MOLECULAR AND OCULAR CHARACTERIZATION OF NOVEL FIBULIN-3 MUTATIONS INVOLVED IN MACULAR DEGENERATION

APPROVED BY SUPERVISORY COMMITTEE

Jennifer Kohler, Ph.D

Benjamin Tu, Ph.D

W. Matthew Petroll, Ph.D

John D. Hulleman, Ph.D

DEDICATION

I dedicate this dissertation to my parents, Danny and Keitha Woodard, whose constant love, support and prayers throughout these past six years have enabled me to persevere.

ACKNOWLEDGEMENTS

When I started at UT Southwestern in 2015, I had no idea that it would be such a roller coaster of a journey for me. Even now as I am writing this section, I can't help but get emotional when I think of everyone who has supported me from the beginning. I first want to acknowledge and thank God for placing me on this graduate school journey and surrounding me with the right people to keep me encouraged. I also want to thank Him for answering my prayers especially when certain seasons of graduate school were very challenging emotionally and mentally.

To my parents, Danny and Keitha Woodard, I love you both so much. Thank you for your constant support and for being my cheerleaders during my time here. Thank you for the sacrifices you've made for our family as well as teaching me certain life lessons at a young age, because now that I'm older, I get it. To my siblings, Danny Woodard II and Kassidy Woodard, I couldn't have asked for better siblings. Y'all are a breath of fresh air to be around and I love you both dearly. Thank you for all of the laughs, "sibling weekends", and fun car rides when we would drive home to Houston. I will miss the fact that we will no longer be in the same city or state, but I'm also looking forward to y'all visiting me in San Diego.

To my mentor, Dr. Hulleman ("Dr. H"), I have appreciated your love of ophthalmology and biochemistry as well as your guidance these past few years. I still remember when I first met with you and we discussed Game of Thrones (before the last season became unbearable to watch). I knew at that exact moment that you would be my mentor. Thank you for welcoming me into your lab as a senior graduate student, supporting

me, and being patient with me when I started in the lab. I also want to thank you for training and developing me as a scientist. While in your lab, I've gained a newfound love for the retina.

To my thesis committee: Dr. Kohler (Jen), Dr. Tu (Ben) and Dr. Petroll, thank you all for your constant support and feedback on my project, and for challenging me to think critically about it. Jen, thank you for being an awesome thesis committee chairperson and I really appreciate you for encouraging me. Ben, you were the first professor I interviewed with at UT Southwestern and I still remember that day like it was yesterday. Thank you for supporting me since I started in the Biological Chemistry program, and even during my lab transition a few years ago. I will definitely miss randomly stopping by your office to have long conversations with you. To Dr. Petroll, thank you for your expertise in ophthalmology and support of my project. I've enjoyed my interactions with you in the hallways of E7. Also, thank you for letting me see the rabbit you were imaging on the Spectralis that one time finally.

I would like to thank each of my incredible lab members (current and former) for making the Hulleman Lab a delight to work in these past few years: Dr. Hui Peng, Dr. Shyamtanu Datta, Dr. Steffi Daniel, Prerana Ramadurgam, Emi Nakahara, Dr. Michael Hayes, and Marian Renwick. I have really enjoyed working with all of you in the lab at one point or another. We've been through so much together: good times, challenging times, and definitely "interesting" times. I want to thank Dr. Hui Peng, Dr. Shyamtanu Datta, and Marian Renwick who made me feel very welcome when I first joined the lab. I really appreciate y'all training me in how to do mouse experiments, your patience in doing so, and

your kindness. To my “ophtha squad”, Dr. Steffi Daniel, Prerana Ramadurgam and Hikaru Ikebe (who I deem as an honorary lab member): where do I even start? I would need to pull up so many pages of our group texts just to recall how amazing our times together were. Seriously, y’all kept me laughing constantly! I definitely cherish our friendship, our coffee times, and our lunches together, especially when life outside of lab was challenging for me. To Emi Nakahara (my “ball of sunshine”), thank you for being such a positive light in the lab and reminding me to not lose hope. Remember to keep that light while you are in graduate school. Last, but not least, to Dr. Michael Hayes: thank you for your guidance and the deep conversations we’ve had in the lab, science and otherwise. Thank you also for the many laughs and for making your lab desk a safe space for me to ask questions.

I also want to say thank you to Dr. Katherine Wert, who helped me to master subretinal injections in mice, which is a very challenging technique. Katherine, thank you for your patience in showing me how to master this and for our chats when we see each other in the E7 hallway.

I can honestly say that the UT Southwestern Graduate School of Biomedical Science has been nothing short of supportive since I started, and I have made some amazing friends along the way. First, I want to say a special thank you to Dr. Nancy Street, who is like a graduate school mom for all of us. Nancy, thank you so much for supporting me, giving me sound advice, and making me feel welcome. I have cherished all of our meetings and conversations on and off campus, and I can’t wait until you come visit me in San Diego so that we can have more. I would also like to say thank you to Carla Childers, the Program

Coordinator for Biological Chemistry. Carla, thank you for always being a listening ear and for your constant encouragement and positivity.

I also want to thank the friends that I've made along the way these past 6 years. To my original squad: Dagimhiwat Legesse (Dagim), Aloysus Lawong (Al), and Busola Alabi, thank y'all for being such a fun, loving group of friends. I enjoyed all our times together hanging out outside of lab and making time to catch up with each other. Dagim, thank you so much for making this last year a blast for me. I enjoy all of our conversations when we're together and I can't for visits with you and Busola in the Bay Area. I also want to thank my peers in the Biological Chemistry program for their support throughout my time in graduate school. I definitely looked forward to in-person WIPS just to catch up with y'all.

To my best friend of 20 years: Maurnica Williams. Girl. What would I do without you? You are my best friend, my sister, and my ride or die. I cannot thank you enough for your love and support throughout these years and I'm so grateful to have you in my life. Thank you for always encouraging me, the many laughs, and also for being my travel buddy. I cannot wait to move to San Diego with you and I'm excited for this next chapter in our lives. I know we will definitely represent and let everyone know that we're from Beyonce's city!

I want to thank all of my extended family: my grandmothers, and numerous aunts, uncles and cousins who have continuously supported and encouraged me throughout this time. Finally, I want to acknowledge two dear friends that I lost who were apart of the UT Southwestern community, Talitha Thomas and Yasmin Abdillahi. I am so grateful for the

great times and conversations we had while you were both here. I am so glad our paths crossed and I miss you both. Heaven gained two angels and one day I'll see y'all again.

MOLECULAR AND OCULAR CHARACTERIZATION OF NOVEL FIBULIN-3 MUTATIONS INVOLVED IN RETINAL DEGENERATION

by

DANAE ROCHELLE WOODARD

DISSERTATION

Presented to the Faculty of the Graduate School of Biomedical Sciences

The University of Texas Southwestern Medical Center at Dallas

In Partial Fulfillment of the Requirements

For the Degree of

DOCTOR OF PHILOSOPHY

The University of Texas Southwestern Medical Center at Dallas

Dallas, Texas

December, 2021

“If all you see is what you see, you will never see all there is to be seen.”

-Dr. Tony Evans

MOLECULAR AND OCULAR CHARACTERIZATION OF NOVEL FIBULIN-3 MUTATIONS INVOLVED IN RETINAL DEGENERATION

DaNae Rochelle Woodard, PhD

The University of Texas Southwestern Medical Center at Dallas, 2021

Supervising Professor: John D. Hulleman, PhD

Distinct mutations in fibulin-3 (F3), a secreted extracellular matrix glycoprotein, have been associated with various ocular diseases including Malattia Leventinese (ML) and the most common macular degenerative disease, age-related macular degeneration (AMD), which ultimately lead to vision loss. AMD is a late onset disease characterized by the progressive loss of photoreceptors and retinal pigment epithelial (RPE) cells that result in irreversible blindness. Although AMD is an etiologically complex disease due to a variety of genetic and environmental risk factors, insight into its pathogenesis can be gained by studying phenotypically similar early-onset monogenic macular diseases. One such disease is ML, a rare macular dystrophy caused by an autosomal dominant Arg345Trp (R345W) mutation in the F3 protein. Previous research has demonstrated that the R345W mutation leads to protein misfolding, inefficient secretion, and accumulation at higher intracellular steady state levels in cultured cells. However, it remained unclear whether other potentially pathogenic or clinically-identified F3 variants recently reported in the human population also share features similar to that of R345W. We hypothesized that secretion defects in one or more F3 mutants

may be a shared mechanism that ultimately contributes to ocular disease. First, I characterized 15 clinically-identified F3 mutations, some of which were identified in patients with AMD, primary open-angle glaucoma (POAG), or had non-discript retinal abnormalities. I found that of the mutants tested, only a single F3 variant, L451F, presented with a significant secretion defect as well as similarities in its biochemical and molecular properties to that of R345W. Subsequently, I generated a retinal disease mouse model of the L451F mutant utilizing recombinant adeno-associated virus (rAAV) in order to robustly evaluate disease phenotypes and uncover how L451F and other F3 mutations (i.e. R345W) are involved in retinal degeneration.

TABLE OF CONTENTS

PRIOR PUBLICATIONS

Peng, H.*, Ramadurgum, P.*, **Woodard, D.R.**, Daniel, S., Renwick, M., Datta, S., Chen, B., Aredo, B., Ufret-Vincenty, R.L. and Hulleman, J.D.[Ω] (2021). Sufficient proteasome activity in aged and degenerating mouse models supports DHFR-based conditional control of protein abundance in the retina. Submitted, *iScience (*- equal contribution, [Ω] - *corresponding author)*

Manna, M.S., Tamer, Y.T., Gaszek, I., Poulides, N., Ahmed, A., Wang, X., Toprak, F.C.R., **Woodard, D.R.**, Koh, A.Y., Williams, N., Borek, D., Atilgan, A.R., Hulleman, J.D., Atilgan, C., Tambar, U.K., and Toprak, E. (2021) A trimethoprim derivative impedes antibiotic resistance evolution. *Nat. Commun*. (2021) May 19;12(1):2949. PMID: 34011959 DOI: 10.1038/s41467-021-23191-z.

Woodard DR, Xing C, Ganne P, Liang H, Mahindrakar A, Sankurathri C, Hulleman JD[#]**,** and Mootha VV[#]. A novel homozygous P388S mutation in TULP1 causes protein instability and retinitis pigmentosa. *Mol. Vis.* (2021); 27:179-190. *([#] - co-corresponding author)*

Woodard DR, Nakahara E, Hulleman JD. Clinically-identified C-terminal mutations in fibulin-3 are prone to misfolding and destabilization. *Sci. Rep.* (2021) Feb 4;11(1):2998. PMID: 33542268 DOI: 10.1038/s41598-020-79570-x.

Ramadurgum P, **Woodard DR**, Daniel S, Peng H, Mallipeddi PL, Niederstrasser H, Mihelakis M, Chau VQ, Douglas PM, Posner BA, Hulleman JD. Simultaneous Control of Endogenous and User-Defined Genetic Pathways Using Unique ecDHFR Pharmacological Chaperones. *Cell Chem. Biol.* (2020) May 21;27(5):622-634.e6. PMID: 32330442 DOI: 10.1016/j.chembiol.2020.03.006.

LIST OF FIGURES

LIST OF SUPPLEMENTARY FIGURES

LIST OF TABLES

LIST OF APPENDICES AND FIGURES

LIST OF DEFINITIONS

ABCR – ATP-binding cassette rim protein

AMD – Age-related macular degeneration

APOE – apolipoprotein E

AREDS – age-related eye disease study

ARMS2 – age-related maculopathy susceptibility protein 2

ARPE-19 – human immortalized retinal pigment epithelium cells

BL – basal lamina

BLamD – basal laminar deposit

BrM – Bruch's membrane

C3 – complement component 3

cbEGF – calcium-binding epidermal growth factor

cGMP – cyclic guanosine monophosphate

CFB – complement factor B

CFH – complement factor H

CNV – choroidal neovascularization

CNS – central nervous system

CRISPR – clustered regularly interspaced short palindromic repeats

CL – Cutis laxa

DHRD – Doyne Honeycomb Retinal Dystrophy

EFEMP1 – epidermal growth factor containing fibulin extracellular matrix protein 1 (the F3 gene)

EGF – epidermal growth factor

ER – endoplasmic reticulum

F3 – fibulin-3

FT – FLAG-tagged

GA – geographic atrophy

GFAP – glial fibrillary acidic protein

GFP – green fluorescent protein

GWAS – genome-wide association study

HEK293A – human embryonic kidney cell line

iPSC – induced pluripotent stem cell

IPM – interphotoreceptor matrix

IRBP – interphotoreceptor retinoid-binding protein

IRES – internal ribosome entry site

IP – immunoprecipitation

IRD – inherited retinal disorder

IS – inner segment

LTBP-4 – latent TGF-binding protein-4

LRAT – lecithin: retinol acyltransferase

ML – Malattia Leventinese

OS – outer segment

PDE – phosphodiesterase

PEDF – pigment epithelium-derived factor

POAG – primary open-angle glaucoma

PS – phosphorothioate

RGC – retinal ganglion cell

ROS – reactive oxygen species

RPE65 – retinal pigment epithelium-specific 65 kDa protein

RPE – retinal pigment epithelium

RP – Retinitis pigmentosa

SD-OCT – spectral domain optical coherence tomography

STR – short tandem repeat

TIMP1 – tissue inhibitor of matrix metalloprotease 1

TIMP3 – tissue inhibitor of matrix metalloprotease 3

TULP1 – tubby-like protein 1

UPR – unfolded protein response

VEGF – vascular endothelial growth factor

WT – wild-type

CHAPTER ONE
INTRODUCTION

1.1 An overview of the human retina

The five senses (sight, hearing, touch, taste and smell) enable us to process our rapidly changing world and are essential for daily function. Of the five, sight has been regarded as the most dominant sense that we use to navigate our environment[1]. Even Aristotle agreed when he stated, "All men by nature desire to know. An indication of this is the delight we take in our senses; for even apart from their usefulness they are loved for themselves; and above all others the sense of sight."[2].

The inner workings of how visual information is transmitted from the eye to the brain remained a mystery for centuries. Today, it is generally understood that light enters the eye and is captured by photoreceptors in the retina, which initiates a cascade of neuronal signals that eventually reach the axons of retinal ganglion cells (RGC) that form the optic nerve (**Fig. 1.1**). The axons in the optic nerve carry neuronal signals to the lateral geniculate nucleus, the visual part of the thalamus, and the superior colliculus in the midbrain that coordinates rapid eye movement, and information is further relayed to higher visual processing centers in the brain that enable us to perceive images of our world.

Ultimately, vision is a result of a complex process whereby vast, intricate networks of neurons and cell circuitries in the retina collectively work together. Unfortunately, this same complexity can also render the retina vulnerable to a variety of environmental and genetic factors, and mutations that can compromise vision with time.

1.1.1 Anatomy of the human eye

Take a quick look around your environment. What do you see? Or think of a loved one's face or a fond memory. What comes to mind? The ability to do these tasks are no small feat and are the result of visual pathways and neural networks in the eye that allow the brain to process and recall visual information[3]. To simply say that the human eye is a complex organ would be an understatement, as it has many tissues, each with unique cellular environments that contribute to its structural integrity and enables it to function similarly to a camera.

Anatomically, the eye can be viewed as a series of tissues that overlap and are classified as either external or internal structures[4] (**Fig. 1.1A**). The external structures are comprised of the conjunctiva, tear film, accessory glands and eyelids, which keep the eye lubricated by secreting mucus and tears; and protect its surface from pathogenic microbes [4, 5]. The internal structures of the eye are categorized into three layers: outermost, middle and innermost layers[4].

The outermost layer consists of i) the sclera, the white outer shell of the eye[6] made up of fibrous collagen that provides stable mechanical support of the eyeball and is connected to extraocular muscles that allow for eye movement[7] and ii) the cornea, a transparent avascular frontal layer responsible for two-thirds of the refractive properties of the eye[4] and acts as a structural barrier that protects against infections[8]. Both tissues act as an outer covering to protect the internal structures of the eye[8].

The middle layer, also known as the uvea, contains i) the iris which controls the size of the pupil[9], thereby dictating the amount of light that reaches the retina[4]; and ii) the ciliary

body which functions to control the focal power of the lens and produces the aqueous humor[10], the fluid that separates the cornea from the lens[11] and iii) the choroid, which is the dense vasculature of the eye that functions as the major nutrient supply for the retina[4, 12].

The innermost layer is comprised of the lens, vitreous humor and the retina[4]. The lens functions by separating the aqueous humor from the vitreous humor in the back of the eye as well as fine-tunes the focus of light onto the retina[13]. The vitreous humor is a fragile, transparent hydrogel made of collagen that separates the retina and the lens[14]. The retina is the nervous tissue of the eye where photons of light are converted into neurochemical energy via action potentials[4], a process that is critical for the visual system of the eye to function properly.

1.1.2 Peeling back the layers of the retina

The relay of visual information from the eye to the brain would be impossible without the retina. The human retina is a 0.5 mm thick, light-sensitive tissue that lines the back of the eye[15]. When light reflects off an object and enters the eye, it is initially refracted through the cornea and lens before reaching the retina[16]. Subsequently, light focused onto the retina causes the activation of distinct neurons embedded within its layers that each play a specific role in vision[17].

The human retina is made up of ten organized cell layers that light passes through to reach the photoreceptors: the inner limiting membrane (1), the nerve fiber layer (2), the ganglion cell layer (3), the inner plexiform layer (4), the inner nuclear layer (5), the middle limiting membrane (6), the outer plexiform layer (7), the outer nuclear layer (8), the external

limiting membrane (9), and finally the photoreceptors (10)[18] (**Fig. 1.1B**). Other neighboring tissues that are important for retinal function and integrity are the retinal pigment epithelium (RPE), Bruch's membrane (BrM) and choroid (**Fig. 1.1B**).

The ten layers of the retina can be categorized as either the inner or outer retina. The inner retina, from the inner limiting membrane (1) to the external limiting membrane (9), contains five highly specialized neurons: ganglion cells, amacrine cells, bipolar cells, horizontal cells and photoreceptors (10). These cells are interconnected by synapses that allow electrical signals to travel from the photoreceptors (10) to the surface of the retina where the RGCs (3) relay processed information to the optic nerve and into the brain[18, 19].

1.1.3 The outer retina and its significance in vision

The outer retina contains the photoreceptor cells (10), RPE, BrM, and choroid. Although each of these layers perform distinct tasks that maintain the health of the retina and supports normal vision, none can function properly without the other[20]. These layers are also the site for many inherited and idiopathic retinal diseases that can lead to vision loss.

1.1.4 Photoreceptors: specialized light-sensing cells in the retina

Humans possess the remarkable ability to perceive color, shape, and motion, and can differentiate between light intensities varied by over nine orders of magnitude[21]. This is possible due to the initial step of vision when light is sensed by a group of specialized, light-sensing neurons called the photoreceptors. The photoreceptors are arguably one of the most important cells in the retina primarily because of their critical role in the initiation of visual

phototransduction whereby photons absorbed by visual pigment molecules are converted into an electrical cellular response. The human retina has ~130 million photoreceptors[21] made up of two types, rods and cones, which work to form the foundation of our daily vision.

1.1.4.1 Rod and cone photoreceptor distribution and structure

The next time you walk into a dimly lit or dark room and it takes a few minutes for your eyes to adjust to your surroundings, you can thank your rod photoreceptors. Rods are highly sensitive to light and operate under dark-adapting conditions, which enables night vision and the ability to see in black and white[22, 23]. Because the human retina is "rod-dominant" (rods make up ~95% or ~120 million of the total photoreceptor cells), it is believed in evolutionary circles that the development of rods were important for our ancestors' survival from predators at night[24].

In contrast, cones make up the remaining ~5% (~6 million) photoreceptors in the human retina and function under ambient and bright lighting conditions. Cone photoreceptor cells are responsible for color vision and high visual acuity[23]. The distribution of rods and cones across the retina varies greatly in certain regions, which in turn affects our perception of light. Despite the daily use of cone-mediated vision in humans, the density of rods far outnumbers cones (20:1), and rods are located primarily in the peripheral retina while cones are present at low densities within this same region[25]. However, this relationship changes in the fovea, a highly specialized rod-free region of the central retina responsible for visual acuity, where cone density is increased by ~200-fold[26].

Rods and cones have five compartments that capture light and transmit signals: a) the outer segment (OS) b) the connecting cilium c) the inner segment (IS) d) the nuclear region and e) the synaptic terminal[23]. The rod OS is the photosensory organelle where photon capture takes place and initiates the process of phototransduction by the following steps: i) a photon of light stimulates rhodopsin, a photo-sensitive G-protein-coupled receptor, and ii) activates the transducin G-protein which in turn iii) activates cyclic guanosine monophosphate (cGMP) phosphodiesterase (PDE) and then iv) hydrolyzes cGMP, reducing its concentration in the OS thereby causing v) the closure of sodium channels and photoreceptor hyperpolarization[27, 28].

Rod and cone OSs comprise hundreds of tightly stacked membrane discs that carry visual pigments (rhodopsin in rods and cone pigment in cones) as well as other transduction components either as transmembrane or peripheral membrane proteins[29]. The connecting cilium functions to connect the OS to the IS, which is the site of metabolic and biosynthetic machinery including the mitochondria, endoplasmic reticulum, Golgi complex, lysosomes and other subcellular organelles[30]; and the nuclear region houses the nucleus[23]. The photoreceptor finally terminates in the synaptic region, which consists of synaptic vesicles that regulate glutamate neurotransmitter release[31].

The integrity and function of the photoreceptors are absolutely crucial for vision. Because of their high metabolic activity due to the constant exposure of light, coupled with their high demand for oxygen and nutrients, photoreceptors are very sensitive to environmental and genetic insults, such as reactive oxygen species (ROS) and mutations,

which could affect their function and disrupt phototransduction[32]. To alleviate these effects, photoreceptors are known to rely on the neighboring RPE cells for protection.

1.1.5 Retinal pigment epithelium functions for maintaining retinal homeostasis

Beneath the photoreceptors lie the RPE, a polarized, pigmented monolayer of epithelial cells that provide structural and functional support to the outer retina[33]. The RPE acts as the blood retinal barrier by separating two distinct environments: the photoreceptor apical side and the BrM/highly-vascularized choroid basal side[34] (**Fig. 1.2**). The polarized nature of the RPE is essential for the health of these two environments and overall retinal health[34, 35]. Given its molecular interactions with the photoreceptors and versatile functions, the RPE is also a critical tissue that aids in vision.

1.1.5.1 RPE and photoreceptor interactions

One direct interaction between the RPE and photoreceptors involve the apical RPE microvilli, 20–30 μm finger-like protrusions that extend into the OSs of rods and cones[36] (**Fig. 1.2**). As many as ~30 photoreceptors can interact with RPE microvilli, which allow the RPE to perform specialized functions essential for photoreceptor support and survival including the diurnal phagocytosis of said photoreceptor OSs, directional transport of nutrients into and removal of waste products from photoreceptors, and visual pigment transport and regeneration[37].

Photoreceptors undergo the daily shedding and renewal of their OS discs, a process that is crucial for maintaining a constant OS length and the prevention of accumulated toxic

photo-oxidative compounds such as ROS[38, 39]. Photoreceptors synthesize new OS discs thereby gradually elongating the OS. To compensate for new OS disc synthesis, the RPE removes the most distal tip of rod and cone OSs by engulfing and degrading the shed tips (disc shedding) by phagocytosis, enabling the daily excitability of photoreceptors and a healthy outer retina [40-42].

The delivery of nutrients such as glucose, retinol, and fatty acids from the choroid blood supply to the photoreceptors is vital for their health and function[43-45]. The RPE mediates this by functioning as a selective barrier that enables the transepithelial transport of nutrients from the choroid to the photoreceptor cells, whilst also directionally transporting metabolic end products (i.e. lactate), ions (Cl-, K+, Na+, HC03 -) and excess water to and from the retina[46, 47].

Another process that occurs between the RPE and photoreceptors is a portion of the visual cycle, which involves the cycling of retinoids, vitamin A derivatives, between the photoreceptor OSs and the RPE[48]. After the absorption of light by rhodopsin in the OS, all-*trans* retinol (a vitamin A isomerization byproduct of light reacting with 11-*cis* retinal within rhodopsin inside the photoreceptors), diffuses across the interphotoreceptor matrix (IPM, also known as the subretinal space) facilitated by the interphotoreceptor retinoid-binding protein (IRBP) and enters the RPE[49]. After esterification of all-*trans* retinol in the RPE by lecithin: retinol acyltransferase, retinal pigment epithelium-specific 65 kDa protein (RPE65) mediates its conversion back to 11-*cis* retinol where it is then oxidized to 11-*cis* retinal and recycled back to photoreceptor OSs[49, 50].

1.1.5.2 The RPE protects the retina from oxidative damage

Beyond the role of regulating photoreceptor interactions, additional functions of the RPE make vision possible such as the absorption of excess light[51]. Similar to photoreceptors, the high metabolism of the RPE and its constant exposure to visible light provides an ideal environment for the formation of ROS that could potentially damage proteins, DNA and lipids[47]. Furthermore, free radicals can also be generated during the phagocytosis of photoreceptor OSs[52].

To help counterbalance the highly oxidative environment of the retina, the RPE employs three lines of defense: i) attenuation of light wavelength and intensity reaching the RPE by macular pigment composed of carotenoids which filters out reactive blue light[53] ii) melanin, the dominant light-absorbing pigment, stabilizes free radicals and reduces light toxicity levels entering the RPE[54] and iii) enzymatic (i.e. superoxide dismutase and catalase) and non-enzymatic (i.e. glutathione, melanin) antioxidants in the RPE which help neutralize reactive oxygen species before they can cause damage to cellular macromolecules[55, 56].

1.1.5.3 RPE secretion mediates retinal integrity

Another important function of the RPE is the secretion of growth factors and proteins that are necessary for the maintaining the structural integrity of the retina and choroid. For example, one of the most prominent growth factors secreted by the RPE include pigment epithelium-derived factor (PEDF). PEDF is a neurotrophic factor that has a dual role in protecting photoreceptors against glutamate-induced or hypoxia-induced apoptosis[57] and

functions as an antiangiogenic factor that inhibits endothelial cell proliferation and stabilizes the endothelium of the choriocapillaris[58].

Proteins expressed and secreted by RPE cells can be localized to either the apical or basal plasma membrane/extracellular space (**Fig. 1.2**). Traditionally, secreted proteins undergo conventional (translocation of proteins from the ER to the Golgi complex, and then to the cell surface via transport vesicles) or unconventional (cell-surface trafficking of proteins via a route that bypasses the Golgi) secretory pathways in cells[59]. The same phenomena occurs in the RPE. However, because of its polarized nature, protein secretion is also regulated by an extra level of complexity and control that stems from sorting proteins apically (e.g.., tissue inhibitor of matrix metalloproteinase 1, TIMP1) or basally (e.g., fibulin-3) to ensure that they are targeted appropriately to the correct cell surface[60-62].

1.1.5.4 Bruch's Membrane, and Choroid

The basolateral region of the RPE also plays a role in forming the blood-retinal barrier due to its proximity to the choroid and is known to mediate a variety of functions that are important for retinal integrity, making the RPE an important cell layer for retinal homeostasis[51, 63]. Whereas the RPE apical microvilli faces the photoreceptor OSs, the RPE basal lamina (BL) interacts with the Bruch's membrane (BrM) and the choroid[33] (**Fig. 1.2**).

The BrM is a thin (2–4 μm), acellular, five-layered extracellular matrix located directly between the RPE and choriocapillaris, a layer of capillaries immediately adjacent to BrM in the choroid[64]. The location of the BrM allows for the exchange of biomolecules, nutrients, oxygen, fluids and metabolic waste between the RPE and choroid. Together, the

RPE, Bruch's membrane, and choroid interact to form the outer blood-retinal barrier that prevents leakage of macromolecules and other potentially harmful agents into the retina, and keeps the microenvironment of the retina and retinal neurons healthy[65].

In summary, the photoreceptors, RPE, BrM, and choroid complex have long been established as having a mutualistic symbiotic relationship in the retina[66]. They each perform individual tasks to support normal vision and while certain cellular and molecular mechanisms aim to protect these layers throughout life, a variety of retinal diseases are known to result in aberrant changes within this complex that ultimately results in loss of vision.

1.2 Vision loss in an ageing society

Imagine waking up one day and not being able to perform simple tasks such as reading this dissertation, watching television or driving. For millions of people, the deterioration or complete loss of vision significantly impacts their daily functioning and quality of life. Furthermore, vision loss affects more than just how people see, but also has implications for physical, cognitive, and mental health issues, which reduce quality of life[67, 68]. This is especially true for the ageing population where eyes naturally exhibit age-related changes in performance, particularly as people reach their sixties and beyond.

1.2.1 Age-related changes in the retina

Ageing is a natural part of life and is characterized by a complex and intraindividual process associated with major cellular and molecular hallmarks, such as accumulation of genetic damage and impaired protein homeostasis, that results in a decline in physiology and

increased vulnerability to death[69, 70]. As we age, our organs, tissues and cells undergo many changes, and the eye is not exempt from this. Ageing in the eye is known to impact the function of its external and internal structures which in turn affects vision. For instance, age-related structural changes to the cornea, such as corneal thickening, can affect the ability of the tissue to refract light and protect itself and the internal structures of the eye[71, 72]. Likewise, common age-related changes in the retina for those over the age of sixty include a decrease in visual acuity, decline in sensitivity of visual field, decreased contrast sensitivity, and increased dark adaptation threshold[73].

At the cellular level, age-related alterations in the retina have been specifically observed in the photoreceptors, RPE and Bruch's membrane. Studies from normal, elderly human donor eyes have shown that rod photoreceptors, but not cones, decrease in density with increased ageing[74]. Moreover, the RPE undergoes several structural changes upon ageing including the atrophy of apical microvilli, loss of melanin granules and accumulation of lipofuscin, an auto fluorescent material known as the "ageing pigment"[47, 75]. Additional age-related changes between the RPE and BrM have also been observed such as BrM thickening, the formation of drusen, yellow deposits comprised of lipids, proteins and cellular debris located between the BL of the RPE and the inner collagenous layer of BrM, and the accumulation of BL deposits (BLamDs) above the BrM[47, 75].

Although to some degree, changes in the retina are considered normal with time, if extensive, they can also have a detrimental effect on vision by increasing the risk for a number age-related retinal diseases such as age-related macular degeneration (AMD), the

prevalence of which is currently raising significant challenges regarding disease prevention and treatment in the world's ageing population[76, 77].

1.2.2 Age-related Macular Degeneration (AMD)

Of the many age-related ocular diseases, AMD is the leading cause of progressive, irreversible visual deterioration and legal blindness in patients over the age of 60 in developed nations[78-80]. Approximately 11 million individuals are affected by AMD in the U.S. alone, with a global prevalence of ~170 million, which is expected to double by the year 2050[81]. In the U.S., the prevalence of AMD is more than double the prevalence of Alzheimer's disease, and has led to an annual $4.6 billion in direct healthcare costs[81, 82]. As the ageing population increases, this expenditure is likewise expected to increase proportionately[81].

1.2.2.1 AMD risk factors contribute to disease complexity

AMD is an ocular disease that involves the posterior portion of the retina called the macula, a specialized region that facilitates central vision and permits high-resolution visual acuity due to its dense concentration of cone photoreceptors[78, 83]. Thus, AMD patients experience a decrease in sharp, central vision as they age. AMD can be triggered by multiple environmental and genetic risk factors that make it etiologically complex. Risk factors such as ageing (>60 years), smoking, high fat consumption, ethnicity and certain mutations in genes are all known risk factors for AMD[84].

Ageing is the most common, unmodifiable risk factor of AMD, whereas cigarette smoking is the most common modifiable risk factor; recent studies have shown that cigarette smokers are at two to three times higher risk for developing AMD[85-87]. Moreover, individuals who consume higher levels of certain of fats (vegetable, monounsaturated, polyunsaturated and linoleic acid) have an elevated risk for AMD, whereas omega-3 fatty acid consumption is associated with a lower risk for AMD in diets low in linoleic acid[84]. The prevalence of AMD has been described predominantly in developed countries such as the United States, Australia, and Europe, and individuals of European descent are more likely to develop AMD compared to individuals of African, Hispanic, or Asian ancestry[82, 88, 89].

In addition to diet and age-related changes, several genetic factors also contribute to advanced AMD. One of the most strongly associated genetic variants leading to increased risk of AMD is the Tyr402His (Y402H) mutant in complement factor H (CFH)[90]. CFH is secreted by the RPE and is a key regulator of the complement system (which involves the *CFH*, *complement factor B* (*CFB*), and *complement component 3* (*C3*) genes)[91]. CFH serves as an inhibitor of the inflammatory response mediated via C3b by acting as a cofactor for cleavage of C3b to its inactive form, and by weakening the active complex between C3b and CFB[92]. The Y402H CFH variant is thought to increase overall complement activation in the retina, thus predisposing one's susceptibility to AMD[90]. Additionally, genes involved in membrane transport (i.e. ATP-binding cassette rim protein, *ABCR*), lipid metabolism (Apolipoprotein E, *APOE*) and age-related maculopathy susceptibility protein 2 (*ARMS2*) have also been associated with advanced AMD[93, 94].

1.2.2.2 Disease stages of AMD

As AMD disease progresses, additional pathological changes are observed in the outer retina (photoreceptors, RPE, BrM, and choroid) (**Fig. 1.3**). In the early stage of AMD, medium-sized soft drusen deposits (>63μm and ≤125μm) in the macula are clinically visible by fundoscopic examination[66]. Intermediate AMD is defined as having one or more large soft drusen (≥125μm) in the macula that are approximately equal to the width of a major retinal blood vessel that crosses the optic disc[95]. Clusters of small, intermediate and large drusen can also be detected in the macula and/or in the peripheral retina, along with hypo- or hyperpigmentary abnormalities in intermediate AMD[95]. The late or advanced stage of AMD are more severe and can occur in two distinct forms: 'wet' AMD (neovascular AMD) or 'dry' AMD (geographic atrophy, GA), both of which causes degeneration of photoreceptors and RPE and ultimately result in vision loss [80] (Fig 1.3).

Wet AMD accounts for 10-15% of AMD cases and is characterized by the abnormal growth of choroidal blood vessels that penetrate up through the BrM and leaks blood into the macula, a process known as choroidal neovascularization (CNV)[66] (**Fig. 1.3B**). This aggressive form of AMD results in fluid accumulation in the retina and/or hemorrhages and causes rapid deterioration of central vision[80]. Fortunately, common therapies for wet AMD (intraocular injections of anti-VEGF inhibitors) halt or reduce CNV quite effectively[96].

In contrast, dry AMD, the most prevalent form of AMD, accounts for ~85-90% of the total cases and is characterized by the excessive accumulation of large drusen between the RPE and BrM that ultimately correlates with atrophy of photoreceptors and RPE cells in the macula[97-99] (**Fig. 1.3C**). The earliest clinical hallmark of dry AMD is the appearance of

drusen. As disease progresses, drusen form between the RPE and the inner collagenous layer of BrM, and are classified based on size, morphology and abundance as either 'hard' or 'soft'. Hard drusen (<63 μm) are described as discrete yellow-white puncta and are considered to be a normal part of ageing[100] whereas soft drusen (>125μm) are larger 'dome shaped mounds' that cluster together, and are highly associated with AMD possibly due to their ability to cause retinal detachment in the macula[101].

1.2.2.3 Disease management strategies for dry AMD

Currently, there are no treatments for dry AMD, however, the use of antioxidant/nutritional supplements to slow disease progression has shown promise for particular disease stages of AMD. For example, in 1996 the National Institutes of Health (NIH) Age-related Eye Disease Study (AREDS) conducted a five year clinical trial that enrolled more than 5,000 AMD patients to test whether nutritional supplements could prevent or slow advanced AMD[102, 103]. The AREDS revealed that patients with intermediate AMD in one eye who took high amounts of antioxidants (beta carotene, vitamins C and E, copper) and zinc reduced their risk of developing central vision loss and advanced AMD by ~19% and ~25%, respectively[104].

Subsequently, in 2006 a second AREDS study (AREDS2) tested whether substituting beta-carotene, which increased the risk of lung cancer in smokers with AMD, with omega-3 fatty acids, lutein and zeaxanthin, would further improve effectiveness in slowing advanced AMD[104, 105]. The rationale for including lutein and zeaxanthin were based on i) previous observational studies suggested a link between higher dietary consumption of these

compounds and decreased risk of developing advanced AMD and ii) these compounds are major constituents comprising the macular pigment and have antioxidative properties[106]. However, the AREDS2 study revealed that lutein and zeaxanthin had no additional overall effect on the risk of advanced AMD, but had an incremental increase in benefit compared to those who those who took the AREDS supplements[104, 107].

Other strategies for slowing or preventing AMD disease progression include lifestyle changes such as smoking cessation and increased physical activity[108]. Currently, several therapeutic avenues are being investigated in dry AMD including drugs with antioxidant properties, inhibitors of the complement cascade, neuroprotective agents, visual cycle inhibitors, gene therapy, and cell-based therapies[109].

For decades, many groups have sought to understand the molecular pathogenesis of dry AMD. However, its heterogeneity and complexity pose a challenge for developing therapies for patients, yet also enables the discovery of key regulators that may influence disease. Advances in current technologies such as genome-wide association studies (GWAS) have opened the door for studying many potential genes involved in dry AMD, particularly those that encode for proteins, such as fibulin-3, located between the RPE and BrM where drusen pathology is observed. These findings have helped to establish a way to both uncover and model AMD disease pathogenesis.

1.3 Fibulin-3 in health and macular degeneration

Fibulin-3 (F3, encoded by the *EFEMP1* gene) has become a protein of significant interest due to its role in a number of pathological diseases that span across various organs,

including the eye[110]. Particularly in relation to macular degenerative diseases, F3 is associated with Malattia Leventinese/Doyne Honeycomb Retinal Dystrophy (ML/DHRD)[111] and more recently with AMD[112-114]. A growing body of evidence suggests that F3 plays an important role in the extracellular matrix (ECM) for maintaining retinal integrity and is a key protein for targeted therapeutics in treating macular dystrophies.

1.3.1 Fibulins: A diverse family of extracellular matrix proteins

The ECM plays vital role in many complex tissues, including the retina[115], and is composed of a variety of proteins and complex carbohydrates that are secreted locally and assembled into an organized meshwork[116]. The major components of the ECM include proteoglycans, growth factors, elastic fibers, extracellular proteases and glycoproteins such as laminins and fibulins[117]. The fibulins have gained traction over recent years because of their diverse cellular and biological functions that are essential for the assembly, maintenance and stabilization of the ECM.

Since the discovery of the first fibulin protein in 1989[118], the fibulin family is known as one of many staples in regulating ECM biology. After all, their family name originates from the Latin word *fibula*, which means clasp or buckle[119]. Made up of eight members, the fibulin family are cysteine-rich ECM glycoproteins and are defined by their structural features, namely i) an N-terminal signaling peptide, ii) a series of canonical calcium-binding epidermal growth factor (cbEGF) domain repeats which are crucial for structural stability and efficient binding to other ECM ligands and iii) a carboxy-terminal (C-terminal) fibulin-type domain[120] (**Fig. 1.4**).

1.3.1.1 The short fibulins and their unique structures and functions

Based on their length and domain structure, the eight fibulins are divided into subfamilies known as class I or class II[121, 122]. The class I fibulins (-1, -2, -6 and -8) have lengthy (>6) cbEGF domains as well as unique N-terminal domains compared to the class II subfamily[119, 121]. For example, fibulin-6 (also known as hemicentin-1) is the largest fibulin (~600 kDa) with six cbEGF domains and an N-terminal von Willebrand factor domain flanked by more than forty immunoglobulin domains[123].

The class II fibulins (-3, -4, -5 and -7) are described as the short fibulins due to their smaller sizes of 50-65kDa (**Fig 1.4**). At the N-terminus, fibulin-3, -4 and -5 have a short signaling peptide followed by a modified cbEGF domain referred to as domain 1 that precedes their canonical cbEGF domains. What makes the modified cbEGF domain 1 atypical is an extra cysteine (Cys) pair at the beginning of the domain and the insertion of a linker region between Cys2–Cys4 and Cys5–Cys6 (numbering refers to the disulfide position within the cbEGF domain) containing 28, 44, or 88 amino acids in fibulin-4, -5, and -3, respectively[120, 124-126]. Structurally, fibulin-3, -4 and -5 are homologous to one another, sharing ~50-60% sequence identity in their cbEGF and C-terminal domains, and are also highly conserved across species[127]. For instance, human, mouse, and rat share a 92% amino acid sequence identity in F3/*EFEMP1*[128].

Ultimately, fibulins 3, -4 and -5 are comprised of five canonical cbEGF domain repeats and a C-terminal fibulin-type domain[121]. The most recently discovered fibulin-7 protein also has a C-terminal fibulin-type domain, but differs from the other short fibulins

because of its three cbEGF domains and an N-terminal Sushi domain which functions as a protein-protein interaction domain and is common in proteins involved in the regulation of the complement system and blood coagulation[129]. Thus, biochemical and structural studies have focused on fibulin -3, -4, and -5 because of their size similarities, sequence homology, and diverse functions within the ECM[125].

Despite their similar structures, the short fibulins have diverse functions and tissue expression patterns that regulate the ECM. During embryogenesis, fibulin-5 (*FBLN5*) is expressed in developing arteries and cardiac valves as well as in many adult tissues including the aorta, lung, uterus and skin. Elastic fiber assembly is mediated through interactions of fibulin-5 with tropoelastin, fibrillin and cross-linking enzymes[130]. *In vivo*, *FBLN5*$^{-/-}$ mice develop disorganized elastic fibers which result in loose skin, vascular abnormalities and emphysematous lung, are reminiscent of phenotypes that resemble Cutis laxa (CL), an inherited connective tissue disorder in humans[130]. A homozygous T–C transition identified at nucleotide position 998 (T998C) of *FBLN5* has also been reported in a consanguineous Turkish family with type 1 autosomal recessive CL[131]. The T998C nucleotide change results in a Ser227Pro substitution at the protein level in the 4th cbEGF domain of fibulin-5, which is predicted to impair elastogenesis[131].

Fibulin-4 has also been shown to be important for ECM assembly. Mice deficient in fibulin-4 die shortly after birth due to disruption of collagen and elastin fibers in their diaphragm[132]. More recent insight into the functional role of fibulin-4 suggests that it may act as a molecular chaperone for the latent TGF-binding protein-4 (LTBP-4) in order to promote elastic fiber assembly[133].

1.3.2 The mysterious case of F3 function

Although F3 is known to be one of many important regulators of the ECM, as well as important for human development and disease[134, 135], many questions remain regarding its exact function. F3 was initially discovered in 1995 as an overexpressed transcript (then known as S1-5) in a patient with Werner syndrome, an inherited disorder that causes premature ageing due to cellular senescence[136]. Within this same study, at the genomic and protein level, F3 was classified as a member of the fibulin family because of its five cbEGF domains and C-terminal fibulin-type domain[136].

Because of its similar structural and sequence properties to fibulin-4 and fibulin-5, F3 was initially speculated to be important for elastic fiber maintenance. However, its lack of interactions with key elastic fiber components, such as elastin and fibrillin, coupled with its inability to compensate for the loss of fibulin-4 and fibulin-5 in mice suggested that F3 has a unique functional role[110]. In 2007, the Mamorstein group gained insight into F3 function after generating *Efemp1-/-* (again, the gene that encodes for the F3 protein) mice by replacing the *Efemp1* gene with a neomycin resistance gene via homologous recombination[137]. They found that *Efemp1-/-* mice bred on the C57BL/6 background displayed hernias at 12 and up to 24 months, in contrast to *EFEMP1-/-* mice bred on the BALB/c background which displayed no herniation, hinting that the function of F3 may be context-dependent and that the lack of F3 can possibly lead to its compensation in certain mouse strains[137]. However, substantial reduction in fascia elastic fibers and several early ageing phenotypes (severe spinal

curvature, periophthalmic lesions, and reduced reproduction and bone densities) were present for *Efemp1-/-* mice regardless of genetic background[137].

The observations of the *Efemp1-/-* in the mouse have also correlated with phenotypes observed with the loss of F3 in humans. An individual recently discovered with biallelic loss of function variants (p.Met107fs and p.Tyr205*) in *EFEMP1* displayed abdominal and thoracic hernias, scoliosis, and translucent skin, akin to phenotypes observed in the *Efemp1* null mice (multiple herniae, premature ageing, and scoliosis)[134]. In contrast to *Efemp1-/-* mice, a skin biopsy revealed that the individual displayed normal elastic fibers[134]. However, it is currently unknown whether elastic fibers were reduced in the individual's fascia. More recently, a novel autosomal recessive Cys55Arg (C55R) variant in F3 was discovered in two siblings that also displayed the some of the aforementioned phenotypes[138], suggesting that this mutant results in loss of F3 function. Loss of F3 in mice and humans have similar systemic phenotypic features, suggesting that F3 may have multiple functions depending on its location in different tissues, unlike fibulin-4 and fibulin-5, which are known for their functional roles of elastic fiber assembly and maintenance[139].

1.3.3 An R345W mutation in F3 causes Malattia Leventinese (ML)

Regardless of limited information about its function, F3 has been well-studied because of its involvement in macular degenerative diseases such as Malattia Leventinese (ML). ML, also known as Doyne Honeycomb Retinal Dystrophy (DHRD), is a rare, early-onset macular dystrophy characterized by the accumulation of drusen between the RPE BL and inner collagenous layer of the BrM. Initially, small radial drusen are typically detected in

the macula in the 3rd and 4th decade of life[140]**.** ML progression correlates with increased drusen number and size which eventually leads to RPE and photoreceptor atrophy and vision loss.

ML is inherited in an autosomal dominant manner and is caused by an Arg345Trp (R345W) missense mutation in F3/*EFEMP1*[111] mapped to chromosome 2, region p16[141]. In 1999, Stone *et al*. identified R345W *EFEMP1* as the singular cause of ML across 39 families, the majority of which were heterozygous, in Australia, Switzerland and the United States[111]. This mutation was also identified in ML patients from a Japanese family[142], a Chinese family[143], and even more recently within a Columbian family[144] with no additional mutations in *EFEMP1*. This indicates R345W F3 has a strong correlation with ML disease and is not due to a founder effect[145].

ML patients are described as having vision symptoms in the early stage of disease such as decreased visual acuity, sensitivity to light (photophobia), and a deficiency in color vision (dyschromatopsia) prior to significant central vision loss[146]. Late stages of the disease typically happen around the 4th or 5th decade where central vision deteriorates due to pigmentary changes in the macula, GA and/or CNV. However, the onset of ML -associated symptoms vary greatly between individuals, including affected family members, suggesting that ML is indeed likely a modifiable disease. For example, whereas the majority of ML patients have been reported to develop drusen, a 62-year-old individual with the R345W mutation was assessed as asymptomatic, demonstrating a lack of complete disease penetrance[147].

1.3.4 R345W F3 is misfolded and inefficiently secreted from the RPE

After discovering that R345W F3 was causal for ML, a key question arose: How does this mutation affect the structural and functional properties of F3? While this is still an open-ended question, Mamorstein *et al.* initially characterized the secretory property of the mutant compared to WT F3, speculating that the mutant was misfolded. Their initial results showed that upon expression in human immortalized retinal pigment epithelium (ARPE-19) cells followed by immunoprecipitation (IP) and western blotting, R345W was more abundant in the cell lysate and less abundant in the media than WT F3[113]. Subsequently, they found that R345W F3 results in protein misfolding due to i) its faster migration under non-reducing conditions compared to WT F3, indicative of a change in intramolecular disulfide bonding and ii) secretion of R345W F3 was significantly reduced coupled with intracellular accumulation in rat RPE-J cell lysates, compared to WT F3[113]. Furthermore, *Hulleman et al*. revealed that R345W secretion is more than meets the eye, and uncovered that aromatic amino acids (arginine, tryptophan, tyrosine) and proline were not well tolerated at the R345 position, resulting in significant reduction of F3 secretion caused by the disruption of disulfide bond formation in the 6th cbEGF domain[100, 148]. This result suggested that the R345W mutation in ML leads to inherent misfolding at the molecular level.

Evidence by Fernandez-Godino *et al*. demonstrated in primary mouse RPE cells from R345W knock-in mice that secreted R345W activates an inflammatory response mediated by C3a[149] (and not C5[150]), which in turn causes sub-RPE deposit formation, suggesting that extracellular R345W may play more of a major role in triggering disease[149]. This study further raises the question of whether the small amount of misfolded, secreted R345W F3 in

ML exerts toxicity in the RPE and neighboring cells and/or is prion-like and alters the structure (i.e. "seeding")[151] of endogenous WT F3, which may also have implications for disease.

1.3.5 R345W F3 leads to sub-RPE deposit formation in mice

In 2007, Fu *et al*. and Mamorstein *et al.* demonstrated that the mutant was pathological by generating an R345W knock-in mouse model that developed deposits between Bruch's membrane and the RPE[152, 153]. In the Fu *et al.* study, chimeric homozygous knock-in mice were generated by injecting blastocysts with the R345W *Efemp1* allele into mouse embryos[152]. Upon analysis, BLamDs akin to drusen in AMD were detected as early as six months of age and progressed in size when mice were aged up to 18 months. RPE abnormalities such as vacuolization also occurred[152], although this latter observation has not been corroborated. Surprisingly, F3 and one of its binding partners, TIMP3, were localized within the deposits[152], similar to a previous report in AMD patients[113].

R345W knock-in mice in the *Mamorstein et al.* study were generated by replacing the endogenous WT allele with either one (heterozygous) or both (homozygous) mutated alleles[153]. Regardless of gene dosage, sub-RPE BLamDs containing membranous debris and mutant F3, coupled with BM abnormalities and degeneration of the RPE, progressed from twelve to 23 months of age[153]. Ultimately, both groups demonstrated that R345W F3 closely recapitulates the pathophysiology of ML patients, making this a valid mouse model to further study the biological pathway(s) involving R345W F3 that initiate ML.

1.3.6 Evidence for F3 in dry AMD

Because of its early age of onset, its well-defined genetic causation, and its similar clinical features to AMD, ML has been a particular disease of interest used for understanding the potential causes of dry AMD. The progression of drusen that results in RPE degeneration and ultimately vision loss is a common theme in both diseases, and although many genetic factors are involved in AMD pathogenesis, there are currently no convincing reports of F3 point mutations in wet or dry AMD. There are also no reports of the R345W F3 in AMD patients, which is not surprising because i) AMD is multifactorial ii) pathology would happen at an earlier age of onset and iii) diagnosis of disease would be ML instead of AMD because of the strong association of the mutant to ML. However, this should not disqualify F3 as one of many important components in AMD pathology.

In fact, a few studies have linked wild-type (WT) F3 to AMD. Histological observations from several AMD human donor eyes revealed that WT F3 accumulates within the RPE and between the RPE and hard drusen[113]. In the same study, *Mamorstein et al.* also observed a similar drusen localization of R345W F3 in ML human donor eyes whereas F3 was not found in the RPE or near drusen of control eyes, suggesting that F3 is mainly associated with pathogenic drusen deposits[113]. It is important to note that although F3 (WT or R345W) was not a component of the drusen in these patients, the close association established the question of whether F3 may somehow play a role in contributing to drusen formation in disease.

Meyer *et al*. conducted a GWAS study that analyzed the genome of AMD and non-AMD patients in order to identify rare copy number variants that would infer the etiology of

AMD[114]. Upon stringent criteria, *EFEMP1* was one of five genes found in three AMD patients whereby an intergenic duplication was discovered less than 1.5 Mb upstream of *EFEMP1* in three AMD patients[114]. Thus, this study suggested that *EFEMP1* levels can be regarded as high risk for AMD in rare cases.

Perhaps the most surprising, a recent study by Cheng *et al.* demonstrated that F3 was overexpressed in the retina-choroid tissues of AMD patients and *in vitro*, serum F3 of wet AMD patients correlates with increased expression of VEGF, a hallmark of CNV[154]. The authors also found F3 overexpression in dry AMD patients in their study, although not to the extent of wet AMD, and thus did not pursue further analysis. Given the heterogeneity of the AMD, it would be interesting to test if F3 overexpression is generally reflected in a larger AMD study, as the authors concluded their results from a small sample population. Taken together, these studies highlight that F3 may be a critical component in the disease processes leading to AMD.

In another study linking *EFEMP1* to AMD, Duvvari *et al.* performed whole-exome sequencing on patients with familial and sporadic cuticular drusen (CD), a clinical subtype of AMD characterized by the presence of at least 50 small (25–75μm) uniformly sized hyperfluorescent drusen, scattered primarily in the macular region[112]. Amongst many ECM genes, their studies revealed rare, heterozygous sequence variants and, specifically, they discovered an Asp49Ala (D49A) F3 mutation that, at the time, was predicted to be damaging to F3 structure and function[112].

Extensive analysis of R345W over years of studies *in vitro* and *in vivo* have helped to pave the way for attempting to understand the pathogenesis of ML and AMD. In this body of

work, I reaffirm the notion that F3 is a key protein important for the development of ML and AMD. I add to the body of knowledge by first determining whether F3 secretion can be used as an indicator of pathology (as observed with the R345W mutation) by performing biochemical and molecular characterization of novel, naturally-occurring F3 mutations (Chapter 2). Next, I model select F3 mutants *in vivo* using recombinant adeno-associated virus technology in order to more robustly characterize and evaluate F3 associated disease phenotypes in the mouse retina (Chapter 3).

Chapter 1 Figures

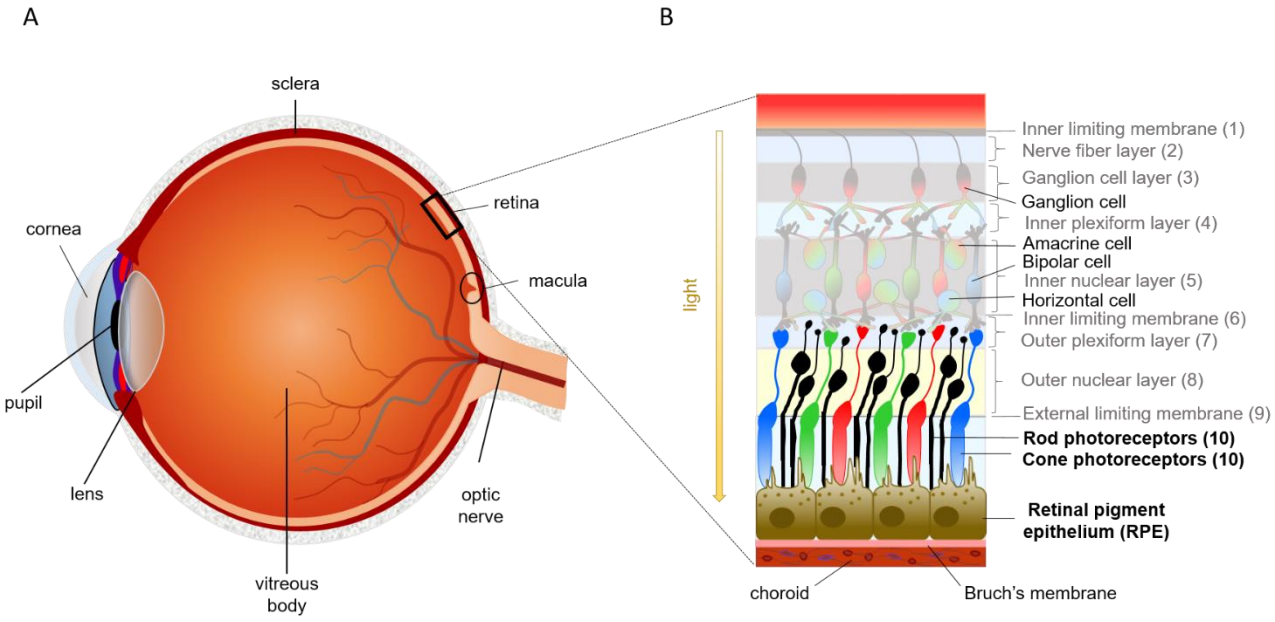

Figure 1.1: Organization of the human retina. (A) The human eye. (B) Distinct layers and cells of the human retina.

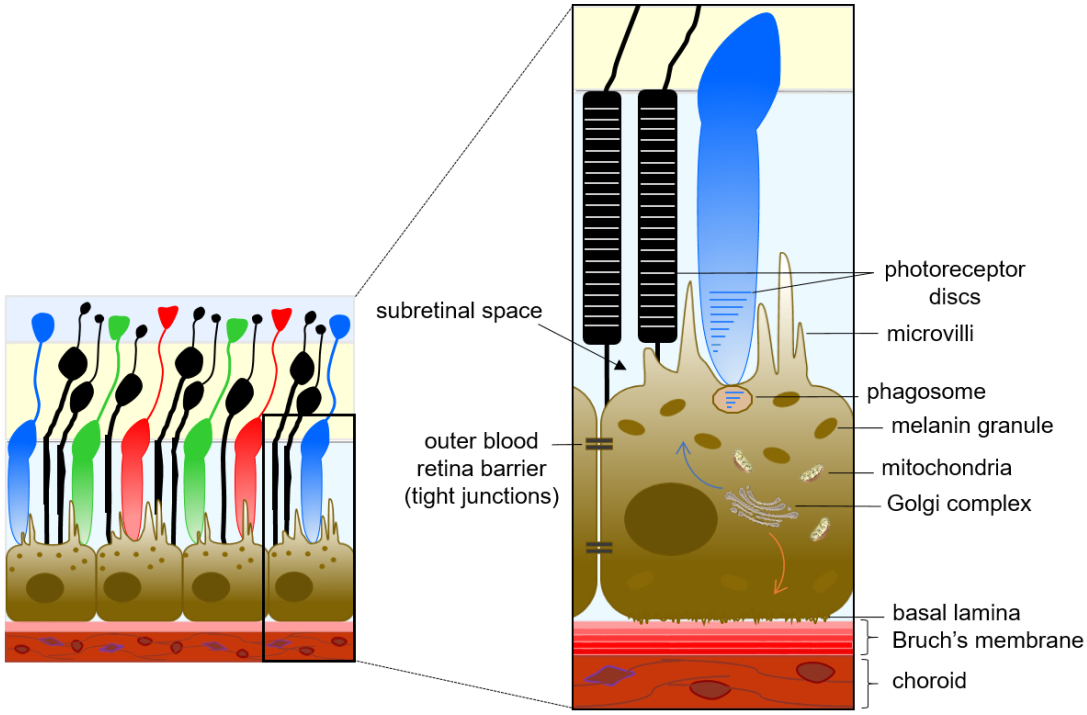

Figure 1.2: The outer retina is essential for maintaining healthy vision. (A) The outer retina. (B) Apical interactions between the photoreceptors and RPE (e.g. photoreceptor disc shedding) and basal interactions of the RPE, BrM and choroid. Black arrow shows the subretinal space located between the photoreceptors and RPE. Blue arrow indicates apical secretion and orange arrow indicates basal secretion in the RPE.

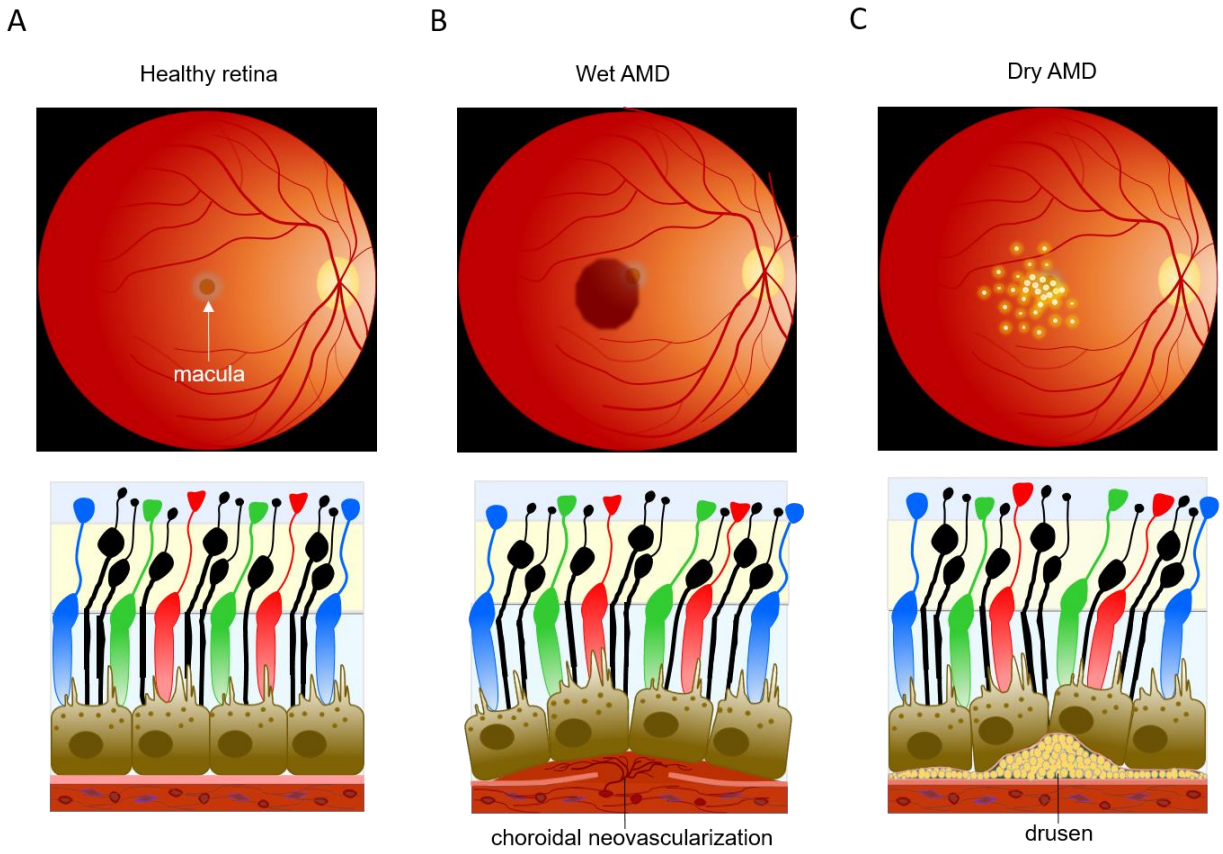

Figure 1.3: Advanced stages of AMD. (A) cross-section of a normal, healthy retina. White arrow indicates the macula. (B) Wet AMD and cross-section showing CNV that leads to fluid buildup in the macula. (C) Dry AMD and drusen accumulation underneath the RPE in the macula.

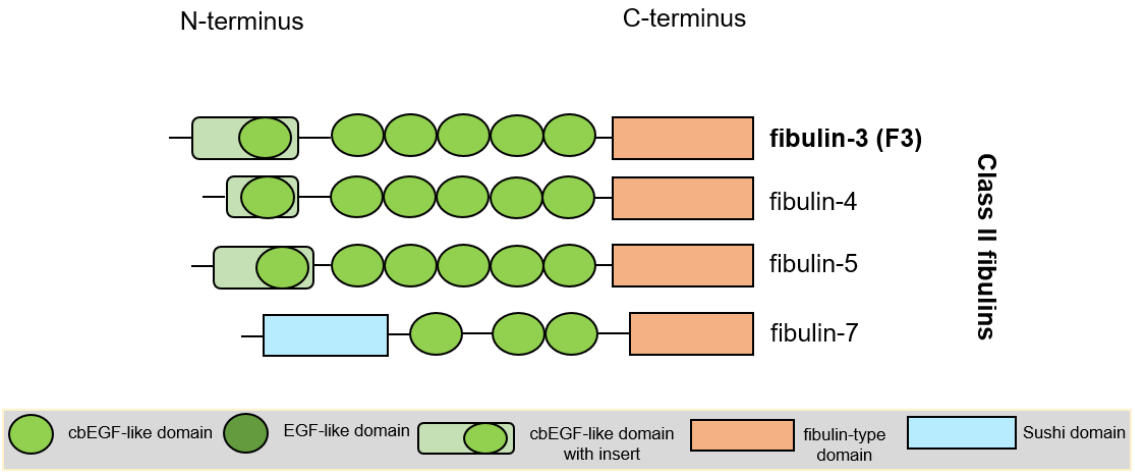

Figure 1.4: The short fibulins and their structures (adapted from Chakraborty *et. al.*[155]). F3 (bolded) is a part of the Class II (short) fibulins.

CHAPTER TWO
CLINICALLY-IDENTIFIED C-TERMINAL MUTATIONS IN FIBULIN-3 ARE PRONE TO MISFOLDING AND DESTABILIZATION

Acknowledgement

This chapter was previously published as **Woodard DR**, Nakahara E, Hulleman JD. Clinically-identified C-terminal mutations in fibulin-3 are prone to misfolding and destabilization. *Sci. Rep.* (2021) Feb 4;11(1):2998. PMID: 33542268 DOI: 10.1038/s41598-020-79570-x. Author contributions: D.R.W. performed all experiments. E.N. generated new F3 constructs. D.R.W. and J.D.H. analyzed data, wrote the manuscript, prepared figures, and all authors reviewed the final manuscript.

2.1 Abstract

Distinct mutations in the secreted extracellular matrix protein, F3, have been associated with a number of ocular diseases ranging from primary open angle glaucoma to cuticular age-related macular degeneration to a rare macular dystrophy, ML. The R345W F3 mutation that causes ML leads to F3 misfolding, inefficient secretion and accumulation at higher intracellular steady state levels in cultured cells. Herein, we determined whether fifteen other clinically-identified F3 mutations also led to similar levels of misfolding and secretion defects, which might provide insight into their potential pathogenicity. Surprisingly, we found that only a single F3 variant, L451F, presented with a significant secretion defect ($69.5 \pm 2.4\%$ of WT F3 levels) and a corresponding increase in intracellular levels ($226.8 \pm 25.4\%$ of WT F3 levels). Upon follow-up studies, when this conserved residue (L451) was mutated to a charged (Asp or Arg) or bulky (Pro, Trp, Tyr) residue, F3 secretion was also compromised, indicating the importance of small side chains (Leu, Ala, or

Gly) at this residue. To uncover potential inherent F3 instability not easily observed under typical culture conditions, we genetically eliminated the sole stabilizing N-linked glycosylation site (N249) from select clinically-identified F3 mutants. This removal exacerbated R345W and L451F secretion defects ($19.8 \pm 3.0\%$ and $12.4 \pm 1.2\%$ of WT F3 levels, respectively), but also revealed a previously undiscovered secretion defect in another C-terminal variant, Y397H ($42.0 \pm 10.1\%$ of WT F3 levels). Yet, glycan removal did not change the relative secretion of the N-terminal mutants tested (D49A, R140W, I220F). These results highlight the uniqueness and molecular similarities between the R345W and L451F variants and also suggest that previously identified disease-associated mutations (e.g., R140W) are indistinguishable from WT with respect to secretion, hinting that they may lead to disease by an alternative mechanism.

2.2 Introduction

Vision loss significantly affects the quality of life of over 200 million middle-aged and elderly people worldwide[156]. In the United States alone, it is estimated that by the year 2050, the number of people who will suffer from either uncorrectable vision defects or blindness will double to more than 20 million[157]. Thus, there is a need for effective ocular therapies for the ageing population and a deeper understanding of the environmental and genetic factors that influence disease[73, 82, 158, 159]. Age-related macular degeneration (AMD) is the leading cause of progressive and irreversible vision loss in individuals over the age of 65 in industrialized nations[82]. AMD is a late-onset disease that results in the degeneration of photoreceptor and retinal pigment epithelial (RPE) cells, compromising an individual's

ability to retain sharp central vision[66, 160]. The most common clinical hallmark of early-stage dry AMD is the formation of yellow, extracellular lipid and protein deposits underneath the RPE known as drusen[66, 80, 97]. The accumulation of drusen eventually correlates with the atrophy of RPE cells followed by the dysfunction of photoreceptor cells, causing irreversible blindness[75, 161]. Dry AMD makes up about 85–90% of AMD cases and there are currently no effective therapies[162, 163].

Although AMD is an etiologically complex disease due to a variety of genetic and environmental risk factors[164-166], insight into its pathogenesis can be gained by studying phenotypically similar, early-onset monogenic macular diseases. One such disease is Malattia Leventinese (ML), a rare macular dystrophy caused by an autosomal dominant Arg345Trp (R345W) mutation in the fibulin-3 (F3) protein, wherein patients develop AMD-like symptoms including drusen formation as early as 20 years of age[111, 147]. Increasing evidence suggests that F3 is involved in AMD including: (1) the accumulation of WT F3 surrounding drusen in AMD patient donor eyes[113], but not around drusen of asymptomatic patients, (2) increased copy number variants near the *EFEMP1* promoter (the gene that encodes for F3) were linked to increased risk for AMD[114], and (3) a sequence variant, Asp49Ala (D49A), was discovered in a patient with cuticular drusen, a clinical subtype of AMD[112]. The combination of these findings strongly suggests that both mutant and WT F3 may play an important role in the development of AMD or AMD-like retinal dystrophies[167].

F3 is a 55 kDa secreted extracellular glycoprotein that belongs to the fibulin family of proteins[126]. While broadly expressed throughout the body during development, F3 is highly expressed in various ocular tissues including the retina and RPE[120, 126, 168]. Several *in vitro*

studies have shown that the R345W F3 mutant, which causes ML, is misfolded, results in a secretion defect, and disrupts protein homeostasis[113, 148, 169-171]. *In vivo* studies have shown that R345W F3 knock-in mice develop basal laminar deposits underneath the RPE, akin to drusen observed in humans[152, 153]. Although these *in vitro* and *in vivo* studies examined and characterized the effect of the R345W variant, additional F3 variants have been identified in the human population, some of which have been linked to disease. These mutations, including the D49A variant mentioned previously, the R140W variant found in a family with primary open-angle glaucoma[172], and the C55R variant found in two patients with recessive Marfanoid syndrome[135], have essentially remained uncharacterized. Additional mutations have been identified in the *EFEMP1* gene in patients with ocular disorders (information obtained through ClinVar[173]), but the clinical significance of these genetic alterations is unclear.

We postulated that secretion defects, as seen with the R345W mutation, may be a universal mechanism by which F3 variants ultimately contribute to ocular disease. In this work, we selected fifteen additional clinically-identified F3 variants (https://www.ncbi.nlm.nih.gov/clinvar), and evaluated their secretion and intracellular accumulation propensities in HEK293A and ARPE-19 cells. New variants that were identified with secretion defects were next evaluated for their ability to activate the UPR and the molecular basis responsible for retention was identified at the amino acid level. Lastly, we determined whether N-linked glycosylation of F3 serves as a unifying stabilizing force, enabling the efficient secretion of subtly unstable mutants.

2.3 Results

2.3.1 Clinical significance and pathogenicity prediction of novel F3 mutations

Previously, we and others have demonstrated that the R345W F3 variant, which causes ML, is inefficiently secreted from cultured cells[113, 148]. We rationalized that additional F3 mutations may also cause secretion defects, serving as a potential universal mechanism by which distinct F3 variants contribute to ocular disease. Using ClinVar, a database that lists mutations present in patients within the human population, we selected fifteen additional clinically-identified, uncharacterized/poorly characterized variants identified in F3 (**Fig. 2.1**). The *EFEMP1* gene that encodes for F3 is one of many genes included within retinal dystrophy panels (https://www.ncbi.nlm.nih.gov/gtr/tests/522537/, https://www.egl-eurofins.com/tests/?testid=MM239) which are typically prescribed for patients with unknown ocular diseases.

We selected a range of F3 missense mutations which have been previously reported in either patients with ocular diseases (D49A, R140W, Y397H, L451F) or identified through other means (remainder). We next recorded their clinical significance (ClinVar), determined their potential pathogenicity (PROVEAN and PolyPhen), and allele frequency (gnomAD, **Table 2.1.1**). As expected, the R345W variant was classified as pathogenic in ClinVar and *in silico* prediction indicated that it is deleterious (PROVEAN score of -3.309) and probably damaging (PolyPhen score of 1.000, **Table 2.1.1**). Due to the extent of study of this mutation, along with documented human and mouse model data, we used the R345W mutation as a benchmark for relevance to ocular disease. However, no other variant was identified as completely fulfilling these three criteria (i.e., simultaneously determined to be

pathogenic, deleterious, and damaging using the aforementioned programs), suggesting that additional metrics, such as secretion propensity, may be needed to provide more information regarding pathogenicity. The variant that resembled R345W the closest in the *in silico* modeling was the Y397H mutation, which was identified as potentially pathogenic (ClinVar), deleterious (PROVEAN score of -3.276) and probably damaging (PolyPhen score of 1.000, **Table 2.1.1**). The clinical significance of the remaining mutations were determined to be benign, likely benign, conflicting interpretations, or uncertain significance (ClinVar, **Table 2.1.1**). A few variants not listed in ClinVar were I220F (previously identified in a control individual[111]) and N249Q and C338A (engineered mutations not present within the human population). Interestingly, 6 out of 10 mutations classified as variants of unknown significance were predicted to be deleterious (PolyPhen) and/or damaging (PROVEAN) to the structure of F3 (**Table 2.1.1**). In contrast, the synonymous F3 variants were predicted to be non-pathogenic (PROVEAN). Many of the variants we analyzed were found at surprisingly high frequencies, including the synonymous E129E variant (most common coding variant, 2.73×10^{-2}), the R387Q variant (most common missense variant, 1.14×10^{-3}), followed closely by the D49A variant (1.05×10^{-3}, **Table 2.1.1**).

2.3.2 Few F3 mutations cause secretion defects

We next determined the secretion propensities of each of the select F3 variants in a cell culture system. Using site-directed mutagenesis, we generated the fifteen new F3 mutations (each construct containing an N-terminal FLAG epitope as described

previously[174], **Fig. 2.1**). We then quantified intracellular (cell lysate) and extracellular (secreted) F3 levels from transfected HEK293A cells using western blotting (**Fig. 2.2A,B**). An additional metric, secretion propensity, which takes into account both intracellular and secreted F3 (the ratio of WT-normalized secreted protein/intracellular), was also calculated (**Fig. 2.2C**).

As we have observed previously[27], C338A F3, a genetically engineered F3 that is not folded due to absence of a required disulfide bond in the 6th calcium-binding EGF domain, and R345W F3 both displayed significant defects in secretion propensity (0.007 ± 0.003 [$p < 0.001$], 0.32 ± 0.04 [$p < 0.001$] of WT F3 levels respectively, **Fig. 2.2A,C**). Interestingly, out of the fifteen newly tested variants, only L451F displayed a significant reduction in secretion propensity (0.38 ± 0.08 [$p < 0.05$] of WT F3 levels), suggesting that this variant may be misfolded (**Fig. 2.2A,C**). These secretion defects were not due to reduced transfection efficiency or expression levels (**Sup. Fig. 2.2A**).

Surprisingly, we observed that the Q226H variant resulted in significantly reduced intracellular ($30.2 \pm 0.9\%$ [$p < 0.001$] of WT) and secreted levels ($27.4 \pm 2.9\%$ [$p < 0.001$)] of WT), which were accompanied by a significant concomitant reduction in *EFEMP1* transcript levels ($23.3 \pm 0.9\%$ of WT, **Sup. Fig. 2.22A**). Even more surprising was that in addition to forming full length F3, this variant formed an intracellular truncated product of ~ 30 kDa through an unknown mechanism (asterisk, **Fig. 2.2A**). While Q226H has intriguing characteristics, it did not fall into our criteria for identifying mutants that behave similarly to R345W, thus we chose not to focus on this variant in this study.

2.3.3 Secretion propensities of F3 in ARPE-19 cells

Because F3 is expressed in retinal pigment epithelial cells (RPE) in the eye[126, 175],we next determined whether F3 secretion propensity defects were also apparent in an RPE-based cell culture system using ARPE-19 cells (**Sup. Fig. 2.2.3A-C**). We selected disease-associated variants as well as those with secretion defects and stably expressed them in ARPE-19 cells. Upon expression of WT, D49A, R140W, R345W, Y397H, and L451F F3 in ARPE-19 cells (**Sup. Fig. Fig. 2.2.3**), we detected significantly lower secretion propensities for R345W (0.21 ± 0.04 [$p < 0.001$]) and L451F (0.44 ± 0.08 [$p < 0.001$]) (**Sup. Fig. 2.2.3C**), a phenomenon similar to what was observed in HEK293A cells (**Fig. 2.2A–C**). Furthermore, analysis of these stable cells by qPCR demonstrated no significant changes in *EFEMP1* transcript levels (**Sup. Fig. 2.2.2B**).

2.3.4 The L451F F3 mutation does not induce an ER stress response

Next, we determined whether an ER stress response was induced due to significantly higher intracellular levels of C338A, R345W, or L451F F3. HEK293A cells were transfected with WT, C338A, R345W, or L451F F3 constructs or treated with tunicamycin (Tm) as an unfolded protein response (UPR) positive control. We performed qPCR using select TaqMan probes (*HSPA5*, *DNAJB9*, and *ASNS*), the levels of which are representative of the triggering of select arms (i.e., ATF6, IRE1 and PERK, respectively) of the UPR. We found that only cells expressing the severely misfolded C338A F3 variant demonstrated a significant increase in *HSPA5* transcript levels compared to cells expressing WT F3 ($302.2 \pm 34.2\%$, **Fig. 2.3**), suggesting that this variant induces ER stress. We observed no significant induction of ER

stress in cells expressing R345W or L451F F3 (**Fig. 2.3**), suggesting that intracellular levels of these variants are not sufficient to disrupt ER homeostasis. These findings are consistent with our previous results[174], but in contrast to other findings[169]. These discrepancies are likely due to the method of DNA introduction, expression level differences, and/or different culture systems.

2.3.5 Charged and aromatic substitutions at position 451 affect F3 secretion

Previously, we demonstrated that substitution of F3 at R345 with aromatic residues or proline also resulted in secretion defects[1482], indicating that the common Arg-to-Trp mutation was not unique in its ability to reduce secretion, but that presence of other sterically-hindering or bulky amino acids would also cause secretion defects. We next decided to explore the molecular basis of how the L451F mutation disrupts F3 secretion in a similar manner. To accomplish this, we generated a panel of substitutions at L451 with diverse amino acid backbones, transfected them into HEK293A cells, and performed western blotting (**Fig. 2.4A**). Mutation from the native leucine residue to other small uncharged residues such as alanine (L451A) or glycine (L451G) did not affect secretion compared to WT F3 ($92.0 \pm 8.4\%$ and $100.6 \pm 3.6\%$ of WT levels, respectively) (**Fig. 2.4A,B**). Replacement of L451 with charged residues such as aspartic acid (L451D) or arginine (L451R) significantly lowered secretion ($68.6 \pm 5.0\%$ [$p < 0.001$], $70.0 \pm 6.0\%$ [$p < 0.01$] of WT levels, respectively) (**Fig. 2.4A,B**). Interestingly, mutation of L451 to a tryptophan (L451W) or tyrosine (L451Y) both resulted in secretion defects ($33.3 \pm 7.7\%$ [$p < 0.01$], $61.3 \pm 2.3\%$ [$p < 0.01$] of WT F3 levels, respectively) (**Fig. 2.4A,B**). Substitution of leucine

to proline (L451P) resulted in an even more drastic secretion defect ($10.3 \pm 4.4\%$ [$p < 0.001$] of WT F3 levels, respectively) (**Fig. 2.4A,B**), possibly due to proline's conformationally-restrictive backbone[176, 177].

The rank-order of secretion propensity for these L451 variants was Pro < Trp < Phe < Tyr < Asp < Arg < Gly ~ Leu (WT) < Ala (**Fig. 2.4C**). Together, these data suggest that, similar to substitutions made at the 345 position, bulky aromatic and restrictive residues at the 451 position are sufficient to cause secretion defects in F3. Supporting this notion, L451 is well-conserved in F3 proteins across species, and reasonably conserved among other human fibulins (**Sup. Fig. 2.24A, B**). Whereas aromatic residues at the 345 position appeared to disrupt disulfide bond formation within the 6th EGF domain[148], possibly causing misfolding of that particular domain, it is unclear why similar residues would also disrupt the folding of the fibulin-type domain where the L451 residue is located. Additional studies will have to be performed to begin to tease out such information.

2.3.6 The N249 N-linked glycan is required for efficient L451F F3 secretion and stabilizes the Y397H F3 variant

Absence of N-linked glycosylation of R345W F3 leads to increased intracellular aggregation and an altered conformation of R345W F3, suggesting that the N-linked glycan is required in order for R345W to maintain a stable, native-like structure[174]. Due to the molecular similarities between R345W and L451F (i.e., mutation to aromatic residues, degree of secretion deficiency, poor tolerance of other amino acids at the position), we postulated that N-linked glycosylation is also a stabilizing force for L451F as well as additional F3 mutants.

To cleanly eliminate the F3 N-linked glycosylation site, we mutated Asn249 to Glu (N249Q) in WT F3 (**Fig. 2.2A**) as well as in a series of variants analyzed in **Fig. 2.5**. Upon elimination of the glycan itself in WT F3 (designated as N249Q), we did not observe a significant change in secretion ($98.8 \pm 6.8\%$) or intracellular ($111.8 \pm 7.0\%$) levels of N249Q compared to WT F3 (**Fig. 2.2A,B**). However, we did observe a significant reduction in N249Q/R345W and N249Q/L451F secretion (15.8 ± 4.6 [$p < 0.001$] and $12.4 \pm 1.2\%$ [$p < 0.001$], respectively, of N249Q F3 levels) (**Fig. 2.5A–C**), especially when compared to fully glycosylated R345W and L451F (compare **Fig. 2.5A–C** to **Fig. 2.2A–C**).

Surprisingly, in the absence of N-linked glycosylation, N249Q/Y397H displayed a significant secretion defect ($42.0 \pm 10.1\%$ [$p < 0.05$] of N249Q F3 levels) (**Fig. 2.5A–C**) that was not previously observable in the glycosylated Y397H variant (**Fig. 2.2A–C**). This observation suggests that the Y397H variant may exhibit a degree of instability which is compensated by the presence of the N-linked glycan at N249. This compensation may be in the form of intrinsic stabilization due to the glycan itself and/or extrinsic stabilization afforded by promoting interactions of F3 with glycan-binding lectins (e.g., calreticulin and calnexin). The secretion of the remaining variants, D49A/N249Q, R140W/N249Q, I220F/N249Q, and N249Q/R387Q were identical to N249Q F3 (**Fig. 2.5A–C**).

2.4 Discussion

In this study, we selected a panel of poorly-characterized, clinically-identified synonymous and missense F3 mutations present in the human population and determined whether these mutations disrupted F3 folding and secretion. Upon initial evaluation, we

found that only R345W and L451F F3 displayed a significant secretion propensity defect compared to WT F3. Subsequent follow-up studies demonstrated a broad intolerance for charged and bulky amino acid side chains at the L451 position, and demonstrated a reliance of L451F and another C-terminal variant, Y397H, on a stabilizing N-linked glycan at N249. Interestingly, many of the N-terminal variants we tested that had no effect on F3 secretion were also of a similar molecular nature to the compromised C-terminal variants (i.e., R140W and R194W versus R345W, and I220F versus L451F), hinting that the positioning of the bulky aromatic variations is important and can compromise secretion in a context-dependent manner, an idea which is supported by our previous studies[178]. It is important to note that since no well-established functional assay exists for the evaluation of F3 variants, we believe that monitoring the secretion and intracellular levels of F3 in cell culture provides a reasonable metric for assessing its degree of folding and its potential to trigger cellular dysfunction and/or influence disease.

Our findings also suggest that the D49A and R140W variants behave differently than R345W or L451F. Given the prevalence of the D49A variant in the human population, its presence in a "predisposition screen in an ostensibly healthy population" (ClinVar), combined with neutral or benign *in silico* predictions, and our secretion results, we believe that this is likely a non-pathogenic polymorphic variant in F3 which may not be involved in AMD. However, it is still possible that other mutations such as R140W might influence disease (primary open angle glaucoma) by mechanisms distinct from R345W or L451F, and therefore may behave differently. Another interesting finding in our study was the Q226H F3 variant. Although this variant is predicted to change *EFEMP1* splicing (ClinVar), it was

surprising to observe a ~ 30 kDa truncated product, especially since our expression constructs lack introns (**Sup. Figure 2.2.1**). Additional studies will be needed to uncover the origin of this product as well as investigate the mechanisms at play that ultimately lead to inherently lower transcript, intracellular, and secreted Q226H levels.

One limitation of our study is that it primarily utilized HEK293A cells. While these cells likely share most of the major protein synthesis, folding and degradation machinery as retinal cells that express F3 (i.e., RPE cells), and are an appropriate model for initial F3 variant screening, we acknowledge that more physiologically relevant model systems are currently accessible. Accordingly, follow-up studies will be focused on evaluating intriguing variants (e.g., L451F) in more relevant model systems, such as CRISPR-modified induced pluripotent stem cells (iPSCs) that have been differentiated into RPE cells or F3 variants knocked into mice to develop an in vivo model system for further analysis.

Overall, little is known about the molecular and cellular influences that regulate F3 secretion and function. Mapping and testing F3 mutations as we have performed, combined with comprehensive ocular phenotypic data, will provide more information regarding whether there are certain 'hot-spots' in F3 that are prone to secretion-compromising or pathogenic mutations. For example, the combination of analogous studies[179-182] have led to the determination that the olfactomedin (OLF) domain is a 'hot-spot' for many pathogenic mutations in myocilin (MYOC). Likewise, we noticed a trend that C-terminal mutations (i.e., mutations occurring after N249, as an approximate midpoint) were more prone to either secretion defects (e.g., R345W and L451F), or further destabilization (i.e., N249Q/Y397H). This approximate region of F3 (amino acids 259–493) has also been shown to bind to tissue

inhibitor of matrix metalloproteinase 3 (TIMP3)[183], a critical extracellular matrix regulatory component that is also associated with Sorsby's Fundus Dystrophy[184]. Failure of F3 to bind to TIMP3 or other known F3 interacting partners[185, 186] due to partial misfolding in its C-terminus may ultimately influence its fate in the cell and at the organismal level. Additionally, recent studies have indicated that the C-terminus of F3 may be the source of amyloid fibrils found in the veins of aged individuals[187], suggesting that this portion of the protein has a propensity for β-sheet formation and aggregation.

While little in-depth knowledge exists for patients with the L451F mutation, we do know that this mutation was identified in two separate unrelated heterozygous individuals, one with retinal dystrophy and the other with congenital nystagmus and otherwise poor ocular workup (information provided by Eurofins Clinical Diagnostics, personal communication). Given our observations of L451F F3 secretion and destabilization, combined with the identification in multiple individuals with eye disease, it is intriguing to speculate that L451F might be a disease modifier or actually trigger ocular disease.

The C-terminal F3 fragility hypothesis doesn't preclude the idea that N-terminal mutations couldn't be detrimental to F3 folding and function. In fact, we would predict that the recently identified C55R F3 mutation, located in the atypical calcium-binding EGF domain of F3 and associated with Marfanoid syndrome[135], could substantially effect F3 secretion and/or redox/disulfide state. Yet, it is important to mention that it is still unclear how the other F3 mutations such as R345W cause diseases such as ML—whether it is due to the escape of misfolded F3 from the cell which wreaks havoc in the extracellular matrix, possibly triggering complement activation[149], or whether it is due to accumulation of poorly

folded intracellular F3, or a combination of both of these possibilities. Ultimately, in the absence of multiple sets of reliable phenotypic patient data, future studies aimed at testing the effects of newly identified (e.g., L451F, Y397H) and rationally-designed (e.g., C338A) mutants in mice will be critical for developing a better understanding of the role of misfolded F3 and its relation to ocular diseases.

2.5 Methods

2.5.1 In silico screening of F3 mutations

F3 (*EFEMP1*) variants were identified using the ClinVar website (https://www.ncbi.nlm.nih.gov/clinvar/). The protein-level consequences of these alterations were then assessed by PROVEAN (http://provean.jcvi.org/index.php) and PolyPhen 2.0 (http://genetics.bwh.harvard.edu/pph2/). Allele frequency of the variation was determined by gnomAD (https://gnomad.broadinstitute.org/, V2.1.1, Ensembl gene ID: ENSG00000115380.14, region: 2.56093102–56151274). Clustal Omega (https://www.ebi.ac.uk/Tools/msa/clustalo/) was used to align UniProt sequences (https://www.uniprot.org/).

2.5.2 Plasmid generation

N-terminal FLAG-tagged (FT) F3 constructs were either generated from pcDNA FT WT F3 or pENTR1A FT WT F3 templates using the Q5 mutagenesis kit (New England Biolabs, Ipswich, MA, USA). pENTR1A constructs were then shuttled into the pcDNA DEST40 vector (Life Technologies, Carlsbad, CA, USA) or pLenti CMV Puro DEST (gift from Eric

Campeau and Paul Kaufman, Addgene plasmid # 17452) by an LR clonase II reaction (Life Technologies) to generate the final construct. The pcDNA FT WT F3 construct is shown in **Sup. Fig. 2.2.1**, and uses a preprotrypsin leader sequence followed by the FLAG peptide, and then the F3 sequence. The plasmid map was made using SnapGene 5.1.7 (GSL Biotech, San Diego, CA, USA). All F3 mutations and plasmids were verified by Sanger sequencing.

2.5.3 Cell culture and transfection

Human embryonic kidney cells (HEK293A, Life Technologies) were cultured at 37 °C with 5% CO_2 in Dulbecco's minimal essential medium (DMEM) supplemented with high glucose, (4.5 g/L, Corning, Corning, NY, USA), 10% fetal bovine serum (FBS, Omega Scientific, Tarzana, CA, USA) and 1% penicillin–streptomycin-glutamine (Gibco, Waltham, MA, USA). Cells were plated at a density of 100,000 cells/well in a 24 well plate and transfected the following day with 500 ng of midi-prepped endotoxin-free plasmid DNA (Qiagen, Germantown, MD, USA) using Lipofectamine 3000 (Life Technologies) as described previously[188]. Forty-eight hours after transfection, fresh serum-free media was added. Cells were harvested and media was collected 24 h later (72 h post transfection). Human immortalized retinal pigmented epithelial cells (ARPE-19, CRL-2302, American Type Culture Collection, Manassas, VA, USA) were cultured in DMEM/F12 media supplemented with 10% fetal bovine serum (FBS, Omega Scientific, Tarzana, CA, USA), HEPES (Corning) and penicillin/streptomycin and glutamine (PSQ, Gibco, Germantown, MD, USA). To generate stably expressing F3 cell lines, ARPE-19 cells were infected with VSV-G-pseudotyped lentivirus packaged with the pLenti CMV Puro vector containing FT F3

variants. Stable populations were selected using puromycin. Cells were plated at a density of 150,000 cells/well in a 12 well plate, changed to serum free media after 24 h, and harvested 24 h later (48 h post plating).

2.5.4 Western blotting

Cells were washed with Hanks buffered salt solution (HBSS, Sigma-Aldrich, St. Louis, MO, USA), then lysed with radioimmunoprecipitation assay (RIPA) buffer (Santa Cruz, Dallas, TX, USA) supplemented with Halt protease inhibitor (Pierce, Rockford, IL, USA) and benzonase (Millipore Sigma, St. Louis, MO, USA) for 3–5 min at room temperature, and then spun at max speed (14,800 rpm) at 4 °C for 10 min. The soluble supernatant was collected and protein concentration was quantified via bicinchoninic assay (BCA) (Pierce). Twenty to thirty μg of soluble supernatant or 20 μL of conditioned media was run on a 4–20% Tris-Gly SDS-PAGE gel (Life Technologies) and transferred onto a nitrocellulose membrane using an iBlot2 device (Life Technologies). After probing for total transferred protein using Ponceau S (Sigma-Aldrich), membranes were blocked overnight in Odyssey Blocking Buffer (LICOR, Lincoln, NE, USA). Membranes were probed with rabbit anti-FLAG (1:5000; Thermo Fisher Scientific, Waltham, MA, USA, cat# PA1-984B) or mouse anti-β-actin (1:1000; Sigma-Aldrich, cat# A1978). All Western blot imaging was performed on an Odyssey CLx (LI-COR) and band quantification was performed using Image Studio software (LI-COR).

2.5.5 Quantitative PCR

Transfected HEK293A or stably expressed F3 ARPE-19 cells were trypsinized (0.25% Trypsin EDTA, Gibco), quenched with full DMEM or DMEM/F12 media, respectively, and centrifuged at max speed (3,000 rpm) at 4 °C for 10 min. Cell pellets were washed with HBSS, centrifuged again, then RNA extraction from cell pellets was performed using the Aurum Total RNA Mini Kit (Bio-Rad). 315–400 ng RNA (HEK293A) or 10–50 ng RNA (ARPE-19) was reverse transcribed using qScript cDNA SuperMix (Quanta Bioscience, Beverly, MA, USA) and the cDNA was diluted 5X in DNase/RNase-free water. cDNA was amplified with TaqMan Fast Advanced Master Mix (Thermo Fisher) and transcripts were detected using h*HSPA5* (cat# hs00607129_gH), h*DNAJB9* (cat# hs01052402_m1), h*ASNS* (cat# hs04186194_m1), and h*ACTB* (cat# hs01060665_g1) TaqMan probe sets. For quantifying F3 (*EFEMP1*) mRNA levels, cDNA was amplified with PowerUp SYBR Green Master Mix (Thermo Fisher). Transcripts were amplified using h*EFEMP1* forward (5′ GGGGATCCTTTGCATGTCAG) and reverse (5′ TGAAACCCAGGACTGCACTG) primers, using *RPLP2* forward (5′ CGTCGCCTCCTACCTGCT) and reverse (5′ CCATTCAGCTCACTGATAACCTTG) primers as a housekeeping gene. Amplification for both TaqMan assays and SYBR Green was performed on a QuantStudio 6 and visualized and quantified using the associated software (Thermo Fisher).

2.5.6 Statistical analysis

To determine statistical significance, samples were compared using a one-sample *t* test using Excel against a hypothetical value of 1 (i.e., unchanged compared to the control). Significance was set at $*p < 0.05$, $**p < 0.01$, and $***p < 0.001$.

Chapter 2 Figures

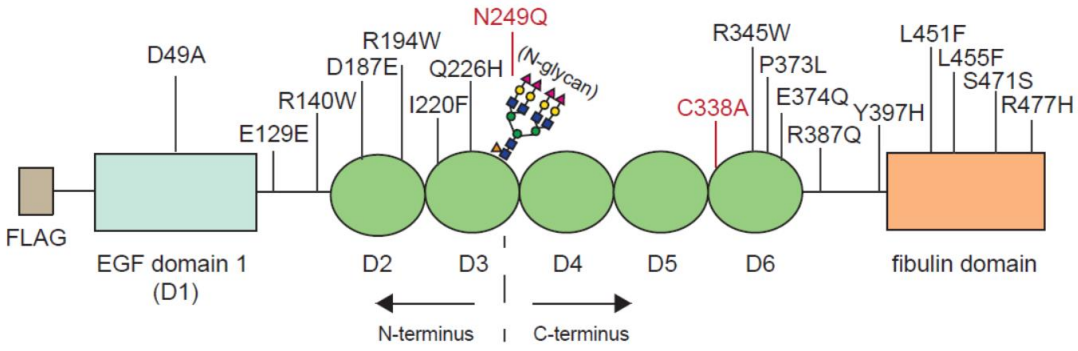

Figure 2.1: Schematic of clinically-identified F3 variants. Genetically-engineered variants are highlighted in red.

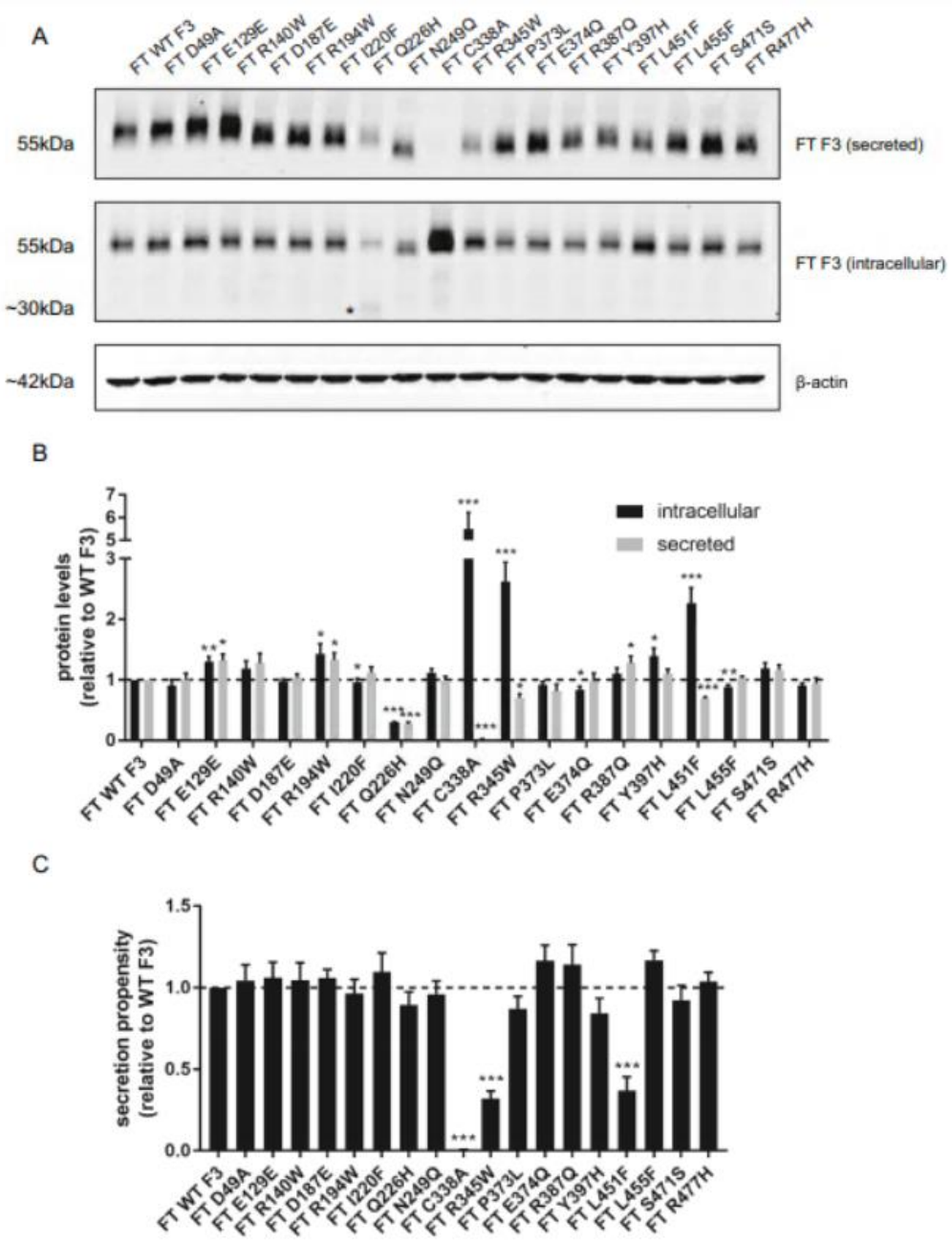

Figure 2.2: Secretion of clinically-identified F3 variants. (A) Western blot of secreted and intracellular levels of F3 variants in HEK293A cells. Asterisk indicates truncated intracellular Q226H band. (B) Quantification of secreted and intracellular levels for each variant. (C) Secretion propensities of F3 variants shown in (A), n≥6, mean ± SEM, (*p<0.05, **p<0.01, ***p<0.001, one sample *t* test vs. a hypothetical value of 1 [i.e., unchanged]).

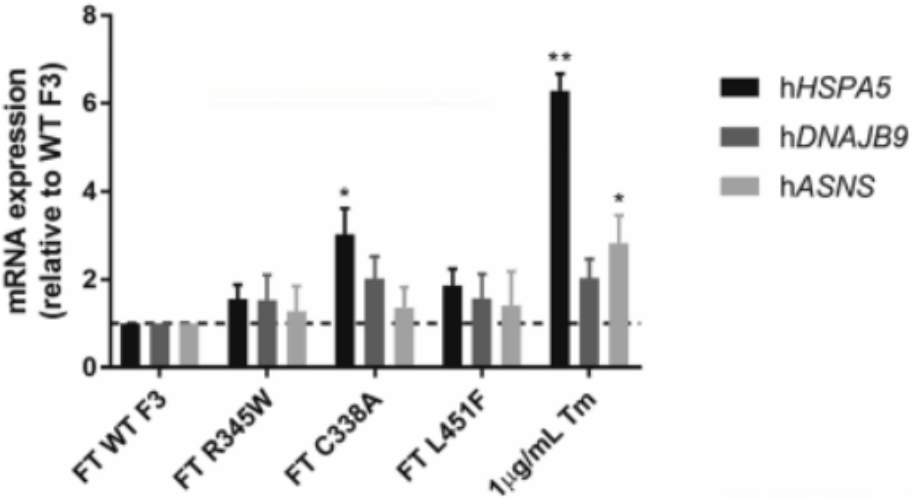

Figure 2.3: L451F F3 does not elicit an ER stress response. qPCR analysis of hHSPA5, hDNAJB9, and hASNS transcript levels with TaqMan probes in WT F3, R345W, C338A, L451F–expressing HEK293A cells and cells treated with 1 μg/mL tunicamycin (Tm), 24 h. n=3, mean ± SEM (*p<0.05, **p<0.01, ***p<0.001, one sample *t* test vs. a hypothetical value of 1 [i.e., unchanged]).

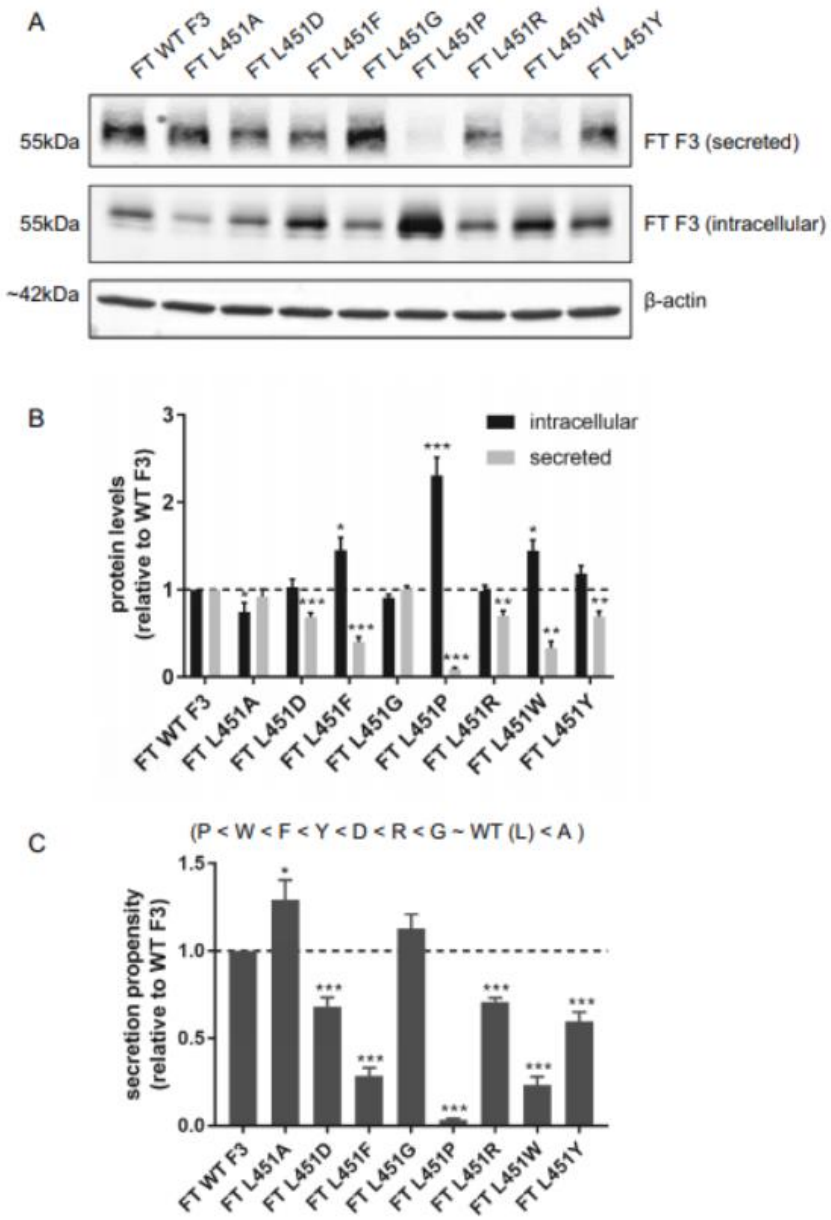

Figure 2.4: Substitution of leucine at position 451 with select residues. (A) Western blot of secreted and intracellular levels of L451F substitution variants. (B) Quantification of secreted and intracellular levels. (C) Secretion propensities L451F substitution variants in (A), $n \geq 4$, mean ± SEM, (*p<0.05, **p<0.01, ***p<0.001, one sample *t* test vs. a hypothetical value of 1 [i.e., unchanged]).

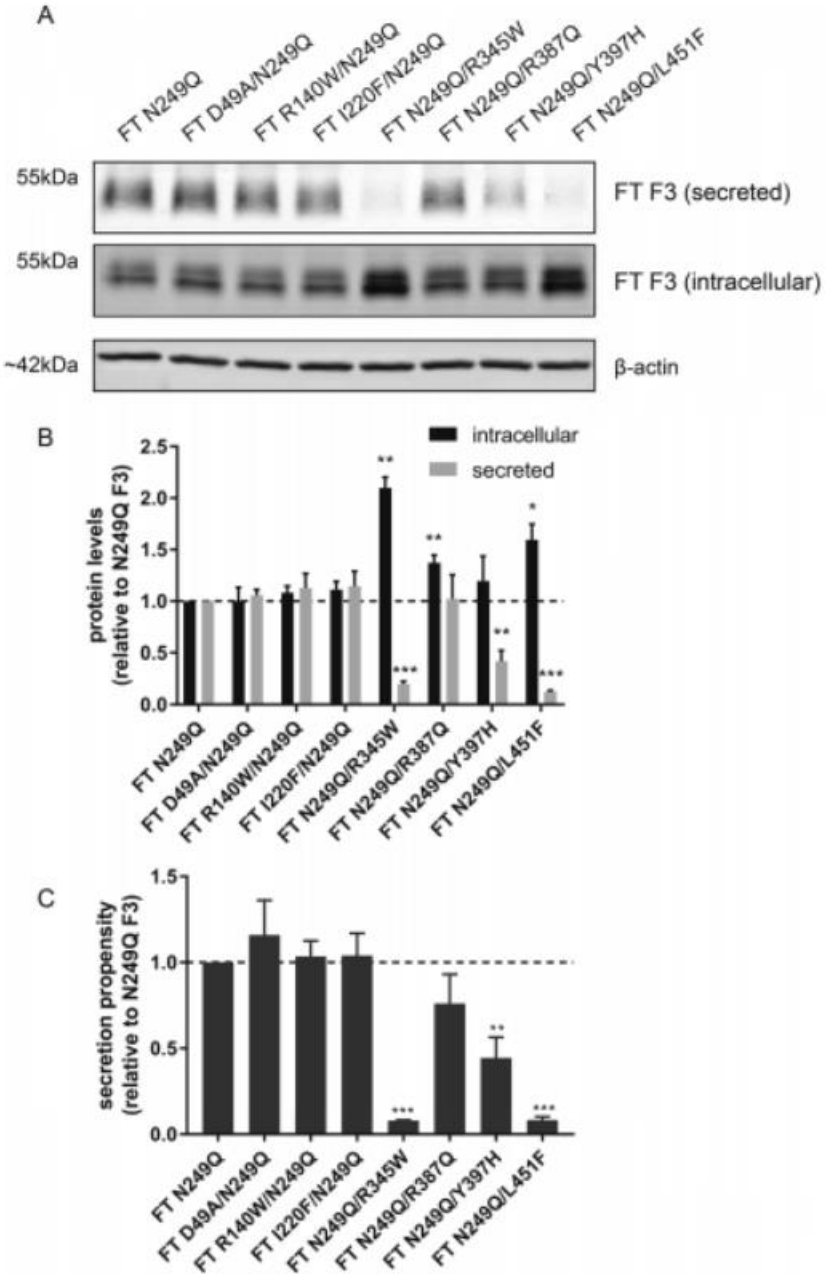

Figure 2.5: Secretion of F3 variants upon genetic ablation of the N-linked glycan. (A) Western blot of secreted and intracellular levels of N249Q F3 variants. (B) Quantification of secreted and intracellular levels. (C) Secretion propensities N249Q F3 variants in (A), $n \geq 4$, mean ± SEM, (*$p<0.05$, **$p<0.01$, ***$p<0.001$, one sample *t* test vs. a hypothetical value of 1 [i.e., unchanged]).

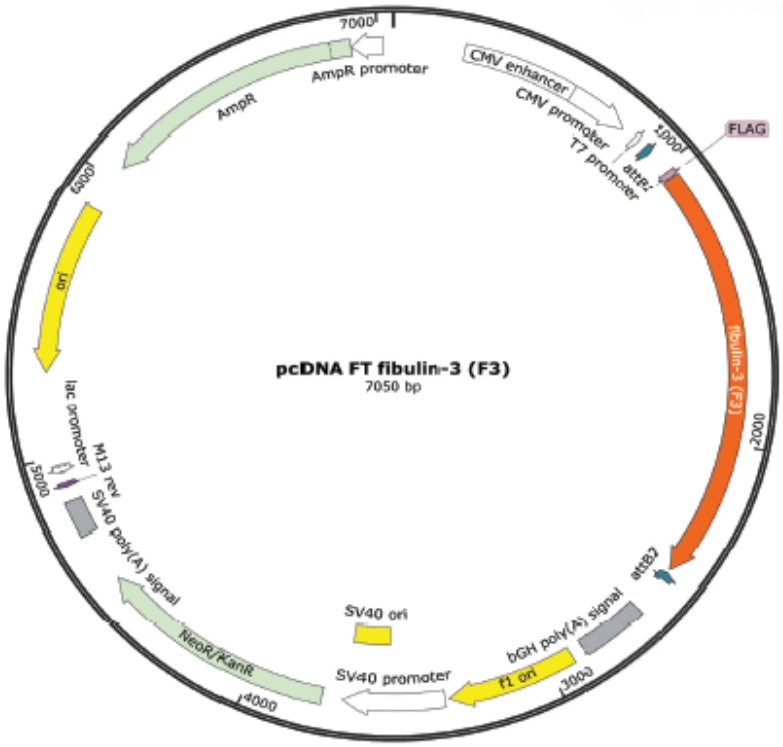

Supplemental Figure 2.2.1: pcDNA FT F3 vector for F3 variants. Plasmid map was generated using SnapGene version 5.1.7, https://www.snapgene.com/.

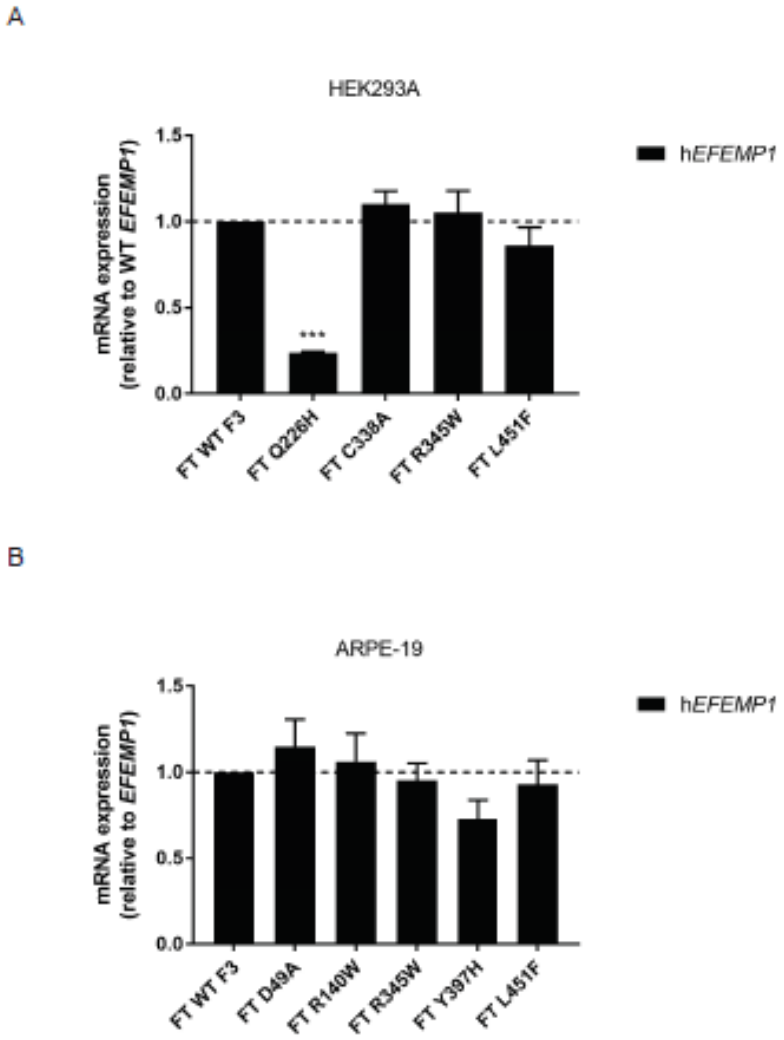

Supplemental Figure 2.2.2: F3 (*EFEMP1*) transcript levels of mutants in (A) HEK293A and (B) ARPE-19 cells. (A) qPCR analysis of h*EFEMP1* transcript levels with SYBR Green EFEMP1 primers in WT F3, R345W, C338A, and L451F-expressing cells. (B) qPCR analysis of h*EFEMP1* transcript levels with SYBR Green EFEMP1 primers in WT F3, D49A, R140W, R345W, Y397H, and L451F-expressing cells. n = 3, mean ± SEM (one sample t-test vs. hypothetical value of 1 [i.e., unchanged]). n = 5, mean ± SEM (*$p<0.05$, **$p<0.01$, ***$p<0.001$, one sample *t* test vs. a hypothetical value of 1 [i.e., unchanged]).

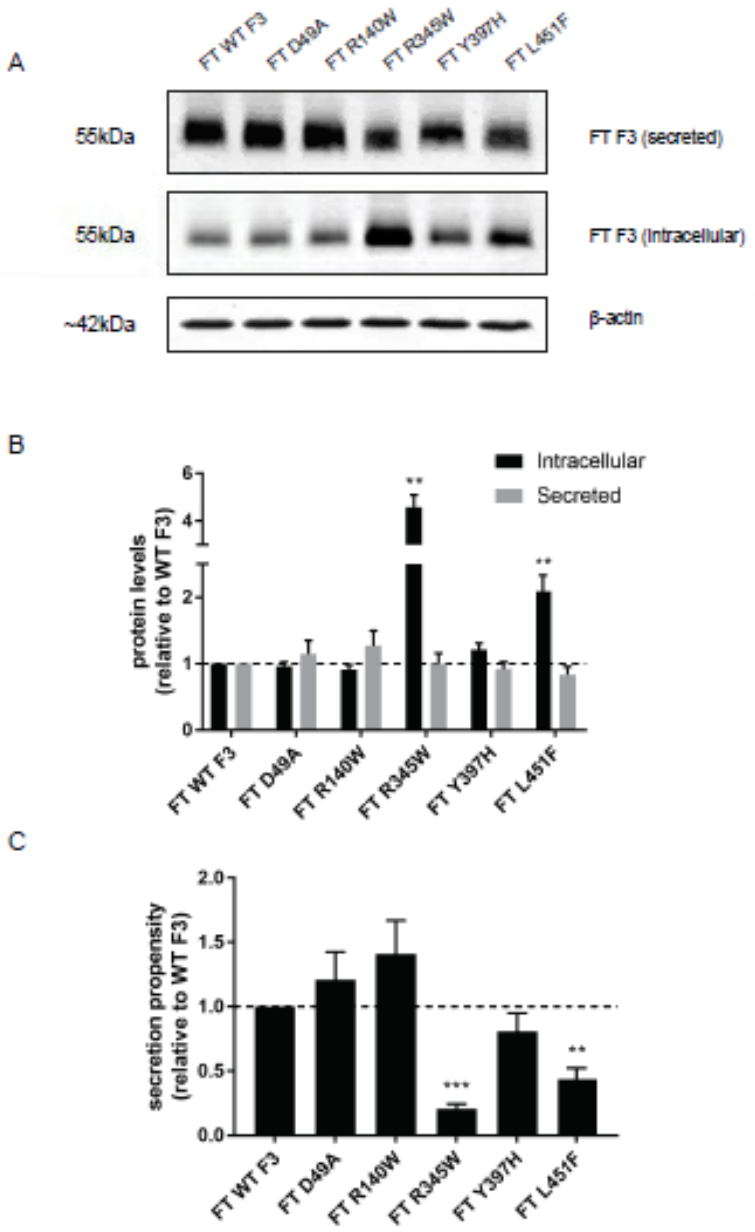

Supplemental Figure 2.2.3: Secretion propensities of F3 in ARPE-19 cells. (A) Western blot of secreted and intracellular levels of F3 variants stably expressed in ARPE-19 cells. (B) Secretion and intracellular levels of F3 variants in ARPE-19 cells and (C) their corresponding secretion propensities, n = 6, mean ± SEM (*p<0.05, **p<0.01, ***p<0.001, one sample *t* test vs. a hypothetical value of 1 [i.e., unchanged]).

Supplemental Figure 2.2.4: Protein alignment near the L451 residue of F3. (A) Clustal Omega alignment of F3 proteins across the indicated species. (B) Clustal Omega alignment of different fibulin proteins at the L451 position.

F3 variant	ClinVar: clinical significance	PROVEAN: impact prediction	PolyPhen 2.0: functional effect prediction	gnomAD: allele frequency
D49A	Conflicting interpretations of pathogenicity	0.384; neutral	0.002; benign	1.05×10^{-3}
E129E	Benign	0.000; neutral	N.A	2.73×10^{-2}
R140W	Uncertain significance	−1.580; neutral	0.997; probably damaging	7.95×10^{-6}
D187E	Uncertain significance	−0.728 neutral	0.389; benign	3.98×10^{-6}
R194W	Uncertain significance	−3.802; deleterious	1.000; probably damaging	1.99×10^{-5}
I220F	N.D	0.904; neutral	0.000; benign	5.97×10^{-5}
Q226H	Uncertain significance	2.873; neutral	0.000; benign	N.D
N249Q*	N.A	−3.965; deleterious	1.000; probably damaging	N.A
C338A*	N.A	−8.812; deleterious	0.999; probably damaging	N.A
R345W	Pathogenic	−3.309; deleterious	1.000; probably damaging	N.D
P373L	Uncertain significance	−1.378; neutral	0.004; benign	5.67×10^{-5}
E374Q	Uncertain significance	−2.287; neutral	0.995; probably damaging	3.98×10^{-6}
R387Q	Likely benign	−2.072; neutral	0.219; benign	1.14×10^{-3}
Y397H	Likely pathogenic	−3.276; deleterious	1.000; probably damaging	N.D
L451F	Uncertain significance	−3.577; deleterious	0.996; probably damaging	1.14×10^{-5}
L455F	Uncertain significance	−2.539; deleterious	1.000; probably damaging	6.36×10^{-5}
S471S	Uncertain significance	0.000; neutral	N.A	1.98×10^{-4}
R477H	Uncertain significance	−3.619; deleterious	1.000; probably damaging	1.41×10^{-5}

Table 2.1.1. Clinical significance, predicted stability scores, and allele frequencies of F3 variants. *Indicates rationally-designed variant.

CHAPTER THREE
CHARACTERIZING F3 VARIANTS IN THE MURINE RETINA

3.1 Introduction

AMD is the most common cause of irreversible vision loss in the elderly population in developed countries[80]. The lack of therapies for dry AMD due to its clinical heterogeneity as well as number of environmental and genetic risk factors poses a current threat for patients' vision and quality of life. In order to understand the disease pathogenesis of dry AMD, ML has been used as a surrogate disease because of its similar clinical and phenotypic AMD-like features, as well as its well-defined genetic cause due to the R345W mutation in the F3 protein[111]. As dry AMD and ML progresses, one commonly observed histopathological marker is the buildup of extracellular material known as basal laminar deposits (BLamDs) located between the RPE and RPE-basal lamina[189-191]. In humans, BLamDs are typically a precursor for eventual drusen formation, sometimes coalescing to form soft drusen[192]. BLamDs, which are the canonical pathogenic feature observed in the ML mouse model at advanced age (mice do not appear to form drusen as humans do[152, 153]), are comprised of complement regulatory proteins[149, 193] and ECM proteins including fibrous long-spacing collagen[194] and F3[195].

F3 is a 55 kDa ECM glycoprotein that is highly expressly in and secreted (apically and basally) from RPE cells in the eye. Interestingly, both WT F3 and the R345W F3 mutant have been found surrounding drusen in AMD and ML human donor eyes[113], respectively, and F3 accumulates within BLamDs in R345W F3 knock-in mice[153]. BLamDs are typically identified as the earliest observable change in the R345W F3 mouse retina by electron

microscopy. In contrast, F3 knockout mice do not develop BLamDs and are protected from environmental stressors that induce BLamDs (i.e., cigarette smoke, and photochemical injury), signifying an important role of F3 in deposit formation[196]. While knock-in mouse models of F3 have helped to increase our current understanding of its involvement in macular degeneration, other *in vivo* modeling approaches, such as the use of adeno-associated viruses (AAVs), to flexibly express mutant proteins of interest, have emerged as a unique tool for further studying disease mechanisms and testing the potential pathogenicity of select variants[197].

AAVs are small (25 nm) nonenveloped, single-stranded DNA viruses with a 4.8 kilobase (kb) genome[198-200]. Recombinant AAV (rAAV) vectors contain two open reading frames, the *rep* and *cap* genes[200]. *Rep* encodes the Rep78, Rep68, Rep52, and Rep40 proteins that are essential for viral life cycle and *cap* encodes for three structural proteins (VP1, VP2, and VP3) that form the viral capsid at a 1:1:10 ratio[200, 201]. *Rep* and *cap* are flanked by two 145 nucleotide long inverted terminal repeats (ITRs) that serve as T-shaped hairpin packaging signals to allow for complementary DNA strand synthesis[202]. rAAV vectors are at the forefront of gene therapy for the treatment of a variety of human diseases, including retinal dystrophies[202, 203]. Most notably, inherited retinal disorders (IRDs), such as Leber's congenital amaurosis (LCA) caused by mutations in the RPE65 protein, have been effectively reversed after a single subretinal (the space between the RPE and photoreceptors) injection of the rAAV2-RPE65 virus, resulting in visual improvement[204-206].

In addition to its use in the clinic, rAAVs have been valuable tools for generating *in vivo* retina mouse models[207]. Moreover, research performed in the Hulleman Laboratory has found that expression levels of F3 in the mouse RPE are significantly lower than those observed in higher order species (porcine), non-human primates (olive baboons), and humans (Dr. Steffi Daniel, Ph.D., personal communication). Thus, we propose that rAAV can be used to quickly evaluate the potential in vivo effects of select F3 mutants while also restoring F3 expression in the RPE to those comparable to what is observed in humans.

Recently, we characterized a novel, clinically-identified L451F F3 mutation *in vitro* and found that its secretion and molecular properties were similar to that of the R345W F3 mutation. In this study, we utilize rAAV technology encoding for human WT, R345W and L451F F3 and examine the expression and potential pathological effects (i.e. BLamDs, RPE abnormalities) of the L451F mutant after expression in the murine RPE. We show that 1 month post-injection, mice display rather wide expression of our F3 rAAVs, primarily being expressed in the photoreceptors and RPE. We next evaluated the protein expression of WT F3 and mutants as well as their ability to induce UPR activation (IRE1, ATF6, and PERK pathways) in the retina/RPE. Lastly, we determined the local distribution of our F3 rAAVs in the mouse retina, as well as whether this led to an immune response.

3.2 Results

3.2.1 Evaluation of F3 AAV expression in the retina

To generate our F3 rAAV mouse model system, we utilized an rAAV plasmid system that includes a rAAV2[MAX(QuadYF, 7m8)] rep/cap vector and a separate F3 transgene plasmid

driven by a hybrid chicken beta actin promoter (cBH). Located after the C-terminus of F3 was an internal ribosomal entry site (IRES) followed by GFP (**Sup. Fig. 3.3.1**). Upon production and purification of 3xFLAG-tagged WT, R345W, and L451F F3 rAAV, as well as a control, CMV-driven GFP rAAV, we verified the purity of the preparation by analyzing the capsid subunits VP1, VP2, and VP3 by silver staining (**Sup. Fig. 3.3.2**). Previously, the rAAV2[MAX] capsid mutant vector was shown to efficiently transduce photoreceptors following intravitreal delivery in 4–6-week-old mice[208], but this method has not been shown to efficiently introduce transgenes into the RPE via the same route of administration. To appropriately introduce our F3 rAAVs into the mouse retina, we performed subretinal injections in order to directly target F3 expression to the RPE. Three weeks post-subretinal injection with CMV GFP rAAV and WT, R345W, and L451F F3 rAAV, we verified rAAV expression by fundoscopic analysis (**Fig. 3.1**). As expected, we did not detect any GFP expression in uninjected control eyes of adult mice (**Fig. 3.1A,F**). In contrast, CMV GFP rAAV conferred high levels of GFP expression that was detectable even in brightfield images (**Fig 3.1 B,G**). Upon increasing the fundus GFP fluorescence intensity, we were able to detect IRES-expressed GFP for WT (**Fig 3.1H**), R345W (**Fig. 3.1I**) and L451F (**Fig. 3.1J**) F3 rAAVs in the mouse retina. We also observed that our F3 rAAVs resulted in ~25-40% coverage of GFP expression in the retina, whereas CMV GFP rAAV resulted in pan-retinal expression, which is consistent with a previous report[208]. These results demonstrate our ability to successfully transduce the retina with F3 rAAV following subretinal injection.

3.2.2 Retinal assessment of F3 rAAV mice

One of the most common challenges of performing subretinal injections is the high risk of injection-induced retinal detachment and/or damage to the retina[209, 210]. To verify that the mouse retinal integrity was not compromised and to observe if there are any changes in the retinal layers, or the presence of observable sub-RPE deposits (i.e., large BLamDs or otherwise amorphous deposits), we utilized spectral domain optical coherence tomography (SD-OCT). We did not detect any abnormal features or changes in retinal thickness in the IR reflectance images of uninjected eyes or F3 rAAV-injected eyes at 1 month post-injection (**Fig. 3.2A-H**). Assessment of the retinal layers revealed no gross anatomical differences in RPE of F3 rAAV-injected mice and we did not detect the presence of sub-RPE deposits. These results suggest that retinal integrity remains intact following injection with F3 rAAV, but these observations did not quantitatively provide F3 expression levels, nor did they precisely confirm its exact expression pattern in the mouse eye.

3.2.3 F3 is overexpressed, but does not activate the unfolded protein response

Because our rAAVs encode for human F3, we next determined F3 (*EFEMP1*) transcript level expression in the retina. We isolated posterior eyecups (which includes the neural retina and RPE/choroid) of mice 1 month post-injection and performed qPCR analysis (**Fig. 3.3A**). As expected, we found that *EFEMP1* levels of WT, R345W, and L451F were highly expressed in the mouse retina compared to Hank's balanced salt solution supplemented with 0.014% Tween-20 (HBSS-T, vehicle) injected mice (**Fig. 3.3B**),

which express endogenous mouse F3 only. Human *EFEMP1* transcript levels were also comparable between WT F3 and mutants, suggesting little variability in F3 expression between each rAAV. These results demonstrate that our F3 rAAVs are able to drive high expression of F3 in the mouse retina.

Previously, Roybal and colleagues demonstrated that high levels of F3 expression (driven by adenovirus, not rAAV) in cultured RPE cells was able to trigger activation of the UPR, and that this activation was significantly more pronounced in cells expressing the R345W mutant[169]. However, Fu *et. al*. found that R345W knock-in mice do not elicit an ER stress response in the retina (as indicated by no change in GRP78 protein levels)[152], and our group has not detected UPR activation when the levels of F3 are appropriately regulated[174, 211].

Nonetheless, to determine whether ER stress is activated in the retina upon high expression of F3 due to rAAV introduction, we performed qPCR to gauge transcript levels of the three major arms of the UPR (m*Asns* [PERK activation], m*Dnajb9* [IRE1 activation], and m*Hspa5* [ATF6 activation]) (**Fig 3.3B**). We observed no significant induction of the UPR for WT, R345W, and L451F, suggesting that the levels of F3 expression mediated by our rAAVs does not lead to overt ER stress in the retina or RPE, and we would speculate that UPR activation does not significantly contribute to ML disease-related observations.

3.2.4 F3 expression in the mouse RPE

Next, we determined whether the F3 rAAVs primarily transduce the mouse RPE. To do this, we isolated the mouse RPE layer by performing RPE flatmounts 1 month post-injection (**Sup. Fig. 3.3.5**) followed by immunofluorescence (**Fig. 3.4**). We first stained with zona-occludens-1 (ZO-1) (**Fig. 3.4C,H,M,R**), a well-known RPE tight junction marker[212, 213], and FLAG for the visualization of each F3 rAAV (**Fig 3.4G,L,Q**). We found that GFP expression from the IRES GFP element of the F3 rAAVs was mostly apparent in the cytoplasm and nuclei, and in some cases, GFP signal was detected at the RPE junctions (**Fig 3.4F,K,P**). We also found co-expression of GFP and FLAG in some, but not all RPE cells (**Fig 3.4J,O,T**), demonstrating that human F3 from our rAAVs are indeed expressed in the RPE. A separate immunofluorescence study was also used to confirm GFP and FLAG (all F3 variants used *in vivo* were 3xFLAG-tagged) co-expression in the RPE (**Sup. Fig. 3.3.6**). We would like to note that detection of co-expression of GFP and FLAG (F3) is challenging, especially since F3 is a secreted protein that would not normally accumulate intracellularly, unless partially or fully unfolded.

3.2.5 F3 rAAV localization and distribution in the mouse retina

Next, we wanted to uncover whether our F3 rAAV transduction was specific to the RPE only, or if it was distributed across the entire retina. Retinal cryosections of mouse eyes 1 month post-injection revealed that, based on IRES GFP localization, WT, R345W, and L451F rAAVs also transduced photoreceptors (**Fig 3.5G,L,Q**), and in some cases, the outer nuclear layer (**Fig 3.5. G,L**), in addition to the RPE. This is likely due to expression of our

F3 rAAV's being driven under the ubiquitous promoter, cBH. To evaluate whether introduction of our F3 rAAVs or mechanical injury (e.g., inducing retinal detachment via injection) induced a pronounced inflammatory response in the retina, we stained for the glial fibrillary acidic protein (GFAP) (**Fig. 3.5C,H,M,R**). GFAP, which is expressed in astrocytes and Muller glia, is a well-known marker for stress in central nervous system (CNS), and its increased immunoreactivity in the retina is usually viewed as an index of gliosis (neural damage)[214-216]. Compared to our HBSS-T control, we found that in our F3 rAAV-injected mice, GFAP was only localized to the ganglion cell layer, where it is normally distributed[217] (**Fig. 3.5 H,M,R**). Additionally, we did not detect GFAP in the inner or outer retina, suggesting that our F3 rAAVs do not elicit an inflammatory response in injected adult mice. It is worth mentioning that although retinal detachment is apparent in some of the brightfield images, this is merely due to how the samples were processed for cryosectioning. We previously confirmed with SD-OCT analysis that the retinal integrity for these mice were not compromised.

3.3 Discussion

There are currently two R345W knock-in mouse models of ML, pioneered by the Mamorstein and Pierce groups, that demonstrated BLamD/sub-RPE deposit formation and progression regardless of gene dosage (heterozygous vs. homozygous)[152, 153]. One important aspect of their studies is the length of time that BLamDs take to form, with deposits becoming noticeable at 12 months in both mouse models[152, 153]. Thus, a more attractive

alternative would be to design a rapid, yet robust F3 mutant animal model where BLamDs develop in a shorter timeframe. rAAVs have several advantages over traditional knock-in approaches, including i) being an economical alternative[218], ii) their use in generating animal models with accelerated disease time course, iii) controlling mutant protein expression with the appropriate serotype, promoter and titer, and iv) monitoring graded levels (early to late stages) of pathological phenotypes. In this study, we utilized rAAV to overexpress human F3 in the mouse retina since recent data shows that endogenous mouse F3 in RPE/choroid is expressed at low levels (data not shown). We wanted to drive F3 expression to more closely match that of endogenous human F3 in the RPE/choroid in order to accurately reflect pathology upon introduction of the R345W and L451F mutants.

The vector serotype (AAV 2/2) and rep-cap plasmid (pACG2-MAX-QuadYF, 7m8) used in this study was previously shown to transduce photoreceptors upon intravitreal injection in the mouse retina[208]. We demonstrated that subretinally injecting this rAAV plasmid system, the F3 transgenes included, were able to transduce the mouse RPE and lead to sufficient F3 overexpression. The same was also true for the CMV GFP rAAV plasmid. We selected the strong and constitutively active cBH promoter to initially assess and drive overexpression of the F3 protein. While CMV is a strong promoter, it is also infamous for being prone to silencing by DNA methylation and histone deacetylation over time in specific cell types and tissues after transduction[219, 220]. Thus, we wanted to avoid this possibility in the RPE. One limitation of our study is that we do not currently have an appropriate control, such

as cBH IRES GFP rAAV, which would allow for a more definitive comparison of IRES GFP expression via fundus, SD-OCT and qPCR. Another limitation is that we are currently unable to gauge how much of human F3 is expressed relative to endogenous F3 within the same mouse retinas, which would ultimately allow for us to determine the extent of human F3 overexpression relative to levels in the mouse.

One of our goals was to generate an F3 rAAV mouse model that rapidly displays BLamDs in a manner of a few months. Similarly, Dinculescu *et al*. utilized rAAV to show that a mutant in the C1QTNF5 protein mimics pathological features (i.e. RPE thinning and cell loss, and basal RPE deposits) of late-onset retinal degeneration in as little as 4 months[197]. Thus, we are optimistic that our approach with F3 rAAV would yield a similar timeframe as well as pathological features to ML for R345W F3. Previously, we found that the L451F F3 mutant is similar in secretion, degree of folding and molecular properties to that of R345W. However, L451F is still unique in that it was found in two heterozygous individuals and is not associated with a specific disease like R345W in ML. It would be interesting to observe if L451F rAAV-injected mice develop BLamD deposits similar to R345W. For instance, if L451F rAAV-injected mice develop BLamDs, one important study would be determine the rate at which the deposits form compared to R345W F3 rAAV BLamDs and compare their components. It is also is possible that BLamDs may not be present in the L451F rAAV-injected mice or that there are distinct changes at the RPE-BrM or other retinal layers that are specific to L451F. Overall, our study successfully demonstrates the use of rAAV for generating an F3 retinal mouse model and which will allow for future characterization of

additional disease-associated mutations in F3, but requires further in-depth electron microscopy of potential ultrastructure changes to the RPE/BrM.

3.4 Methods

3.4.1 rAAV production

The pAAV cBH 3X FT WT F3 IRES eGFP rAAV vector was produced by VectorBuilder and the R345W and L451F rAAV vectors were generated via restriction digest and ligation. AAVpro293T cells (Clontech) were triple transfected in T175 flasks with an rAAV helper plasmid (pHelper), an AAV2/2-based rep-cap plasmid: pACG2-MAX-QuadYF, 7m8, also called AAV2/2 MAX (provided by Dr. Daniel Lipinski) and transgenes: pAAV cBH 3X FT WT F3 IRES eGFP (Vector Builder), pAAV cBH 3X FT R345W F3 IRES eGFP, and pAAV cBH 3X FT L451F F3 IRES eGFP (**Sup. Fig. 3.3.1**). Plasmids were transfected in equimolar ratios (1:1:1) along with 1 μg/μl polyethylenimine (PEI) in high-glucose DMEM and 24 h post-transfection the media was changed to high-glucose DMEM supplemented with 2% FBS and 1% penicillin-streptomycin-glutamine (Gibco, Waltham, MA, USA). Seventy-two hours post media change, cells and media were collected followed by the addition of chloroform and vortexed for 5 min. 5M NaCl was added to the aqueous phase, vortexed briefly, and centrifuged at 4,000 x g for 5 min at 4^{o}C. After collecting the supernatant, polyethylene glycol (PEG) 8000 (50% w/v) was added, the samples were vortexed briefly, and then incubated on ice for 1 h. Samples were centrifuged for 30 min at 3000 × g at 4°C, the supernatant discarded, and the pellets were dried at RT for up to 15 min by inverting the

tube. The pellets were then resuspended in 50mM HEPES buffer (pH 8.0), vortexed for 5 min at RT, and incubated at 37^{o}C for 30 min with the addition of 1 M $MgCl_2$ and 1μL benzonase. Samples were then loaded onto an iodixanol gradient and spun in a T170 rotor at 63,000 rpm for 90 min at 4^{o}C. Virus was collected by puncturing the 40% iodixanol layer with an 18G needle and ten drops were collected per tube. The virus fractions were transferred to a 100K 0.5 ml Amicon filter, spun twice at 14,000 rpm for 6 min followed by buffer exchange with HBSS-T and spun again for 6 and 8 min, respectively. The virus was eluted by inverting the filters into a new collection tube, spun at 1,000 x g for 2 min (final volume is ~20μL). Viral titers for determined by a Quant-iT PicoGreen dsDNA kit (Thermo Fisher Scientific) and 3μL of purified rAAV was run on a 4–20% Tris-Gly SDS-PAGE gel (Life Technologies) followed by visualization of capsid subunits via silver staining (**Sup. Fig. 3.3.2**).

3.4.2 Subretinal Injections

Animal experiments were approved by the Institutional Animal Care and Use Committee (IACUC) of UT Southwestern Medical Center. Two month old C57BL/6 mice were anesthetized with an intraperitoneal injection of ketamine/xylazine cocktail (120/16 mg/kg). Eyes were temporarily proptosed and an incision was made immediately below the limbus using a 23 G needle at an angle to avoid touching the lens. Subretinal delivery of F3 rAAV was performed by inserting a 33G ½ blunt needle connected to an rAAV-filled Hamilton syringe in the incision at a 45 degree angle (**Supp Fig. 3.3.3**). The needle was then pushed slowly across the eye, careful not to hit the lens, until resistance was felt, indicating that the

needle reached the retina. A half microliter of rAAV at a titer of 1 x 10^{11} viral genomes/mL (10^{8} vg/eye) was injected over the course of 30 seconds and afterward the needle was slowly removed over the course of 30 seconds from the mouse eye. Each mouse received bilateral injections of either F3 rAAV, GFP rAAV or HBSS-T) injections. After injections, bacitracin zinc and polymyxin B sulfate ointment were applied to both eyes.

3.4.3 Fundoscopy and SD-OCT

One month post-injection, mice were anesthetized with an intraperitoneal injection of ketamine/xylazine cocktail (100/10 mg/kg) followed by pupillary dilation with Tropicamide Ophthalmic Solution 0.5%. GenTeal eye gel was applied to prevent dry cornea and fundus images were taken using a Phoenix Micron Retinal Imaging Microscope (Phoenix Technology Group). SD-OCT images were acquired using a Heidelberg Spectralis HRA + OCT system (Heidelberg Engineering, Heidelberg, Germany). For retinal imaging, horizontal scans were obtained for every eye with the optic nerve head at the center. SD-OCT scans were acquired in automatic real-time (ART) mode, averaging 9 frames per image. Each volume covered 30°×30° and consisted of 31 horizontal and 6 radial B-scans (768A-scans each), 240μm apart.

3.4.4 Immunostaining

Eyes were harvested and fixed in 4% paraformaldehyde (PFA) for 2 h at room temperature (RT). For flatmounts, after fixation, eyes were incubated in 1X phosphate-buffered saline (PBS). Under a light microscope, the anterior segment and lens were removed and the RPE was dissected from the neural retina and placed in a 48 well plate containing 1X PBS.

Tissues were washed with 1X PBS, incubated with 0.1% Triton X-100/1X PBS, and then blocked in 10% goat serum in 0.1% Triton X-100/1X PBS for 2 h at RT. Tissues were then incubated in primary antibodies (anti-mouse FLAG M2 (1:200) Sigma Aldrich cat# F1804, anti-rabbit ZO-1 (1:500) Invitrogen cat# 40-2200) made in blocking solution overnight at 4^{o}C. Twenty-four hours post primary antibody incubation, tissues were washed in 1X PBS and incubated with secondary antibodies (Alexa Fluor 633 goat anti-mouse (1:1000) and Alexa Fluor 546 goat anti-rabbit (1:100) Invitrogen) overnight at 4^{o}C. The following day, samples were washed with 1X PBS, incubated with DAPI for 20 mins at RT, washed again with 1X PBS. Approximately 12-16 radial cuts were made to flatten the RPE followed by mounting with antifade diamond mounting media onto glass microscope slides. Images were acquired using a 63X oil objective on a Leica SP8 confocal microscope (Buffalo Grove, IL)

For cryosections, after fixation, eyes were incubated with 10% sucrose in 1X PBS for 24 h at 4°C followed by 18% sucrose in 1X PBS for an additional 24 h at 4°C. The following day, eyes are embedded in Optimum Cutting Temperature media and placed at -80 ^{o}C to solidify. Twelve micron thick cryosections were dried overnight at RT, then placed on a slide warmer set at 60 ^{o}C for 30 min and cooled for 10 min at RT. Sections were washed with 1X PBS, incubated with 0.1% Triton X-100/1X PBS, and blocked in 10% goat serum in 0.1% Triton X-100/1X PBS for 2 h in a black slide holder tray. Sections were incubated in primary antibodies (mouse anti-FLAG M2 (1:200, Sigma Aldrich cat #F1804), rat anti-GFAP (1:500, ThermoScientific cat #13-0300) overnight at 4^{o}C. The next day samples were washed in 1X

PBS followed by secondary antibody incubation (Alexa Fluor 546 goat anti-mouse (1:1000) Invitrogen cat #A11003, Alexa Fluor 633 goat anti-rat (1:1000) Invitrogen cat #A21094 or Alexa Fluor 594 goat anti-rabbit (1:1000) Invitrogen cat #A11012) overnight at 4^{o}C. The following day, sections were washed with 1X PBS, incubated with DAPI for 20 min at RT, washed again with 1X PBS and covered with a glass cover slip after placement of ProLong Diamond Antifade Mountant (Invitrogen) onto samples. Images were acquired using a 63X oil objective on a Leica SP8 confocal microscope (Buffalo Grove, IL)

3.4.5 Quantitative PCR

RNA isolation was carried out using the Aurum Total RNA isolation kit (Bio-Rad #732-6820; Hercules, CA, USA). Samples were reverse-transcribed to cDNA using qScript cDNA Supermix (Quantabio #101414-106; Beverly, MA, USA). For quantifying F3 (*EFEMP1*) mRNA levels, cDNA was amplified with PowerUp SYBR Green Master Mix (Thermo Fisher). Transcripts were amplified using h*EFEMP1* forward (5′ GGGGATCCTTTGCATGTCAG) and reverse (5′ TGAAACCCAGGACTGCACTG) primers, and m*RPLP2* forward (5′ CGTCGCCTCCTACCTGCT) and reverse (5′ CCATTCAGCTCACTGATAACCTTG) primers as a housekeeping gene. Amplification for SYBR Green was performed on a QuantStudio 6 Real-Time PCR system and visualized and quantified using the associated software (Thermo Fisher).

3.4.6 Statistical analysis

To determine statistical significance, samples were compared using one-way ANOVA. Significance was set at $*p < 0.05$, $**p < 0.01$, and $***p < 0.001$.

Chapter 3 Figures

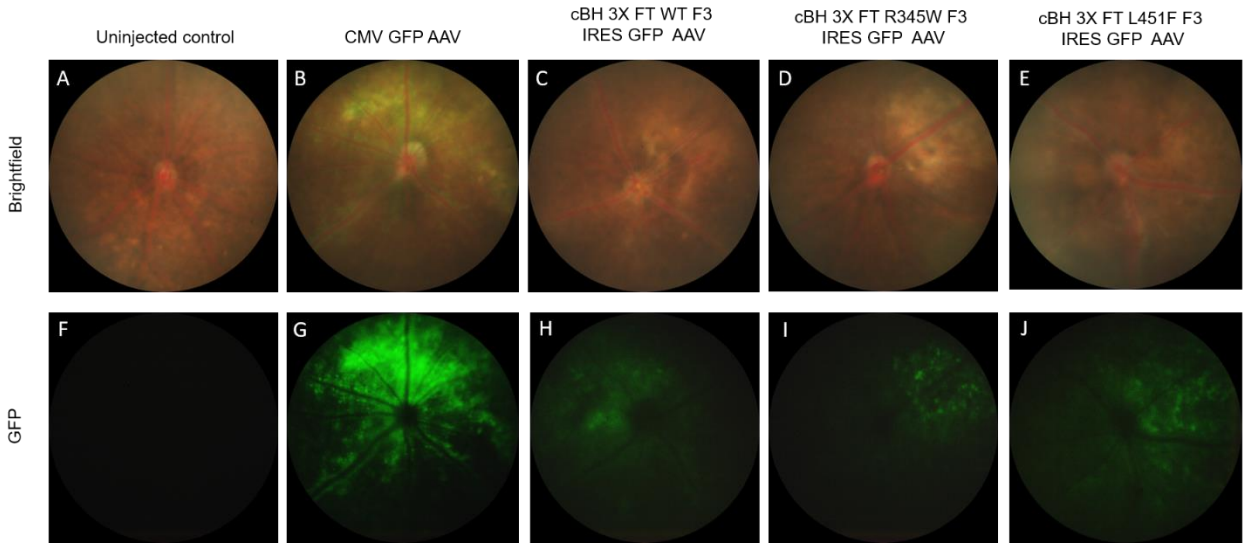

Fig 3.1: Retinal fundus assessment of F3 rAAV expression in the mouse retina. Brightfield and fluorescent fundus images of (A,F) un-injected control adult mouse retina at one month. (B,G) CMV GFP rAAV, (C,H) 3X FT WT F3, (D,I) 3X FT R345W F3, and (E,J) 3X FT L451F F3 rAAV expression in adult mouse retinas.

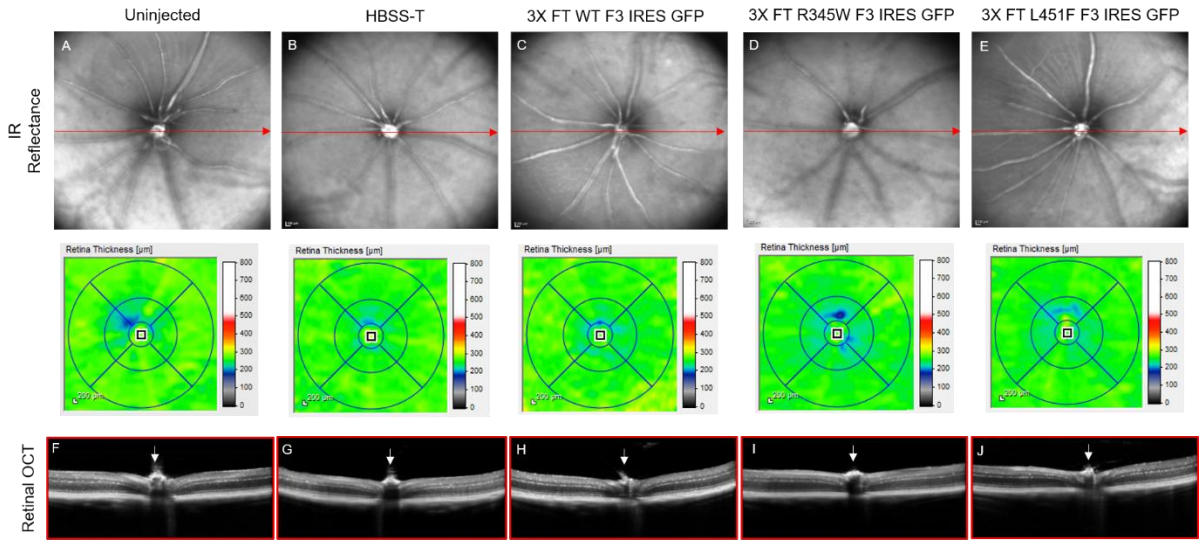

Fig 3.2: SD-OCT of F3 rAAV-injected mouse retinas. Red arrows in top panels (A-E) indicate a horizontal B-scan. Bottom panel (F-J) shows corresponding retina cross-section. *En face* retina thickness is shown under each corresponding IR reflectance image (A-E). White arrow indicates optic nerve head. Scale = 200µm.

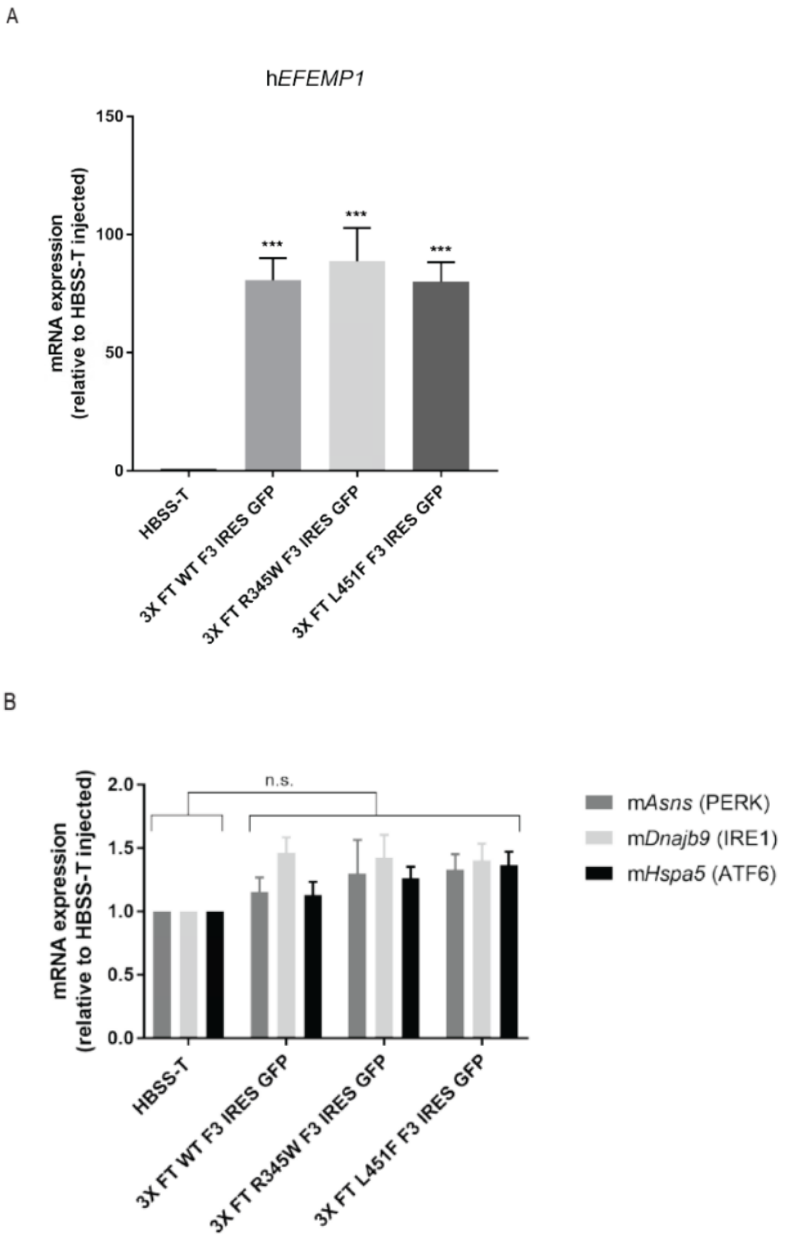

Fig 3.3: *EFEMP1* and UPR transcript levels of F3 rAAV in the mouse retina. (A) qPCR analysis of h*EFEMP1* transcript levels post-subretinal injection. Biological replicates, n=3, ***$p < 0.001$, one-way ANOVA. (B) m*Hspa5*, m*Dnajb9*, and m*Asns* transcript levels with TaqMan probes in WT, R345W and L451F F3 rAAV and HBSS-T injected mouse retinas. Biological replicates, n=3, n.s. = not significant, one-way ANOVA.

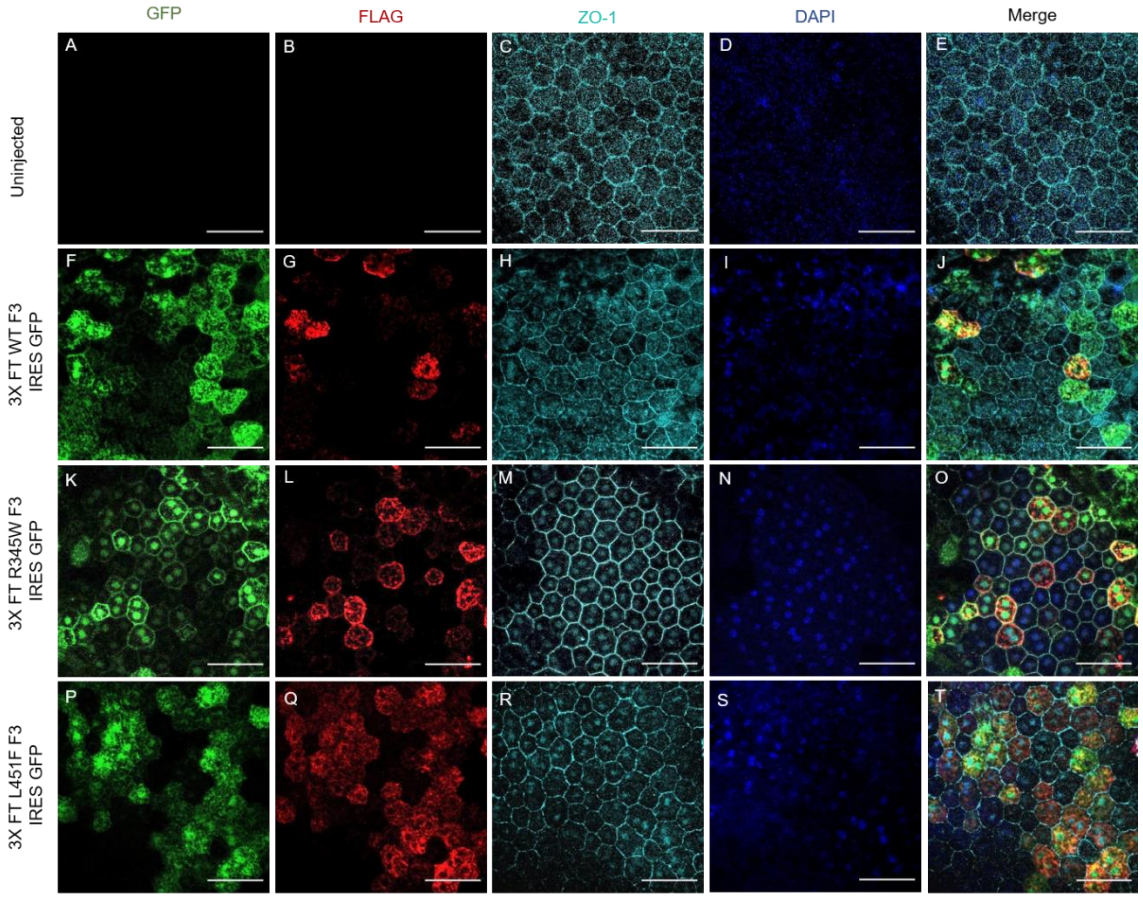

Fig 3.4: Immunofluorescence of F3 rAAV-injected mouse RPE flatmounts. Flatmounts were stained with, FLAG, ZO-1 and DAPI. Scale = 50 μm.

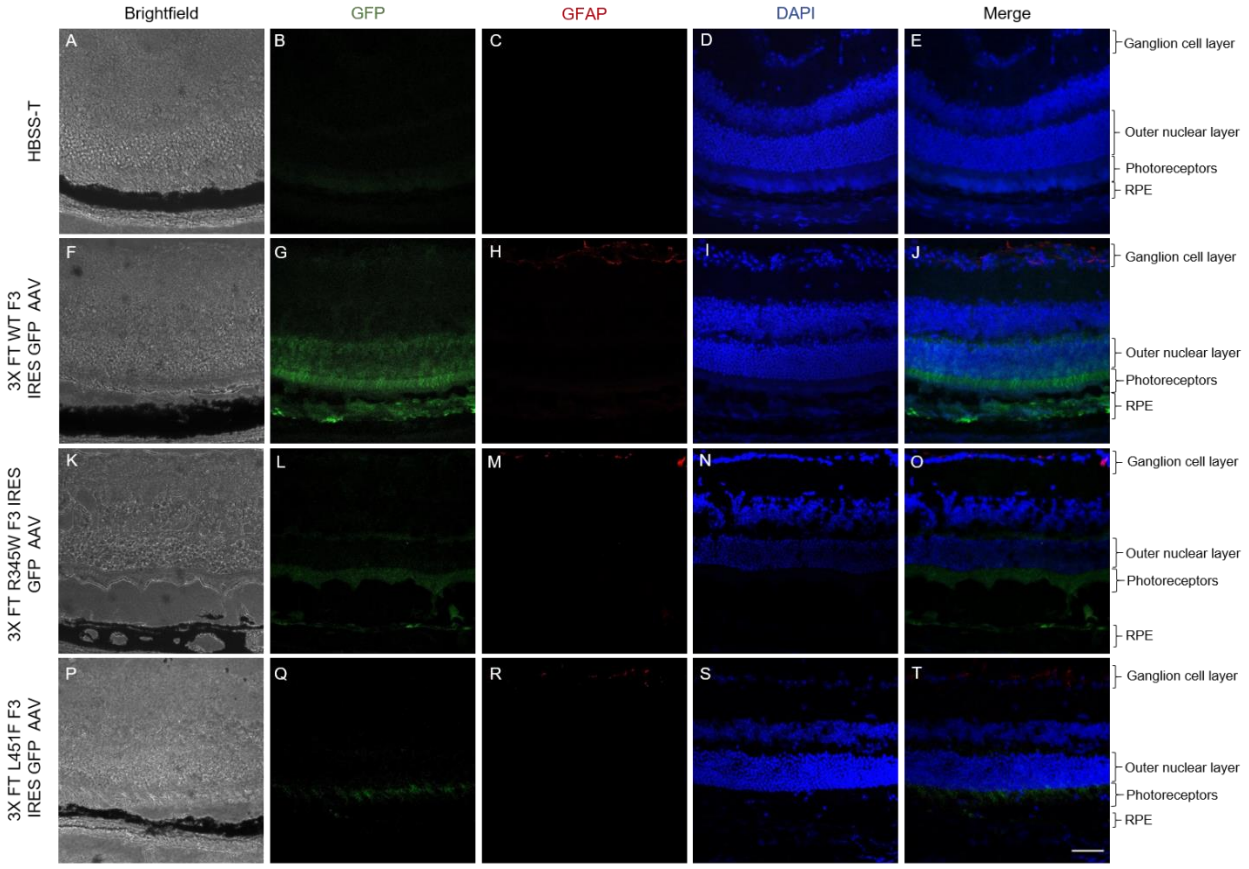

Fig 3.5: Retinal distribution of F3 rAAV-injected mice. Representative cryosection images showing F3 rAAV expression 1-month post-injection. Sections were stained with GFP, GFAP, and DAPI. Scale = 50 μm.

Supplementary Fig 3.3.1: Plasmid map of cBH 3X FT WT F3 IRES GFP vector used for rAAV production. The CMV enhancer is highlighted in white and the cBH promoter in red. F3 coding sequence is highlighted in blue and the R345W and L451F mutant positions are labeled. Downstream of the F3 sequence is an IRES (dark grey) followed by an eGFP (green).

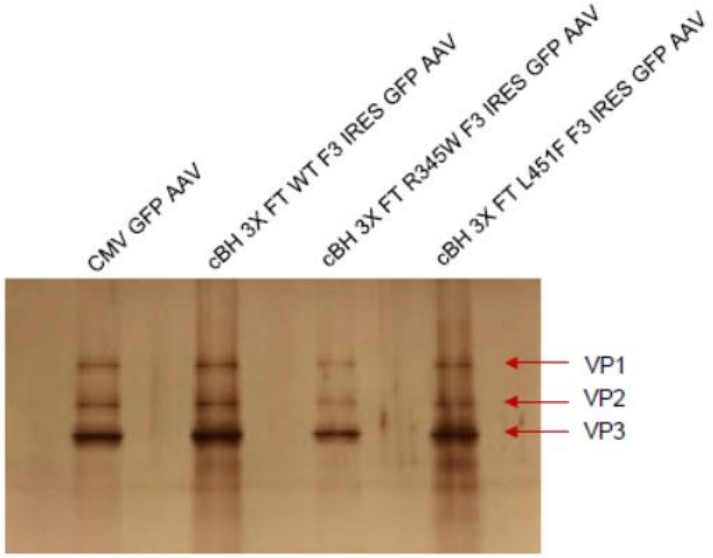

Supplementary Fig 3.3.2: Silver stain of rAAV capsid subunits after purification. VP1, VP2, and VP3 are at a 1:1:10 ratio, consistent with previous studies[221, 222].

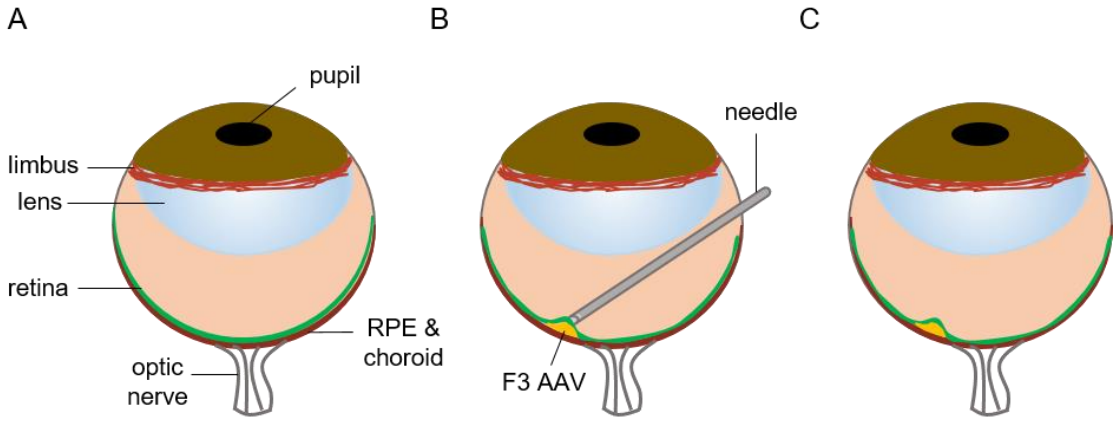

Supplementary Fig 3.3.3: Subretinal injection technique in the mouse eye. (A) Anatomy of a normal, uninjected mouse eye. (B) Injection across the mouse retina using a blunted needle to deliver genetic material to the subretinal space. (C) Bleb of F3 rAAV post-injection.

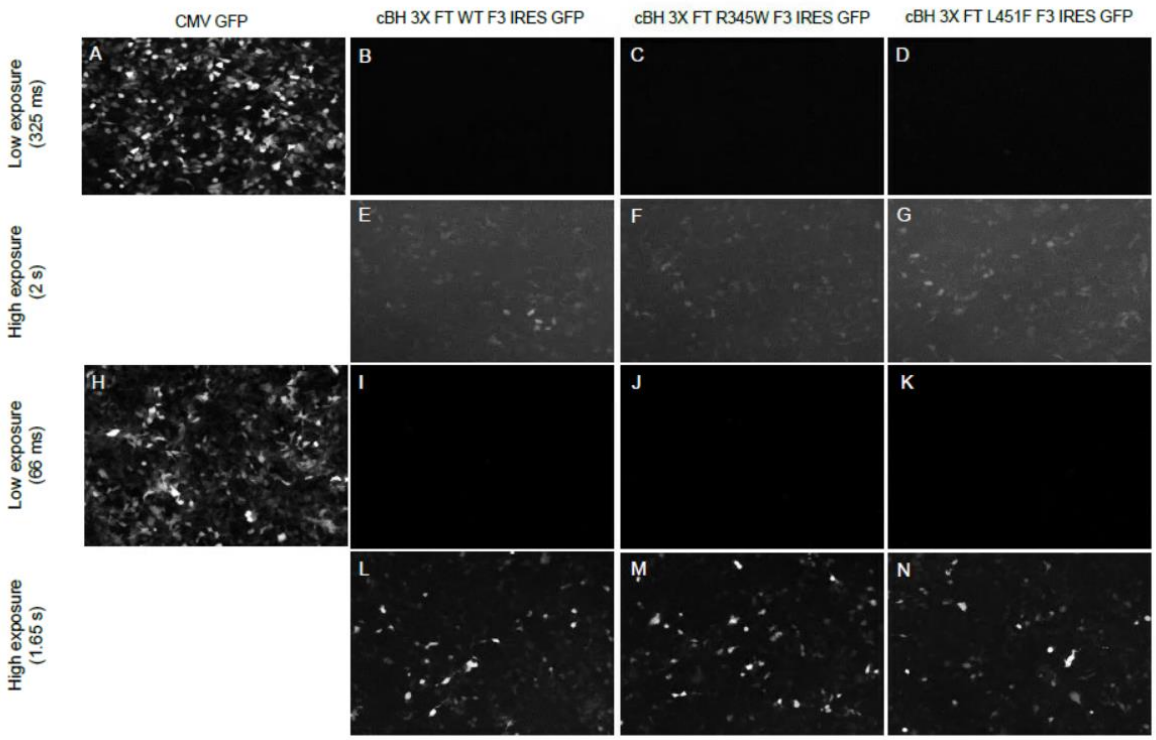

Supplementary Fig 3.3.4; Transduction of F3 rAAV constructs in HEK293A cells. At 24 h (A-G) and 48 h (H-N) post-transduction, F3 rAAV is only detected at high exposure (E-G and L-N) whereas CMV GFP rAAV is detected initially at low exposure. MOI=1.

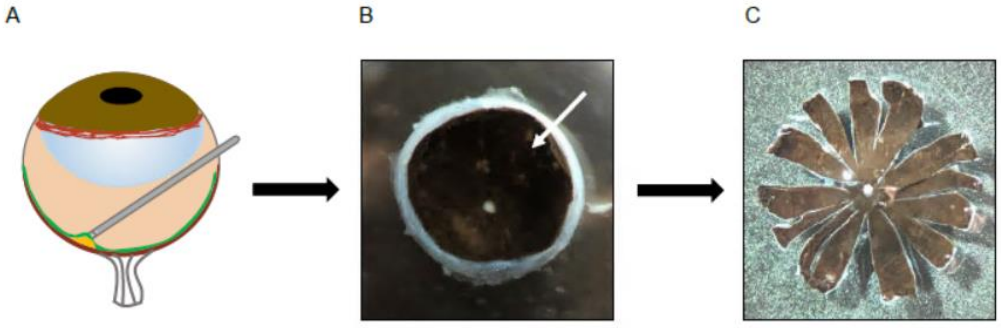

Supplementary Fig 3.3.5. Generation of mouse RPE flatmounts. (A) Subretinal injection. (B) Isolation of RPE/choroid. Arrow indicates RPE. (C) Radial cuts of RPE mounted onto a microscope slide.

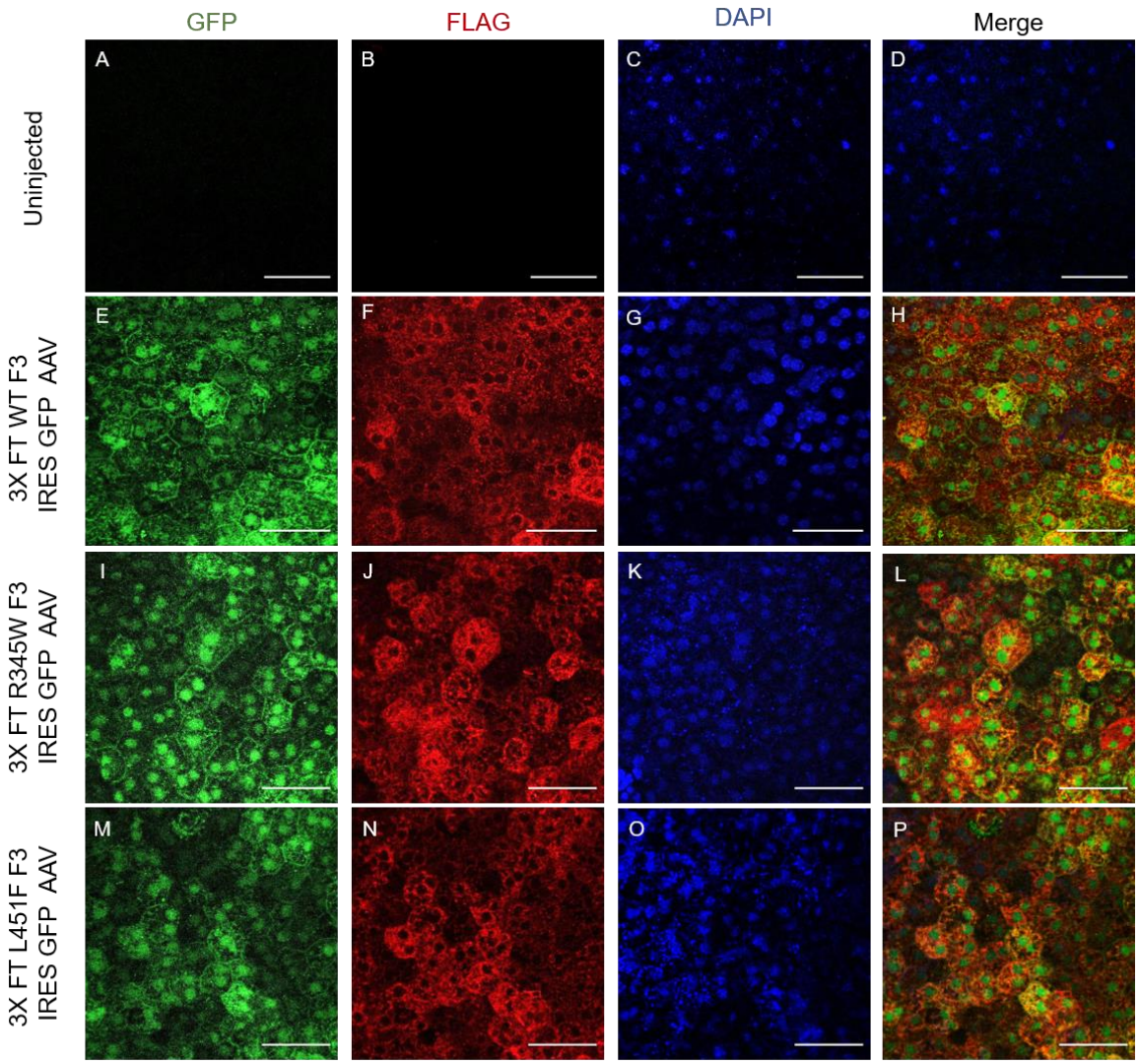

Supplementary Fig 3.3.6. Immunofluorescence of RPE flatmounts. F3 rAAV-injected 2-month-old mice stained with GFP and FLAG. Scale = 50 μm.

CHAPTER FOUR
CONCLUSIONS AND FUTURE DIRECTIONS

4.1 Conclusions

4.1.1. F3 secretion is indicative of pathology in a context-dependent manner

My published work on F3 has firstly demonstrated that secretion can be indicative of pathology, depending on the mutation (Chapter 2). To date, the R345W is the most well-studied F3 missense mutation in relation to ML and leads to several phenotypic features that resemble complex macular degenerative diseases like AMD. Because of the obvious secretion defect in R345W that has been repeatedly observed by our group and others, we hypothesized that a significant reduction in secretion could be used as a marker for F3 misfolding and pathology. Accordingly, we tested a large panel of F3 mutations found in patients with ocular disease or otherwise undisclosed potential abnormalities. Our results in Chapter 2 partially support our hypothesis as seen with the L451F F3 mutation being the only variant with a significant secretion defect and, to our surprise, having a secretion and molecular profile similar to that of R345W.

The fact that the majority of F3 variants of unknown significance (most of which were missense mutations like R345W) evaluated were not sensitive to secretion in our *in vitro* studies, even ones that were reported in patients presumably with retinal dystrophies (i.e. Y397H, L455F, and R477H), begs the question of whether using secretion as a metric for misfolding and pathology is appropriate for characterizing these mutants. Additionally, *in silico* analysis of most of the clinically identified mutants that were

predicted to be deleterious/probably damaging to F3 structure was also not reflected by a significant reduction in secretion, in contrast to observations with R345W F3 in our study. It is possible that these mutations may not perturb F3 folding and secretion to the point of initiating disease. In this case, perhaps it would be better to look at other ways that these mutants are associated with disease independent of secretion propensity, such as F3 function (which is currently unknown), profiling protein binding partners, changes in subcellular localization relative to WT F3, or changes to the structure of the ECM.

It is also possible that we are limited by current cell culture systems (HEK293A and ARPE-19) for uncovering how these mutants behave *in vitro*, and ultimately it would be ideal to test whether these mutants exhibit pathological features in primary RPE cells, whether porcine, human or mouse, as well as in the retina.

4.1.2 F3 has a misfolding problem that is likely well-tolerated in cells

We are the first to report L451F as another misfolded, destabilized and inefficiently secreted F3 mutant. Initially, before we obtained any clinical information, we hypothesized that this mutation was identified in a patient with a monogenic macular degenerative disease like ML. However, after receiving information about the two unrelated patients, one with congenital nystagmus and another with retinal dystrophy, this led us to believe that L451F can result in phenotypic variation, which is a classic feature of a genetic modifier. Like R345W, it is highly likely that L451F is autosomal dominantly inherited and results in a gain of function mechanism since it appears to be

misfolded, is inefficiently secreted, and the patients who harbor this mutation do not appear to have any symptoms related to F3 deficiency.

As far as R345W and L451F misfolding, it is unclear why the accumulation of these mutants in cells does not elicit an ER stress response. UPR activation is a well-known event that occurs for many misfolded proteins, especially those famously involved in neurodegenerative diseases such as Alzheimer's (tau protein and amyloid-β[223, 224]), Parkinson's (α-synuclein[225]), and even IRDs such as retinitis pigmentosa (RP, e.g., the P23H mutation in rhodopsin[226, 227]). In fact, several *in vitro* and *in vivo* studies, including ours in Chapters 2 and 3, suggest that ER stress doesn't play a crucial role as a signal of retinal disease for the misfolded R345W and L451F mutants.

One exception to these observations is a study by the Roybal group where R345W was overexpressed using an adenoviral vector in ARPE-19 cells, which led to increased GRP78/BiP and X-box binding protein (XBP1) transcript and protein levels. However, this result is likely due to the overexpression R345W using a high multiplicity of infection (≥25) in cells, which is sufficient for triggering the UPR, even when overexpressing WT F3[169, 174]. Furthermore, in knock-in R345W mice, no upregulation of GRP78/BiP in the mouse retina has been observed even at advanced age (18 months) [152].

Another interesting phenomena is that the R345W and L451F misfolded mutants do not appear to be degraded, but rather retained intracellularly. One possibility is that their misfolded conformations are well-tolerated intracellularly, at levels that do not exceed the ER homeostasis network capacity. Therefore, the cell may not recognize these

mutants as toxic or damage-associated. Another possibility may be due to passive ER retention, in which misfolded proteins accumulate due to failure of exiting the ER because of the absence of exit signals (possibly because it is difficult to unfold and extract disulfide-rich proteins such as F3 from the ER) or the inability to functionally and/or structurally present them[228]. This may also explain why there is no activation of the UPR and in our studies and others. However, in the context of disease, it is also important to consider whether R345W and L451F F3 misfolded accumulation is secondary to RPE dysfunction due to inability of the RPE to no longer control secretion during degeneration. Thus, it is possible that the secreted, misfolded R345W and L451F, rather than misfolded intracellular F3, is more likely to contribute to disease pathogenesis.

4.1.3. F3 secretion of R345W and L451F contribute to macular degeneration

Despite protein quality control mechanisms, such as ER associated degradation (ERAD), some misfolded proteins, are still able to exit the cell, which can cause downstream consequences that lead to a disruption of protein homeostasis and disease[229, 230]. Several *in vitro* and *in vivo* studies suggest that secreted R345W may be more detrimental in causing disease (ML) since its presence induces BLamD formation and complement activation of C3a, which are key observations in response to an abnormal ECM[152, 153]. This same phenomena may be true for the L451F mutation as well. In Chapter 3, although we were able to successfully introduce our rAAV mutants into the mouse RPE,

we were unable to detect any obvious BLamDs 1 month post-injection, which may not be an ideal timeframe for visualizing the mouse retina. However, we are optimistic that we will observe *in vivo* retinal phenotypes for R345W, consistent with previous studies, and perhaps uncover novel retinal phenotypes associated with the L451F F3 mutant. These studies will likely require ageing injected mice out to extended time points as well as utilizing transmission electron microscopy.

4.2 Future Directions

4.2.1 F3 misfolding and secretion in physiologically relevant in vitro systems

Because F3 is secreted from RPE cells, monitoring its secretion, including F3 mutants, in a relevant RPE-based culture system aside ARPE-19 cells would be beneficial. Although widely used in studies linked to retinal degeneration because of their RPE-like properties (i.e. morphology, polarization, and ability to phagocytose photoreceptor OSs), several reports have cautioned against prolonged ARPE-19 cell line use because they i) lack features of mature RPE, such as pigmentation and expression markers such as *RPE65*, and ii) are spontaneously immortalized, which deems them less likely to recapitulate native RPE because of structural and functional changes within the cells[231]. Nonetheless, if properly cultured, polarized and differentiated, ARPE-19 cells may be an appropriate model system[232].

One alternative approach to more accurately test several F3 mutants' secretion properties would be to establish a primary human fetal or adult RPE cells. Primary RPE cells are the gold standard culture system because they re-establish pigmented epithelial

monolayers with apical microvilli that express key mRNA, miRNA, and proteins essential for RPE function as well as several other important native features such as polarized secretion of growth factors and mediating transepithelial transport of fluid[233]. Introduction of select F3 mutations in primary RPE cells would not only allow for additional confirmation of secretion defects and misfolding, but would enable further characterization such as similarities and/or differences in binding partners (i.e., TIMP3) compared to WT F3 as well as determining morphological or functional changes in the RPE. For instance, evaluating RPE barrier function by transepithelial resistance (TER) measurements would be useful to assess normal primary human fetal RPE, which develop high TER (>400 Ωcm^2)[234], are well as TER for cells in which the F3 mutants are introduced.

Another primary cell culture system is the use of porcine RPE cultures, which have already been established in our laboratory. Established porcine RPE cells have several features including the expression of RPE65, localization of ZO-1 to tight junctions and Na^+, K^+-ATPase to the apical membrane[235]. Recently, we transduced porcine cell cultures with our control rAAV (CMV GFP) and cBH 3x FT WT, R345W and L451F F3 IRES GFP rAAV constructs (**Sup. Fig. 3.3.1**). We observed that 24 h post-transduction, GFP expression could be detected for CMV GFP rAAV, but not for the F3 rAAV constructs (data not shown), possibly due to the presence of the IRES GFP element (which can result in lower GFP signal than GFP directly driven by a promoter)

or due to serotype incompatibility. Thus, initial optimization studies should seek to verify F3 expression in the porcine culture prior to secretion analysis.

4.2.2 Enhancing expression of F3 rAAV

In chapter 3, we were able to verify expression of our F3 rAAV constructs in the mouse RPE. A important next step would be to generate F3 rAAV constructs that i) improve GFP expression since the IRES GFP element results in inherently low GFP fluorescent levels[236], ii) are driven by an RPE-specific promoter, and iii) the use of additional vector serotypes that are compatible with transducing the retina/RPE.

Using a GFP fluorescent reporter allows for us to visualize expression and validate the success of the subretinal injection technique in the retina. Because of the IRES GFP element, we aim to improve GFP expression in a manner that allows for increased transduction efficiency *in vitro* (**Sup. Fig. 3.3.4**) and most importantly, *in vivo* compared to our current study in Chapter 3, but also does not lead to retinal toxicity[237]. We recently attempted to insert 3x FT F3 IRES GFP sequence into a plasmid that contains a CMV enhancer-chicken β-actin promoter with a shortened intron (known as smCBA[238, 239]), in the hopes of improving GFP expression while also retaining constitutive activation in the retina. However, these studies have resulted in unsuccessful generation of these constructs.

Another important study would be to drive F3 expression specifically under an RPE-specific promoter versus using a ubiquitous promoter, which could lead to targeted expression of F3 in other cells in the neural retina. Common RPE-specific promoters such

as bestrophin-1 (BEST1) or RPE65 would ensure targeted expression of F3 to the RPE. However, one consideration would be to monitor expression levels of F3 under these promoters to ensure that F3 levels are overexpressed, which can be verified at the protein and transcript level.

To transduce F3 rAAV in the mouse retina, we used the AAV2/2[MAX] mutant serotype in our studies, which proved successful. A recent report suggests that commonly used rAAV serotypes (rAAV 2, rAAV5, rAAV8, and rAAV9) can transduce the RPE and photoreceptors upon subretinal delivery in adult mice[240-242]. Thus, utilizing additional serotypes would allow for testing retinal tropism, transduction, and determining whether AAV2/2[MAX] is the only optimal serotype for F3 rAAV RPE specificity.

4.2.3 Resolving the structural properties of F3

While it is clear that R345W and L451F F3 are misfolded and accumulate intracellularly *in vitro*, several questions remain as to the true nature of F3 misfolding. Does misfolding in this context mean that the mutants self-assemble to form aggregate species (disordered or prefibrillar)? Do the mutants form intracellular amyloid fibrils? Are the mutants considered prion-like proteins?

In chapter 2, we established that the C-terminal region of F3 is prone to misfolding and destabilization, which is exacerbated upon removal of the N-linked glycosylation site. Surprisingly, a recent study by Tasaki *et al*. found evidence of F3 amyloids in the large intestinal veins of elderly individuals[187]. Upon biophysical analysis,

the C-terminal region containing residues 437-493 showed a high tendency for amyloid fibril formation versus the N-terminal region[187]. Interestingly, a synthetic peptide containing F3 residues 437-456, which includes L451, formed nonbranching straight amyloid fibrils[187]. Therefore, we hypothesize that the L451F mutation in F3 may rapidly exacerbate amyloid fibril formation through promotion of hydrophobic interactions, especially since we have observed that the full length L451F mutant is misfolded. Currently, we are utilizing synthetic peptides (residues 437-456 that include either WT F3 sequence as a control, the L451F mutant, or a L455F control mutant) to test our hypothesis. The peptide containing the L455F mutant will be used to determine whether amyloid fibril formation is specific to only L451F or whether a general substitution to phenylalanine is sufficient to drive aggregation. After initial monomerization of the peptides, a Thioflavin T kinetic assay will be performed in order to monitor the presence of F3 amyloid fibrils.

Additional methods to resolve not only the C-terminal region of F3, but full-length F3 would also be useful in future studies. Although WT F3 is monomeric, secondary structural characterization of it is lacking, and there is currently no crystal structure of F3 available. To begin to investigate the structure of F3, a starting point would be to obtain a circular dichroism (CD) spectrum detailing F3 secondary structure. CD spectroscopy would allow for us to directly determine whether F3 is an intrinsically disordered protein in its native form, which a previous study suggested due to its predicted binding promiscuity, multifunctionality and multiple posttranslational

modification sites[110]. CD spectroscopy would also enable more thorough elucidation of the structural properties in the N- and C-terminal F3 region (alpha helix vs. beta-sheet content) and provide insight as to how the R345W and L451F mutants influence F3 folding, thermal and chemical stability, binding properties and conformational changes.

4.2.4 Targeting R345W and L451F F3 for degradation

Although we show that R345W and L451F F3 intracellular accumulation does not lead to significant ER stress, a combination of intracellular and secreted F3 mutants may trigger disease and lead to deposit formation and eventual blindness. Therefore, a therapeutic approach to target R345W and L451F for degradation would be attractive. Furthermore, our group recently reported that removal of even WT F3 is well-tolerated in various ocular tissues, including the retina/RPE, and may serve as a potential therapeutic strategy for reducing sub-RPE deposit formation in disease[175]. The use of antisense oligonucleotides (ASOs) has garnered attention within the last decade for the treatment of ocular diseases, including IRDs such as RP[243-245].

ASOs are single-stranded DNAs (~18-20 base pairs) that are complementary to an mRNA target of interest, with the goal of reducing the gene expression of said target by induction of RNase H endonuclease activity, which cleaves the DNA-RNA heteroduplex[246]. Several studies have shown the use of ASOs in mouse retinal degeneration models[247-249]. Using this approach, studies of optimizing the design and screening of F3 ASOs for i) their uptake and stability *in vivo* which is dependent on backbone (i.e. phosphorothioate (PS)) and chemical modifications (i.e. methoxyethyl

(MOE))[250, 251], ii) their ability to penetrate the mouse RPE and iii) sufficient concentration for knockdown of mutant F3 levels *in vitro* and *in vivo*.

As a starting point to these studies, we recently designed a non-targeting 2'MOE gapmer ASO with a 5' Cy3 fluorescent reporter and an F3 2'MOE gapmer ASO that targets mouse F3 for degradation. After transfection of the F3 2'MOE gapmer ASO into a stably-expressed mouse F3 ARPE-19 cell line where F3 is fused to an enhanced Gaussia luciferase (eGluc), we were unable to detect a reduction in eGluc (and therefore F3) activity up to 72 h. Subsequently, we tested whether our non-targeting, fluorescently labeled Cy3 ASO could transduce the mouse RPE. We found that whereas the photoreceptors were transduced upon intravitreal injection, subretinal injection did not result in RPE transduction. These studies highlight the unique challenges to overcome for future optimization of using ASOs as a means to target F3 in the RPE *in vitro* and *in vivo*.

4.2.5 Long-term evaluation of sub-RPE deposits in F3 rAAV-injected mice

At 1 month post-injection, we did not detect the presence of sub-RPE or basal laminar deposits. Therefore, long-term retinal evaluation of the mice will be necessary. Recently, Dinculescu *et al*. observed basal RPE deposits starting at 4 months in their rAAV-induced mutant C1QTNF5 driven by an RPE-specific BEST1 promoter following subretinal delivery in mice[197]. Similarly, in our F3 rAAV mouse model, we hypothesize that sub-RPE deposits may be visible at around 3 months, and will progressively accumulate and lead to prominent features of retinal degeneration (i.e. photoreceptor

atrophy, RPE abnormalities, overall retinal thinning, loss of retinal function) as the mice age.

To begin monitoring mice for deposits, subretinal injections have been performed on mouse pups (p4-p5) to allow for ageing up to one year. At designated timepoints (3, 6, 9, and 12 months) post injections, F3 rAAV IRES GFP expression will be confirmed using fundoscopy and retinal integrity will be assessed by SD-OCT. Electroretinography will also be used to assess whether there are changes in visual function of the mice at the corresponding timepoint and subsequently analysis via histology and electron microscopy will be used to determine the presence of sub-RPE BLamDs.

APPENDIX A.

Acknowledgement

I want to acknowledge another major project in the lab that focuses on a protein expressed in the eye named tubby-like protein 1 (TULP1) and its implication in Retinitis pigmentosa (RP). This project was initially my rotation project in the lab, but quicky birthed into a novel finding that led to a publication: Woodard DR *et. al.* A novel homozygous missense mutation p.P388S in *TULP1* causes protein instability and retinitis pigmentosa**.** *Mol. Vis.* (2021); 27:179-190. Author contributions: D.R.W. performed all *in vitro* experiments.

4.1 Abstract

Retinitis pigmentosa (RP) is an inherited retinal disorder that results in the degeneration of photoreceptor cells, ultimately leading to severe visual impairment. We characterized a consanguineous family from Southern India wherein a 25 year old individual presented with night blindness since childhood. The purpose of this study was to identify the causative mutation for RP in this individual as well as characterize how the mutation may ultimately affect protein function. We performed a complete ophthalmologic examination of the proband followed by exome sequencing. The likely causative mutation was identified and modeled in cultured cells, evaluating its expression, solubility (both with western blotting), subcellular distribution, (confocal microscopy), and testing whether this variant induced endoplasmic reticulum (ER) stress (quantitative PCR [qPCR] and

western blotting). The proband presented with generalized and parafoveal retinal pigmented epithelium (RPE) atrophy with bone spicule-like pigmentation in the midperiphery and arteriolar attenuation. Optical coherence tomography scans through the macula of both eyes showed atrophy of the outer retinal layers with loss of the ellipsoid zone, whereas the systemic examination of this individual was normal. The proband's parents and sibling were asymptomatic and had normal funduscopic examinations. We discovered a novel homozygous p.Pro388Ser mutation in the *tubby-like protein 1* (*TULP1*) gene in the individual with RP. In cultured cells, the P388S mutation does not alter the subcellular distribution of TULP1 or induce ER stress when compared to wild-type TULP1, but instead significantly lowers protein stability as indicated with steady-state and cycloheximide-chase experiments. These results add to the list of known mutations in *TULP1* identified in individuals with RP and suggest a possible unique pathogenic mechanism in *TULP1*-induced RP, which may be shared among select mutations in *TULP1*.

4.2 Introduction

Inherited retinal disorders (IRDs) caused by autosomal dominant, recessive, and X-linked mutations comprise more than 2 million cases of ocular diseases worldwide[252]. The most common IRD, retinitis pigmentosa (RP), affects 1 in 3,000 individuals worldwide and is characterized by the degeneration of retinal photoreceptor cells beginning with the atrophy of rods and the secondary death of cones[253]. Clinical

symptoms of RP include night blindness followed by the loss of peripheral, and eventually, central vision[254].

Currently, more than 30 genes have been associated with autosomal recessive RP[255]. Mutations in the *tubby-like protein 1* (*TULP1*; Gene ID: 7287, OMIM: 602280) gene have been shown to contribute to autosomal recessive RP[256-259]. *TULP1* belongs to the tubby-like gene family that encodes for a 542 amino acid cytoplasmic, membrane-associated protein found exclusively in retinal photoreceptor cells[260]. Previously, the TULP1 protein was demonstrated to be required for normal photoreceptor function through promotion of rhodopsin transport and localization from the inner to outer segments[261], potentially in an F-actin-dependent manner[262]. In addition, in vivo studies have confirmed that mice lacking *Tulp1* display early-onset photoreceptor degeneration due to the loss of rods and cones[263]. Recently, Lobo et al. demonstrated that certain RP-associated autosomal recessive missense mutations in the *TULP1* gene can cause the protein to accumulate within the endoplasmic reticulum (ER), leading to prolonged and possibly detrimental ER stress, providing a surprising but speculative molecular mechanism by which mutations in *TULP1* can induce retinal degeneration[264].

In the present study, we identified a novel homozygous missense mutation p.Pro388Sser (P338S) in *TULP1* in a consanguineous family from Southern India who presented with autosomal recessive RP. We explored whether the P388S TULP1 mutant demonstrated any differences in solubility, subcellular localization, or activated cellular stress responses. Our observations revealed that there are no differences in transcript

levels between P388S and wild-type (WT) *TULP1*, and the P388S mutation does not induce overt ER stress within cells. Furthermore, we found that P388S localized similarly to WT TULP1 in transfected human embryonic kidney (HEK293A) and human immortalized retinal pigmented epithelial cells (ARPE-19). However, we found that P388S steady-state levels were significantly reduced and that P388S was more rapidly degraded than WT TULP1 through cycloheximide-chase assays. Our results suggest that certain mutations in *TULP1* may affect protein stability, which may, in turn, contribute to RP disease pathogenesis.

4.3 Results

4.3.1 Proband from a consanguineous family in Southern India

A 25-year-old man (Study ID: SIO221) born of a consanguineous marriage in Andhra Pradesh, India, an area where we previously identified unique autosomal recessive mutations linked to eye disease[265], presented with a history of night blindness since childhood. Best-corrected visual acuity (BCVA) in both eyes was 20/60. He had no nystagmus. Intraocular pressure and anterior segment examinations were normal. Fundus examination revealed a symmetric generalized and parafoveal RPE atrophy with bone spicule-like pigmentation in the midperiphery and arteriolar attenuation (**Fig. 4.1A,B**). The optic nerve head was normal in appearance. Fundus autofluorescence revealed a parafoveal ring of hypo autofluorescence corresponding to the area of RPE atrophy and a patchy decrease in autofluorescence throughout the retina in both eyes (**Fig. 4.1C,D**).

Optical coherence tomography scans through the macula of both eyes showed atrophy of the outer retinal layers with loss of the ellipsoid zone (EZ) and a thin epiretinal membrane (**Fig. 4.1E,F**). For comparison, an age-matched healthy control patient was imaged using the same modalities (**Fig. 4.1G–L**). There was no evidence of posterior staphyloma in the patient. The patient's axial lengths were 24.47 mm and 24.25 mm, respectively. Systemic examination was normal. The examined parents and sibling (pedigree shown in **Fig. 4.2A**) were asymptomatic and had normal funduscopic examinations.

4.3.2 Exome sequencing identifies a novel homozygous mutation in the *TULP1* gene

Exome sequencing of the proband, followed by application of filtering criteria (described in Methods and the flowchart provided in **Appendix Fig. 4.2**), revealed ten possible homozygous mutations (**Appendix Fig. 4.3**), only one of which was in a gene (*TULP1*) known to cause RP[266]. This variant, a homozygous missense mutation (NC_000006:g.35471576G>A; NM_003322:c.1162C>T; NP_003313:p.Pro388Ser) in exon 12 of the *TULP1* gene, results in a substitution of proline by serine in a conserved amino acid position (**Fig. 4.2B**). Aside from the potentially pathogenic mutation in *TULP1*, the only known pathogenic mutation (p.Arg89His) that was identified in the affected individual was in the *INS* gene (Gene ID: 3630, OMIM: 176730; Appendix Fig. 4.4), which is associated with hyperproinsulinemia, a disease not known to result in the described ocular phenotype[267]. Nonetheless, the P388S *TULP1* mutation is a novel

variant absent from the 1000 Genomes Project database, the Genome Aggregation Database (v2.1.1), the TOPMed database (freeze 5), and the GenomeAsia 100 K Project database[268]. Segregation of the variant in the consanguineous pedigree was examined with Sanger sequencing to reveal that the parents are heterozygous for the mutation (**Fig. 4.2A**, Appendix Fig. 4.5). P388 is a highly conserved residue among the species tested, including mammals (**Fig. 4.2B**) with a $GERP^{2+}$ score[269] of 4.95 (**Fig. 4.2C**). *In silico* prediction indicates that the change to proline at this position could possibly perturb protein function or contribute to pathogenicity with a PolyPhen-2 score[257] of 0.997 (probably damaging), a CADD score[270]of 26.9, and a PROVEAN score[271] of −7.9 (deleterious). Analysis of known mutations in *TULP1* showed an enrichment of mutations occurring in the C-terminus of TULP1 (> amino acid 300), with P338S falling within this region (**Appendix Fig. 4.6**).

4.3.3 P388S displays similar subcellular localization to WT TULP1

Previously, WT TULP1 has been shown to localize near the plasma membrane and in the nuclear compartments of COS-7 cells[272]. A separate study suggested that missense mutations in TULP1 shift its sub-cellular trafficking, resulting in ER localization[264]. Therefore, we tested whether the P388S mutant displayed localization differences compared to WT TULP1 in cultured cells. HEK293A cells (STR verified, **Appendix Fig. 4.1**) were transiently transfected with eGFP, WT TULP1 eGFP, or P388S TULP1 eGFP constructs and analyzed for green fluorescence and counterstained with phalloidin, which binds to F-actin, using laser-scanning confocal microscopy (**Fig. 4.3A–C**). As expected,

expression of eGFP showed the fluorescent signal distributed evenly across the cytoplasm in cells (**Fig. 4.3A**). WT TULP1 eGFP was localized near the plasma membrane as well as in the nuclear compartments of cells (Figure 4.3B) similar to previous reports in COS-7 cells[262, 272]. Surprisingly, we found that localization of P388S TULP1 eGFP was similar to that of WT TULP1 eGFP in that it also localized predominantly near the plasma membrane and in the nuclear compartment of cells (**Fig. 4.3C**), suggesting that there are no differences in cellular distribution between WT and P388S TULP1. To confirm that these observations were not cell type-dependent, we also transfected human immortalized RPE (ARPE-19) cells (also STR verified, **Appendix Fig. 4.1**) with the constructs indicated above and observed that P388S TULP1 eGFP again localized similarly to WT TULP1 eGFP in the nucleus and near the plasma membrane of the cells (**Appendix Fig. 4.7**).

4.3.4 Protein expression and solubility of P388S TULP1

Because we did not detect obvious differences between WT and P388S TULP1 at the sub-cellular level, we investigated other potential biochemical differences that might partially explain the RP phenotype observed in the patient with the presumed pathogenic variant, p.Pro388Sser in *TULP1*. We employed a biochemical approach to detect the expression and solubility of WT and P388S TULP1. Using HEK293A cells, we transfected WT TULP1 eGFP and P388S TULP1 eGFP, and isolated the soluble and insoluble protein fractions from the cells 24 h later. WT TULP1 eGFP and P388S TULP1

eGFP in the soluble and insoluble fractions migrated as predicted at a molecular weight of about 100 kDa (Figure 4.4A, TULP1 is about 70 kDa[263], and eGFP is about 26–28 kDa[273]). WT TULP1 and P388S TULP1 were similarly more abundant in the RIPA-soluble fraction, as expected based on previous findings[263] (**Fig. 4.4A**). However, we detected a significant 27.7±13.8% and 22.2±12.4% decrease in soluble and insoluble P388S TULP1 protein levels compared to WT TULP1, respectively (**Fig. 4.4B**). Furthermore, these observed differences were not due to variations at the transcript level, as qPCR revealed no statistically significant difference between WT and P388S *TULP1* (**Fig. 4.4C**).

4.3.5 P388S is degraded more rapidly than WT TULP1

Because we observed a significant reduction in P388S TULP1 protein steady-state levels compared to WT TULP1 (**Fig. 4.3A,B**), we hypothesized that this may indicate that P388S TULP1 is less stable in vitro. To more definitively address whether there were any differences in stability at the protein level between WT TULP1 and P388S TULP1, transfected HEK293A cells were treated with cycloheximide (CHX), a translation elongation inhibitor, over the course of 9 h. With western blotting, we observed a gradual decrease in protein levels for WT and P388S TULP1 under CHX treatment over time (**Fig. 4.5A,B**). Initially, we observed an 18.4±18.2% reduction in P388S levels, compared to a 4.8±5.5% reduction in WT TULP1 after 1 h of treatment with CHX (25 μM, Figure 4.5A–C, not statistically significant). After 3 h of CHX treatment, we observed a

statistically significant 48.7±7.90% reduction in P388S levels, in contrast to the stability of WT TULP1 (5.00±12.3%, **Fig. 4.5A–C**, $p<0.01$, *t* test), indicating that P388S is more rapidly degraded at this time point. Finally, at 9 h, we detected a 74.1±11.6% reduction in P388S, whereas WT TULP1 displayed only a 53.6±3.10% reduction in protein levels (**Fig. 4.5A–C**, $p<0.05$, *t* test). These data suggest that P388S is generally more unstable and has a higher turnover rate compared to WT TULP1.

4.3.6 P388S TULP1 does not induce ER stress

Missense mutations in *TULP1* have been shown to induce ER stress *in vitro*[264]. Similarly, we hypothesized that P388S TULP1 may also induce ER stress in cells. To test this hypothesis, we transfected HEK293A cells and performed qPCR using TaqMan probes that are representative downstream genes of unfolded protein response (UPR) pathway activation[170]. To measure changes in ER stress, we selected the heat shock protein 70 family protein 5 (*HSPA5*, *ATF6* activation, Gene ID: 3309, OMIM: 138120), DnaJ homolog subfamily B member 9 (*DNAJB9*, *IRE1* activation, Gene ID: 4189, OMIM: 602634), and asparagine synthetase (*ASNS*, *PERK* activation, Gene ID: 440, OMIM: 108370) genes. We measured the mRNA expression levels of each gene in HEK293A cells expressing either WT or P388S TULP1 and detected no statistically significant differences in the *HSPA5*, *DNAJB9*, and *ASNS* transcript levels (**Fig. 4. 6A**), suggesting that the presence of P388S does not induce ER stress within cells. We also confirmed these observations at the protein level by analyzing the GRP78 (*HSPA5*) levels (**Fig. 4.6B,C**). We found that P388S did not induce statistically significant cellular stress

in cultured cells when compared to WT TULP1. These results suggest that the P388S TULP1 variant likely contributes to RP by an alternate mechanism other than ER stress.

4.4 Discussion

More than 25 mutations in *TULP1* have been implicated in RP and LCA, including splice-site, frameshift, nonsense, and missense mutations[259, 274-280] (**Appendix Fig. 4.6**). In the present study, we characterized the P388S TULP1 variant found in an individual with autosomal recessive RP. When monitoring TULP1 sub-cellular localization in HEK293A and ARPE-19 cells, as well as ER stress markers as a consequence of *TULP1* expression, we found no obvious differences between WT TULP1- or P388S TULP1-expressing cells. These observations are in contrast to a previous report showing that missense mutations in *TULP1* can induce ER stress in cultured cells[264]. The present study results suggest that not all mutations in *TULP1* induce cellular stress that could potentially lead to disease. In cultured HEK293A cells, we showed that in comparison to WT TULP1, the P388S mutant protein is unstable and has a faster turnover. Additional RP-associated mutations in *TULP1* (R311Q and R342Q) were also speculated to cause destabilization of the protein in separate studies[281]. Furthermore, upon closer examination of previous data[264], although not specifically elaborated upon in that particular publication, two other mutations in *TULP1*, I459K and F491L, also appear to show a greater than or equal to 45% reduction in apparent steady-state levels relative to WT TULP1. Although largely speculative, the culmination of these results suggest that

a reduction in protein stability might be a phenomenon shared among particular *TULP1* variants.

The extent of reduction in protein stability or steady-state levels (on average, about 25%) may not fully explain how the P388S *TULP1* mutation causes RP, but this observation indicates that the protein is likely partially misfolded and may be nonfunctional. To address this possibility, an ideal experiment would be to introduce P388S TULP1 into *Tulp1*$^{-/-}$ mice to determine whether it can compensate for the loss of *Tulp1,* which is beyond the scope of this study. Nonetheless, the present findings suggest the possibility of another avenue other than ER stress by which select mutations in *TULP1* may lead to disease, and support the idea that evaluation of TULP1 protein stability should be considered when characterizing newly identified mutations in TULP1 associated with RP in vitro.

4.5 Methods

4.5.1 Study participants

This study was approved by the Institutional Review Board of the Srikiran Institute of Ophthalmology and followed the tenets of the Declaration of Helsinki. The proband and his family members were recruited and examined after informed consent was received. All participants underwent detailed ophthalmologic evaluations including fundus examination by a retina fellowship-trained ophthalmologist.

4.5.2 Exome sequencing

Approximately 4 ml of blood was drawn from each subject by venipuncture and stored in BD Vacutainer blood collection tubes with K2EDTA (Becton Dickinson, Franklin Lakes, NJ) at 4° C. Genomic DNA from peripheral leukocytes was isolated using the QIAsymphony automated DNA extraction system and QIAsymphony DNA Midi Kit (Qiagen, Hilden, Germany) per manufacturer's protocols.

We performed exome sequencing on genomic DNA of the proband. Library construction and target enrichment were performed using the IDT xGen Exome capture kit (Coralville, IA). The libraries were then sequenced to mean 100X on-target depth on an Illumina sequencing platform (San Diego, CA) with 150 base pairs paired-end reads. Sequences were aligned to the human reference genome b37, and variants were called using the Genome Analysis Toolkit (Cambridge, MA)[282] and annotated using SnpEff[283].

We filtered for rare missense, nonsense, splicing, or frameshift homozygous mutations with a minor allele frequency (MAF) less than 0.01 in the 1000 Genomes Project and genome aggregation (gnomAD) databases. Variants with a Genomic Evolutionary Rate Profiling ($GERP^{2+}$) score greater than 2.0 and a Combined Annotation Dependent Depletion (CADD) score greater than 15 were considered. Known RP susceptibility-conferring genes[266] were screened with priority. Sanger sequencing was used to validate variants of interest in the proband and family members.

4.5.3 Generation of *TULP1* constructs

The cDNA encoding for WT human *TULP1* was purchased from the DNASU Plasmid Repository (HsCD00820883, Tucson, AZ). To generate the P388S mutation, Q5 site-directed mutagenesis (New England Biolabs, NEB, Ipswich, MA) of full-length human *TULP1* was performed using the following primers: 5′-CGG GCA GAA CTC ACA GCG TGG-3′ and 5′-TTG TCA AAG ACC GTG AAG CGG-3′. To generate the C-terminal green fluorescent protein (GFP)-tagged WT and P388S *TULP1*, Gibson Assembly (HiFi Master Mix, NEB) was used to insert a Kozak sequence (DNA sequence: GCCACC) upstream of the *TULP1* start codon, and a flexible linker (amino acids: GGGGS) separating *TULP1* and enhanced GFP (eGFP). This TULP1-GGGGS-eGFP DNA was inserted into the peGFP-C1 vector backbone via the SalI and NheI restriction sites. All constructs were verified with Sanger sequencing.

4.5.4 Cell culture

Human embryonic kidney (HEK293A, Life Technologies, Carlsbad, CA) cells were cultured at 37 °C with 5% CO_2 in Dulbecco's minimal essential medium (DMEM) supplemented with high glucose (4.5 g/l, Corning, Corning, NY), 10% fetal bovine serum (FBS, Omega Scientific, Tarzana, CA), and 1% penicillin-streptomycin-glutamine (Gibco, Waltham, MA). For a 24-well plate, cells were plated at a density of 100,000 cells/well, and for a 12-well plate, cells were plated at a density of 180,000–200,000 cells/well. Cells were transfected the following day with either 500 ng (24 well) or 1 μg

(12 well) of midi-prepped endotoxin-free plasmid DNA (Qiagen, Germantown, MD) using Lipofectamine 3000 (Life Technologies) according to the manufacturer's protocol. Forty-eight hours after transfection, fresh media was added, and the cells were harvested 24 h later (72 h post transfection) and processed for western blotting or quantitative PCR (qPCR). As a positive control for some experiments, cells were treated with tunicamycin (an unfolded protein response inducer, 1 μM, 24 h, Sigma cat# T7765, St. Louis, MO) and processed similarly for western blotting or qPCR. Human immortalized RPE (ARPE-19, CRL-2302, American Type Culture Collection, Manassas, VA) cells were cultured in DMEM/F12 media supplemented with 10% FBS (Omega Scientific), HEPES (Corning, Corning, NY), and penicillin/streptomycin and glutamine (PSQ, Gibco, Germantown, MD). For a 24-well plate, ARPE-19 cells were plated at a density of 100,000 cells/well and transfected the following day with 500 ng of midi-prepped endotoxin-free plasmid DNA (Qiagen) using Lipofectamine 3000 (Life Technologies). All cells used were verified for authenticity using short tandem repeat (STR) profiling (Appendix Fig. 4.1, University of Arizona Genomics Core, Tucson, AZ). Note that STR verification cannot distinguish among different variants of the 293-based cell lines (i.e., 293 versus 293A versus 293T).

4.5.5 Confocal microscopy

A glass-bottom 24-well plate (MatTek Corporation, Ashland, MA) was coated with 1X poly-D-lysine (Sigma Aldrich), rinsed with water, and allowed to dry at room temperature. HEK293A or ARPE-19 cells were plated at a density of 100,000 cells/well

and transfected the following day with 500 ng of midi-prepped endotoxin-free plasmid DNA (Qiagen). Forty-eight hours after transfection, fresh media was added, and 24 h later (72 h post transfection), the cells were washed twice with 1X PBS (Fisher BioReagents, cat# BP2944100, Waltham, MA) followed by incubation with 4% paraformaldehyde (PFA; Electron Microscopy Sciences, Hatfield, PA) for 20 min. After PFA incubation, cells were washed with 1X PBS. For the ARPE-19 cells, the cell nuclei were stained with 300 nM 4’,6-diamidino-2-phenylindole (DAPI), dilactate solution (Molecular Probes, Eugene, OR). For membrane staining, the HEK293A cells were washed twice with 1X PBS, fixed in 4% PFA, permeabilized in 0.1% Triton X-100 for 3 min, and washed again in 1X PBS. Cells were incubated in blocking buffer (1% bovine serum albumin [BSA] in PBS) for 10 min followed by Alexa Fluor™ 633 Phalloidin (1:50 dilution in PBS; Molecular Probes) for 20 min and washed twice with 1X PBS before being imaged using a 63X oil objective on a Leica SP8 confocal microscope (Buffalo Grove, IL).

4.5.6 Western blotting

Cells were washed with Hanks buffered salt solution (HBSS, Corning), lysed with radioimmunoprecipitation assay (RIPA) buffer (Santa Cruz, Dallas, TX) supplemented with Halt protease inhibitor (Pierce, Rockford, IL) and benzonase (Millipore Sigma) for 3–5 min, and spun at maximum speed (21,000 ×g) at 4 °C for 10 min. The soluble supernatant was collected, and the protein was quantified via bicinchoninic assay (BCA) assay (Pierce). The insoluble pellet fractions were further washed in HBSS and

centrifuged, and the pellet was resuspended in 1X sodium dodecyl sulfate (SDS) buffer containing 0.83% β-mercaptoethanol (BME) and sonicated (30% amplitude, pulse 10 s on/off). Thirty micrograms of soluble supernatant were run on a 4–20% Tris-Gly SDS–polyacrylamide gel electrophoresis (PAGE) gel (Life Technologies) alongside the equivalent amount of insoluble protein and transferred onto a nitrocellulose membrane using an iBlot2 device (Life Technologies). After probing for total protein transferred using Ponceau S (Sigma), the membranes were blocked overnight in Odyssey PBS Blocking Buffer (LI-COR, Lincoln, NE). Membranes were then probed with mouse anti-GFP (1:1,000; Santa Cruz, cat #sc-9996), mouse anti-glucose-regulated protein 78 (GRP78, 1:1,000; Santa Cruz, cat #sc-376768), or rabbit anti-β-actin (1:1,000; LI-COR, Lincoln, NE, cat# 926–42210). Blots were imaged on an Odyssey CLx and quantified using ImageStudio (both from LI-COR).

4.5.7 Quantitative PCR

Transfected HEK293A cells were trypsinized (0.25% Trypsin EDTA, Gibco), quenched with DMEM, and centrifuged at maximum speed (21,000 ×g) at 4 °C for 10 min. Cell pellets were washed with HBSS and centrifuged again, and then RNA extraction from the cell pellets was performed using the Aurum Total RNA Mini Kit (Bio-Rad, Hercules, CA). Four hundred nanograms of RNA were reverse transcribed using qScript cDNA SuperMix (Quanta Bioscience, Beverly, MA) according to vendor recommended parameters (5 min at 25° C, 30 min at 42° C, 5 min at 85° C), and the cDNA was diluted 5X in DNase/RNase-free water. cDNA was amplified with TaqMan Fast Advanced

Master Mix (Thermo Fisher; Applied Biosystems, Waltham, MA (cat# 4444963), 20 sec at 95° C [initial denaturation], 1 sec at 95° C, 20 sec at 60° C, 40 cycles). TaqMan probes used were h*TULP1* (cat# hs00163236_m1), h*HSPA5* (cat# hs00607129_gH), h*DNAJB9* (cat# hs01052402_m1), h*ASNS* (cat# hs04186194_m1), and h*ACTB* (cat# hs01060665_g1; Thermo Fisher; Applied Biosystems) and quantification was performed using QuantStudio 6 Real-Time PCR software (Thermo Fisher; Applied Biosystems).

4.5.8 Cycloheximide-chase assay

Twenty-four hours after transfection with the WT TULP1 eGFP or P388S TULP1 eGFP constructs, the HEK293A cells were treated in 24-well plates with cycloheximide (25 μM; Alfa Aesar, Haverhill, MA, cat# J66901-03) for 0, 1, 3, 6, and 9 h. Cells were washed with HBSS, harvested at each time point, and then processed for western blotting. Membranes were probed with mouse anti-GFP and rabbit anti-β-actin and imaged/quantified as described above.

Appendix A Figures

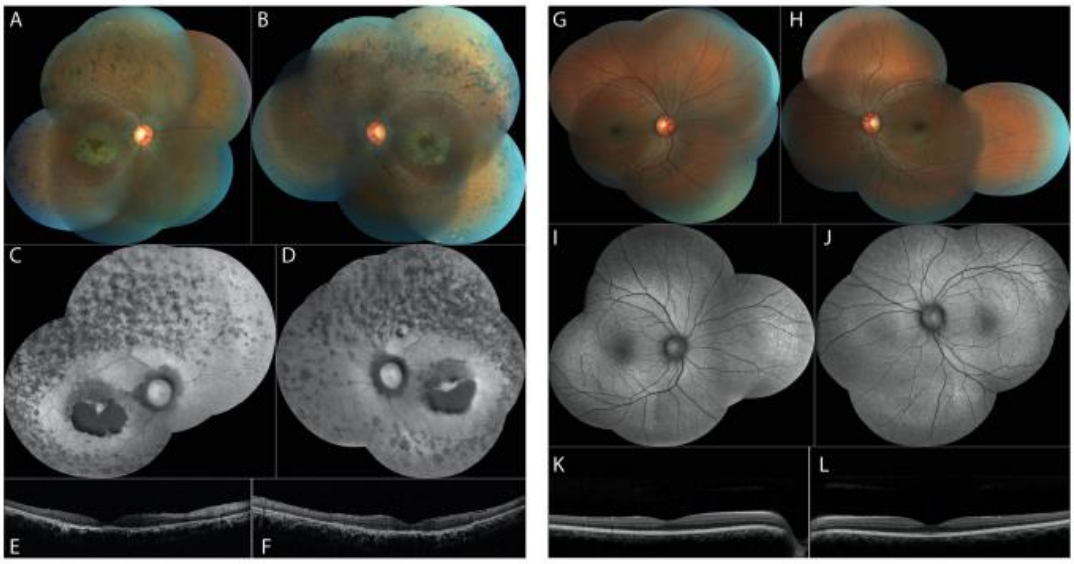

Figure 4.1: Clinical characterization of the proband. (A, B) Fundus photographs of the patient's right and left eyes showing parafoveal RPE atrophy, bone spicule-like pigmentation, and arteriolar attenuation. (C, D) Fundus autofluorescence images showing parafoveal hypoautofluorescence corresponding to the area of RPE atrophy and a patchy decrease in autofluorescence throughout the retina in both eyes. (E, F) OCT scans through the macula showing outer retinal atrophy with loss of the ellipsoid zone. (G–I) Fundus photographs, autofluorescence, and OCT images of an age-matched control subject.

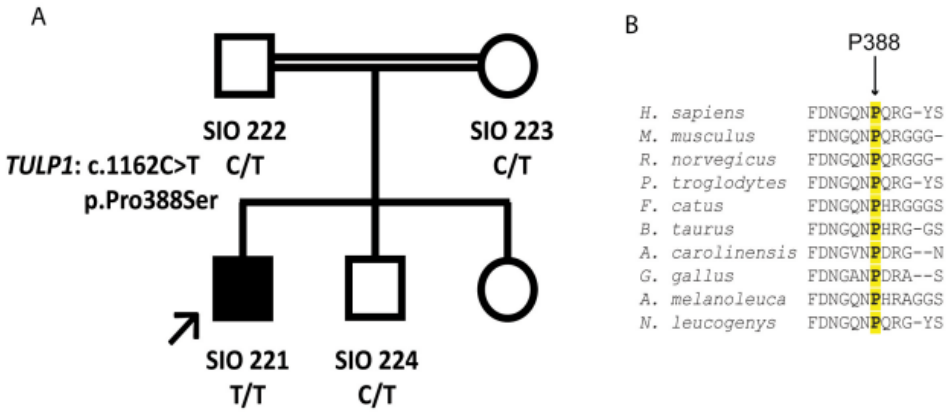

C

	GERP^{++}	CADD	PolyPhen-2	PROVEAN
P388S TULP1	4.95	26.9	0.997	-7.9
			probably damaging	deleterious

Figure 4.2: Pedigree and *in silico* analysis of the pathogenic mutation. (A) Pedigree of the consanguineous family with variant segregation based on Sanger sequencing. (B) Multiple sequence alignment of TULP1 amino acid residues across species. Arrow indicates highlighted TULP1 residue. Alignments were performed using Clustal Omega multiple sequence alignment software. (C) *In silico* prediction findings related to the P388S mutation.

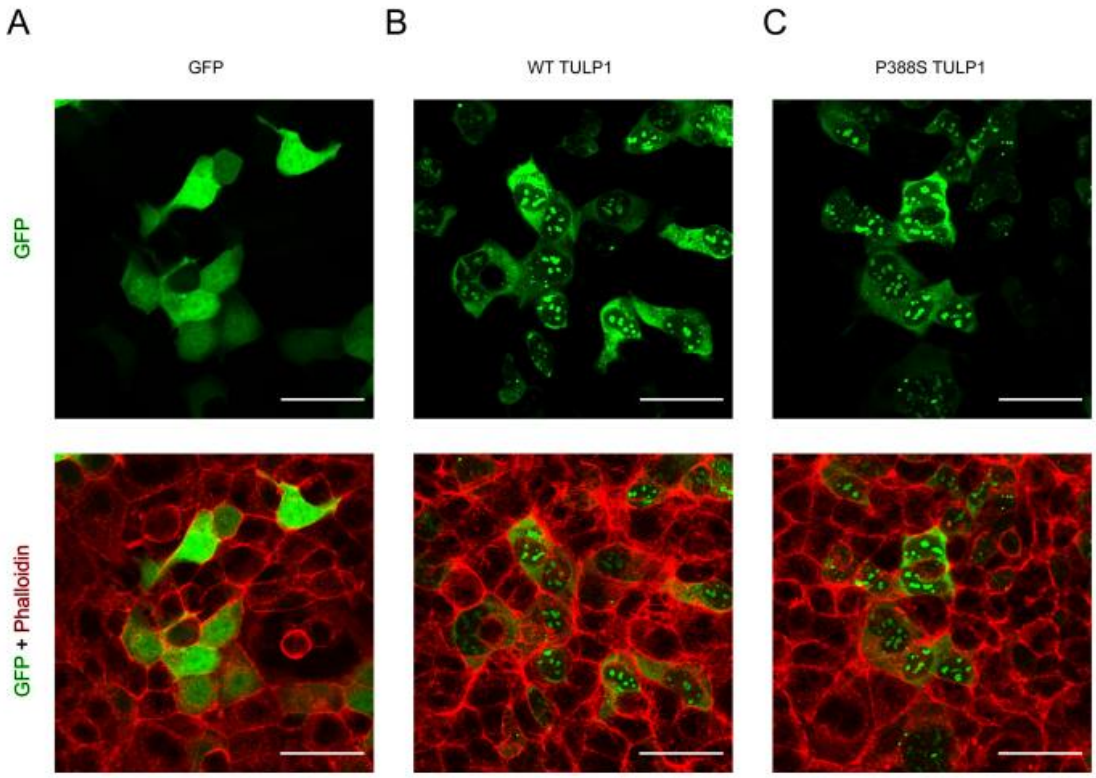

Figure 4.3: Sub-cellular localization of WT TULP1 and P388S TULP1. Representative confocal microscopy images of HEK293A cells transfected with (A) green fluorescent protein (peGFP-C1), (B) wild-type (WT) TULP1 enhanced GFP (eGFP), or (C) P388S TULP1 eGFP constructs (green) and stained with Alexa Fluor 633 phalloidin (red). Scale bar = 50 µm. TULP1 eGFP images are representative n≥5 biological, independent replicates. Phalloidin images were representative of n≥3 separate independent wells of a single transfection experiment.

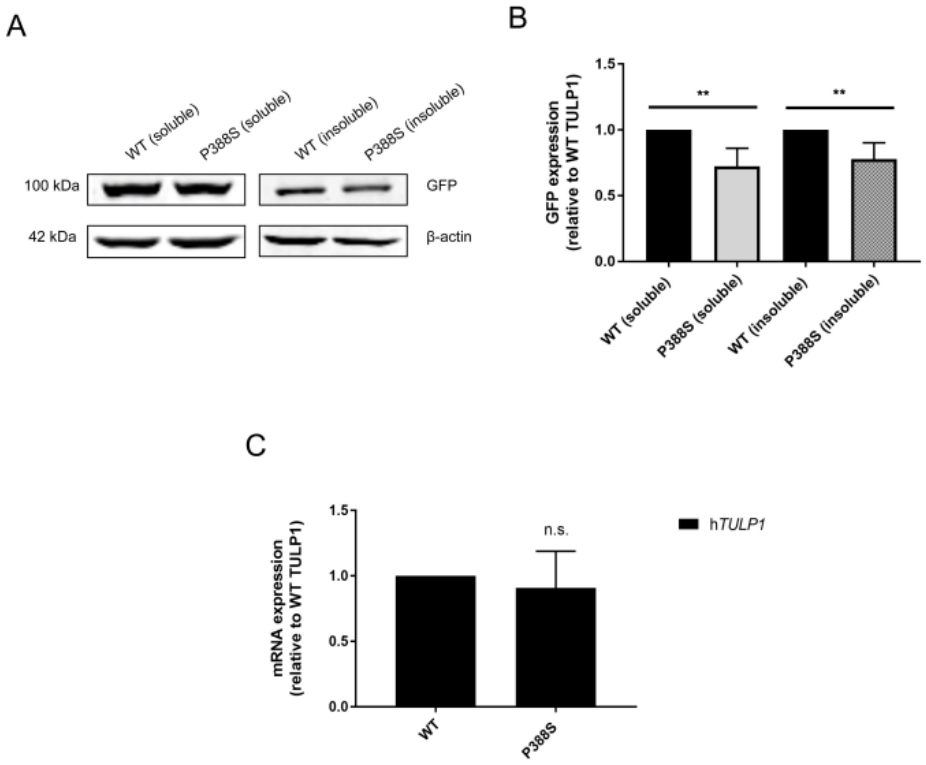

Figure 4.4: Characterization of the P388S TULP1 variant. (A) Western blot of WT and P388S TULP1 eGFP levels in soluble and insoluble fractions. (B) Quantification of WT and P388S TULP1 eGFP expression in soluble and insoluble fractions of western blot in (A), n≥5, mean ± standard deviation (SD; **p<0.01, one-sample *t* test versus hypothetical value of 1 [i.e., unchanged]). (C) qPCR of *TULP1* mRNA expression from WT and P388S TULP1 eGFP-transfected HEK293A cells. Representative data of n≥3 independent experiments, mean ± SD; n.s., not significant.

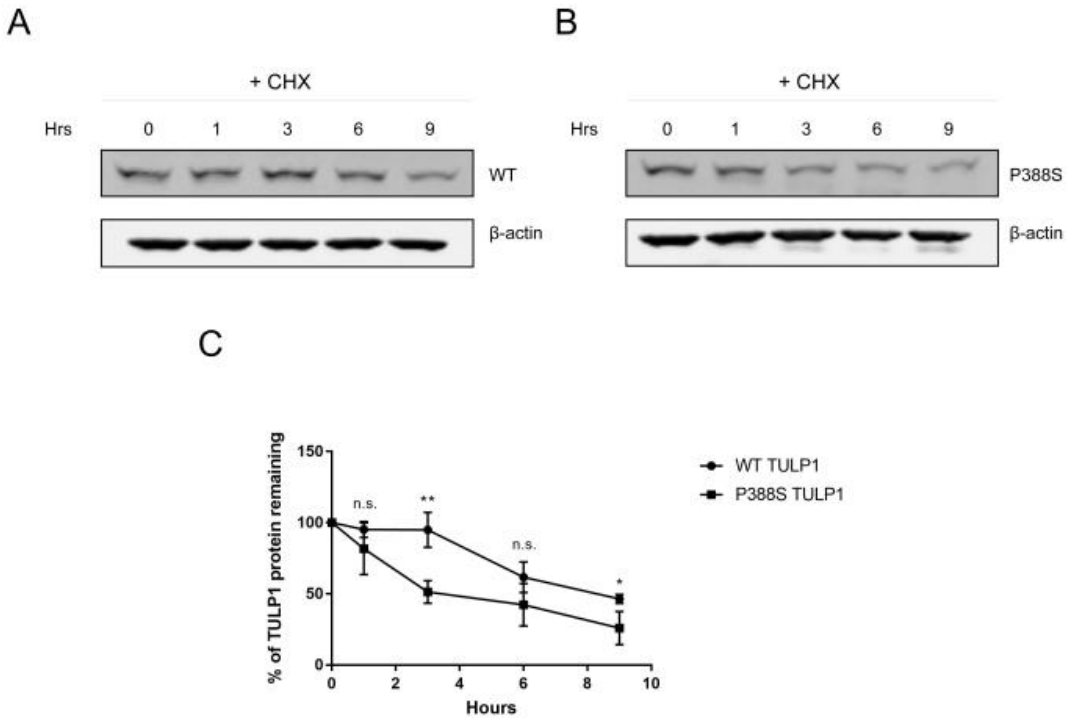

Figure 4.5: Cycloheximide chase of WT and P388S TULP1. (A, B) Western blots of WT and P388S TULP1 eGFP stability in HEK293A cells treated with 25 μM cycloheximide (CHX) and harvested at the indicated time points. (C) Quantification of western blot from (A) and (B) showing percentage of TULP1 remaining over time when treated with CHX. (●) indicates WT TULP1 eGFP, and (■) indicates P388S TULP1 eGFP. n=3 independent experiments, mean ± SD; *$p<0.05$, **$p<0.01$, two-tailed *t* test compared to each WT value, n.s., not significant.

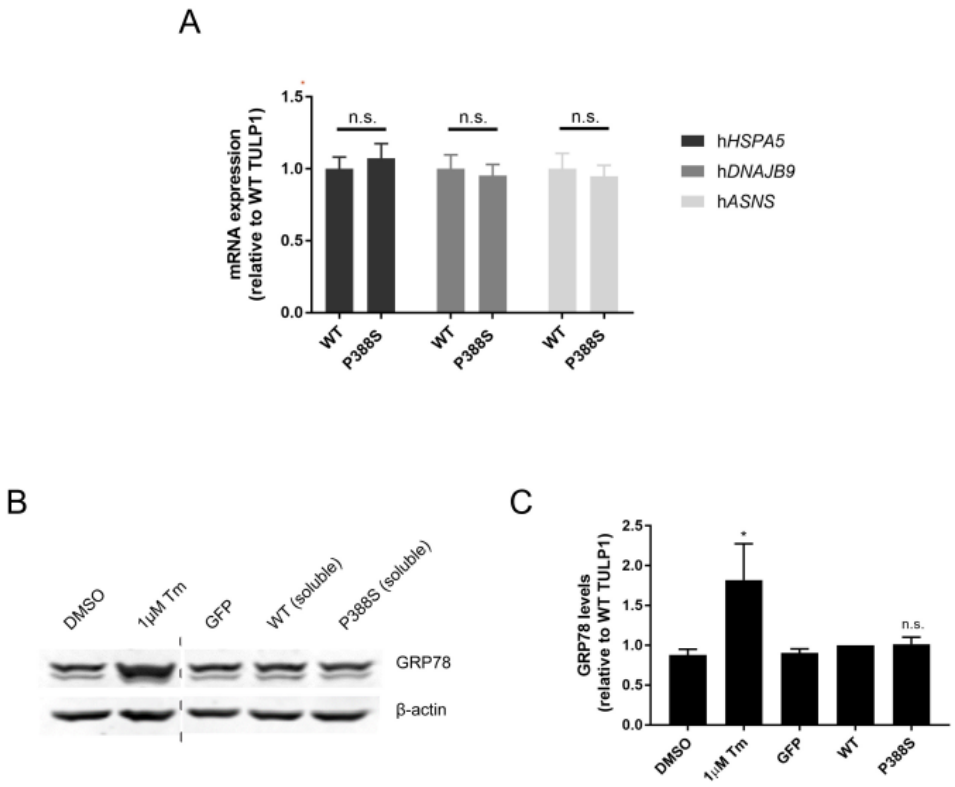

Figure 4.6: P388S TULP1 does not activate the ER stress response. (A) qPCR of h*HSPA5*, h*DNAJB9*, and h*ASNS* transcript levels with TaqMan probes in WT or P388S TULP1 eGFP-expressing HEK293A cells. (B) Western blot showing GRP78 expression in eGFP-, WT TULP1 eGFP-, or P388S TULP1 eGFP-transfected HEK293A cells. One microgram per milliliter tunicamycin (Tm) was used as a positive control to analyze GRP78 induction. (C) Quantification of western blot in (B). n=3 biological independent experiments, mean ± SD; *$p<0.05$, **$p<0.01$, one-sample *t* test versus hypothetical value of 1 (i.e., unchanged), n.s., not significant.

Reference STRs

Sample Name	D5S818	D13S317	D7S820	D16S539	VWA	TH01	AM	TPOX	CSF1PO	Multiple Profiles Seen	Match Comments
ARPE19-p5	13 13	11 12	9 11	9 11	16 19	6 9.3	X Y	9 11	11 11	NO	Sample matches ARPE-19 above the 80% match threshold. This is considered a match to ARPE-19 (ATCC).
HEK-293A-p8	8 8	12 14	11 11	9 13	16 19	7 9.3	X X	11 11	12 12	NO	Sample matches 293T above the 80% match threshold. This is considered a match to 293T (DSMZ).

Additional STRs

Sample Name	D3S1358	D21S11	D18S51	Penta_E	Penta_D	D8S1179	FGA
ARPE19-p5	14 15	28 29	12 16	7 11	11 13	13 13	23 23
HEK-293A-p8	15 17	30.2 30.2	17 17	7 15	9 9	12 14	23 23

Appendix Fig 4.1: Demonstration of STR verification of the HEK293A and ARPE-19 cell lines.

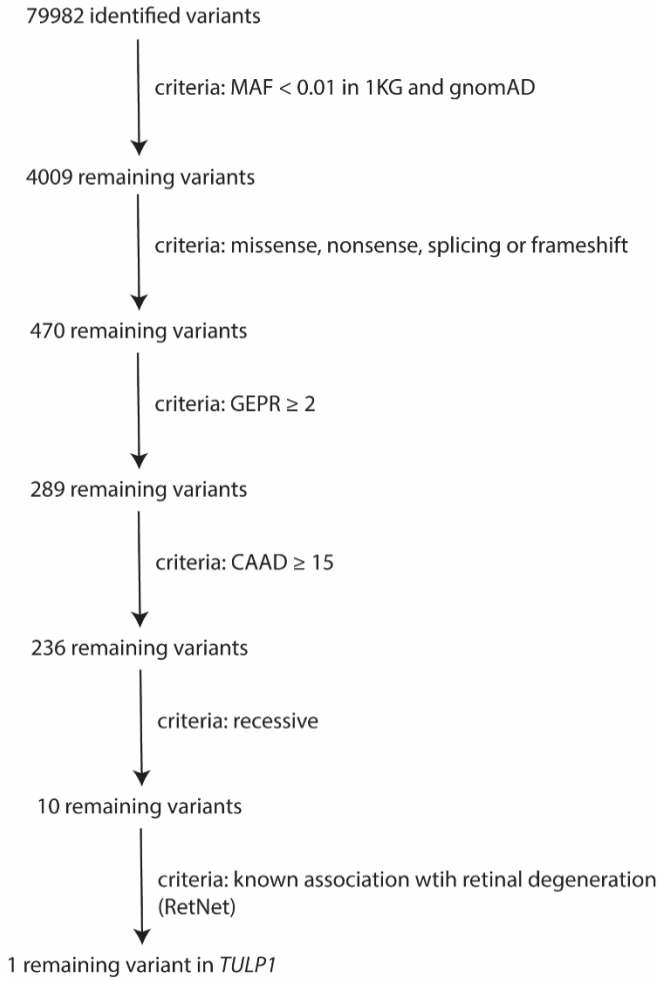

Appendix Fig 4.2: Flowchart of exome sequencing parameters used to identify pathogenic recessive mutations in RP.

chromosome	position	reference allele	alternative allele	dbSNP ID	variant quality score recalibration	variant type	annotation effect	annotation impact	protein change	gene
1	145139088	C	CG	rs150935736	6.18	INS	splice_acceptor_variant&splice_donor_variant&intron_variant	HIGH	.	NUDT4P1
12	52756723	G	T	rs745916213	3.01	SNP	missense_variant	MODERATE	p.Thr331Asn	KRT85
12	114384194	C	G	rs563542363	1.25	SNP	missense_variant	MODERATE	p.Lys498Asn	RBM19
13	73409415	C	T	rs200956787	4.79	SNP	missense_variant	MODERATE	p.His378Tyr	PIBF1
13	78216919	G	C	rs770729617	3.73	SNP	missense_variant	MODERATE	p.Glu676Gln	SCEL
6	26509316	C	T	rs781175779	1.17	SNP	missense_variant	MODERATE	p.Pro499Ser	BTN1A1
6	33172447	T	G	rs552817372	7.38	SNP	start_lost	HIGH	p.Met1?	HSD17B8
6	35471576	G	A	.	5.26	SNP	missense_variant	HIGH	p.Pro388Ser	TULP1
6	43270023	G	A	rs757872915	5.77	SNP	missense_variant	MODERATE	p.Gly383Arg	SLC22A7
6	51735388	A	G	rs552199185	3.58	SNP	missense_variant	MODERATE	p.Leu2467Pro	PKHD1

Appendix Fig 4.3: Ten genes identified in the proband were found to be in accordance with autosomal recessive inheritance.

chromosome	position	reference allele	alternative allele	dbSNP ID	variant quality score recalibration	variant type	annotation effect	annotation impact	protein change	gene
11	2181149	C	T	rs28933985	3.24	SNP	missense_variant	MODERATE	p.Arg89His	INS

Appendix Fig 4.4: Identification of the Arg89His known pathogenic variant in the *INS* gene in the proband.

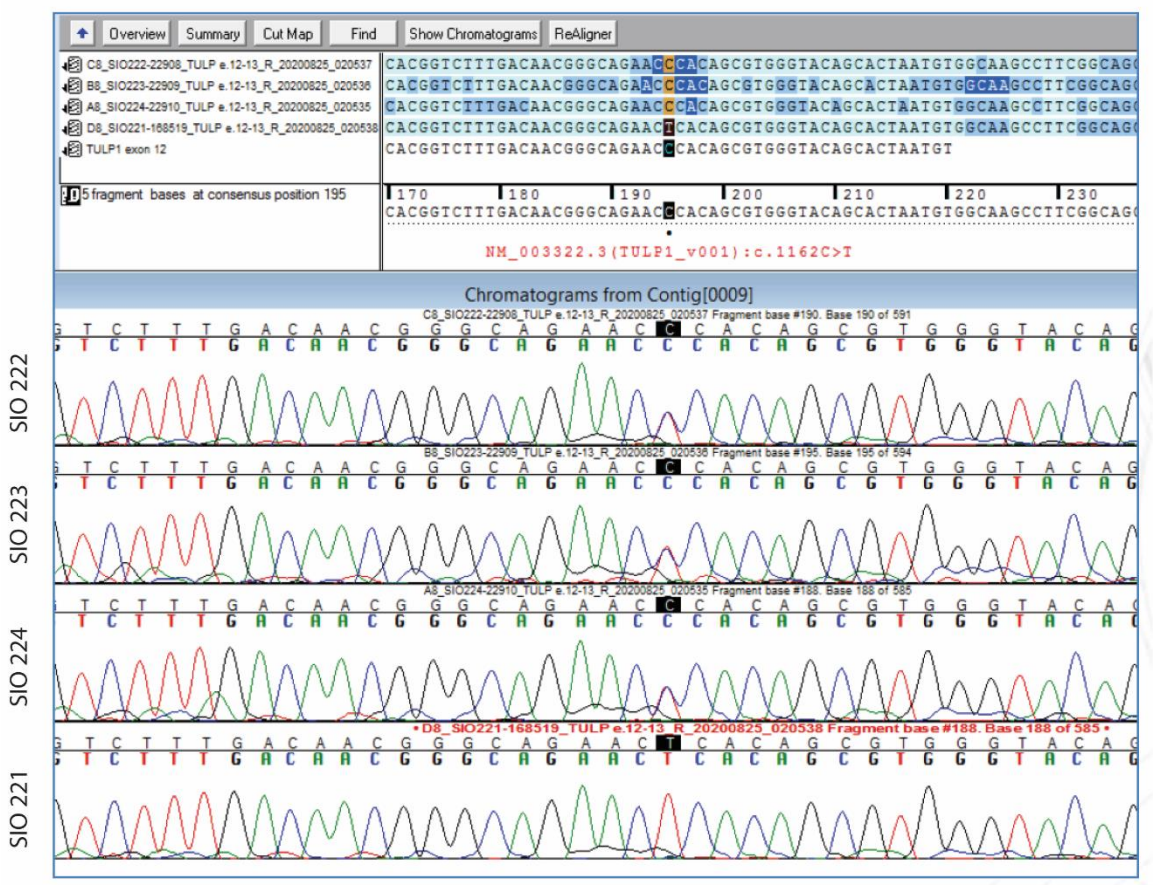

Appendix Fig 4.5: DNA sequencing chromatogram analysis of TULP1 variant in proband and family members.

Table S3

TULP1 variant	corresponding SNP	associated disease	citiation
D94Y		LCA	Beryozkin et al (2014) Invest. Ophthalmol. Vis. Sci.
S210X		RP	Glockle et al (2014) Eur. J. Hum. Genet. *
A245V	dbSNP:rs62636707	RP	Uniprot (https://www.uniprot.org/uniprot/O00294)
K261T		RP	Uniprot (https://www.uniprot.org/uniprot/O00294)
Q301X		"TULP1 retinal degeneration"	Li et al (2001) Invest. Ophthalmol. Vis. Sci.; Jacobson et al (2014) Invest. Ophthalmol. Vis. Sci.
Q301fsX8		early onset RP	Paloma et al (2000) Invest. Ophthalmol. Sci.
R311Q		RP	Hebrand et al (2011) Eur. J. Hum. Genet.
R311W/Q492R		LCA	Tajiguli et al (2016) Sci. Rep.
G319D/R482W		RP	Consugar et al (2015) Genet. Med.
Y321D		LCA	Wang et al (2013) J. Med. Genet.
Y321D/R400Q		"TULP1 retinal degeneration"	Jacobson et al (2014) Invest. Ophthalmol. Vis. Sci.
R342Q		RP	Hebrand et al (2011) Eur. J. Hum. Genet.
N349K		RP	Kannabiran et al (2012) Mol. Vis.
D355V		LCA	Wang et al (2013) J. Med. Genet.
D355V/G368W		"TULP1 retinal degeneration"	Jacobson et al (2014) Invest. Ophthalmol. Vis. Sci.
R361X/R420S		LCA	Glockle et al (2014) Eur. J. Hum. Genet.
G363R		cone/cone-rod dystrophy	Boulanger-Scemama et al (2015) Orphanet J. Rare Dis.
G368W	dbSNP:rs387906837	LCA	Hanein et al (2004) Hum. Mut.
R378H	dbSNP:rs148749577	RP	Uniprot (https://www.uniprot.org/uniprot/O00294)
T380A		LCA	McKibbin et al (2010) Arch. Ophthalmol., Ajmal et al (2012) Mol. Vis.
F382S	dbSNP:rs121909076	RP	Kondo et al (2004) Invest. Ophthalmol. Vis. Sci.
G385R		LCA	Wang et al (2015) Invest. Ophtalmol. Vis. Sci.
P388S		RP	this study
R400W	dbSNP:rs387906836	LCA15/"TULP1 retinal degeneration"	Hanein et al (2004) Hum. Mut.; Jacobson et al (2014) Invest. Ophthalmol. Vis. Sci.
R400Q		RP	Singh et al (2009) Invest. Ophtalmol. Vis. Sci.
E402X		LCA	Hanein et al (2004) Hum. Mut.
A405P		RP	Ge et al (2015) Sci. Rep.
R416C		RP	Katagiri et al (2014) PLoS One
R419W		retinal dystrophy	Sanchez-Alcudia (2014) Invest. Ophthalmol. Vis. Sci.
R420P/F491L	dbSNP:rs121909073, dbSNP:rs121909074	RP	Hagstrom et al (1998) Nat. Genet.
R420S		cone dysfunction	Roosing et al (2013) Ophthalmol.
P426L/F506L		LCA	Wang et al (2013) J. Med. Genet.
R440X		LCA	Wang et al (2015) Invest. Ophtalmol. Vis. Sci.
W450X		LCA/Coat's-like changes	Beryozkin et al (2014) Invest. Ophthalmol. Vis. Sci.
T454M	dbSNP:rs138200747	RP	Hagstrom et al (1998) Nat. Genet.
I459K	dbSNP:rs121909075	RP	Hagstrom et al (1998) Nat. Genet.
L461V		RP	den Hollander et al (2007) Invest. Ophthalmol. Vis. Sci.
R482Q		RP	Ajmal et al (2012) Mol. Vis.
R482W/L504fsX140	dbSNP:rs121909077	RP	den Hollander et al (2007) Arch. Ophthalmol.
Q492R		LCA	Tajiguli et al (2016) Sci. Rep.
P499S		RP	Ge et al (2015) Sci. Rep.
F506L		LCA	Wang et al (2013) J. Med. Genet.
FA531-532 dup.		LCA/RP	Mataftsi et al (2007) Invest. Ophthalmol. Vis. Sci.
F535S		LCA	Eisenberger et al (2013) PLoS One
			* = additional mutations identified in USH2A, ABCA4, PRCD identified in this patient

Appendix Fig 4.6: Known mutations in TULP1 identified in patients with RP or LCA.

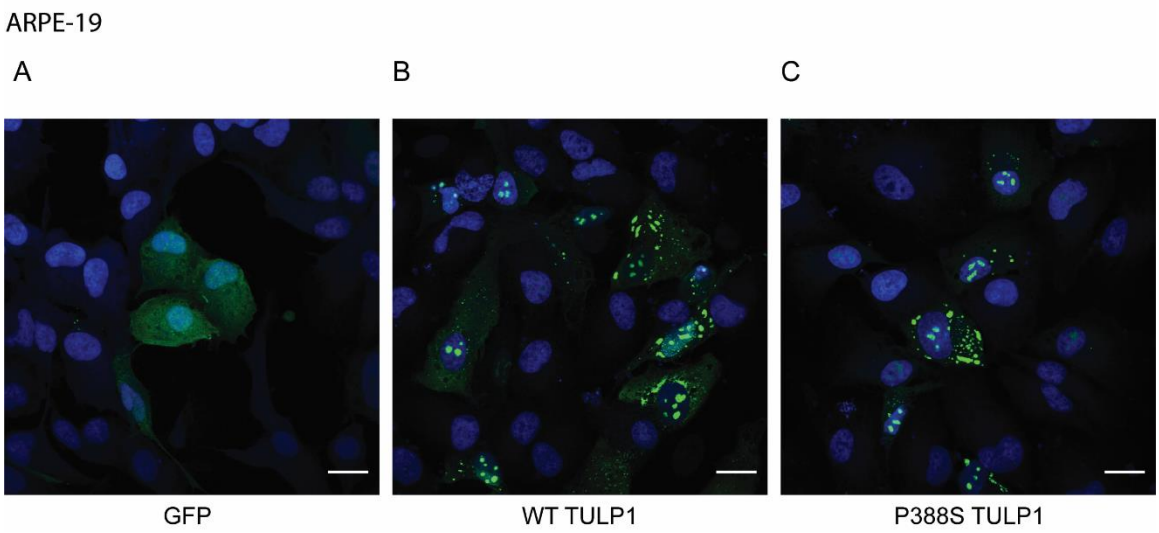

Appendix Fig 4.7: Sub-cellular localization of WT TULP1 and P388S TULP1 in ARPE-19 cells.

BIBLIOGRAPHY

1. Majid, A.; Roberts, S. G.; Cilissen, L.; Emmorey, K.; Nicodemus, B.; O'Grady, L.; Woll, B.; LeLan, B.; de Sousa, H.; Cansler, B. L.; Shayan, S.; de Vos, C.; Senft, G.; Enfield, N. J.; Razak, R. A.; Fedden, S.; Tufvesson, S.; Dingemanse, M.; Ozturk, O.; Brown, P.; Hill, C.; Le Guen, O.; Hirtzel, V.; van Gijn, R.; Sicoli, M. A.; Levinson, S. C., Differential coding of perception in the world's languages. *Proc Natl Acad Sci U S A* **2018,** *115* (45), 11369-11376.
2. Aristotle. Metaphysics. *Cambridge: Harvard University Press* **1933,** *17 & 18*.
3. Ajina, S.; Bridge, H., Blindsight and Unconscious Vision: What They Teach Us about the Human Visual System. *Neuroscientist* **2016,** *23* (5), 529-541.
4. Pradeep, T.; Mehra, D.; Le, P. H., Histology, Eye. In *StatPearls*, Treasure Island (FL), 2021.
5. Akpek, E. K.; Gottsch, J. D., Immune defense at the ocular surface. *Eye (Lond)* **2003,** *17* (8), 949-56.
6. Coudrillier, B.; Pijanka, J.; Jefferys, J.; Sorensen, T.; Quigley, H. A.; Boote, C.; Nguyen, T. D., Collagen structure and mechanical properties of the human sclera: analysis for the effects of age. *J Biomech Eng* **2015,** *137* (4), 041006.
7. Boote, C.; Sigal, I. A.; Grytz, R.; Hua, Y.; Nguyen, T. D.; Girard, M. J. A., Scleral structure and biomechanics. *Prog Retin Eye Res* **2020,** *74*, 100773.
8. Sridhar, M. S., Anatomy of cornea and ocular surface. *Indian J Ophthalmol* **2018,** *66* (2), 190-194.
9. Bouffard, M. A., The Pupil. *Continuum (Minneap Minn)* **2019,** *25* (5), 1194-1214.
10. Janssen, S. F.; Gorgels, T. G.; Bossers, K.; Ten Brink, J. B.; Essing, A. H.; Nagtegaal, M.; van der Spek, P. J.; Jansonius, N. M.; Bergen, A. A., Gene expression and functional annotation of the human ciliary body epithelia. *PLoS One* **2012,** *7* (9), e44973.
11. Goel, M.; Picciani, R. G.; Lee, R. K.; Bhattacharya, S. K., Aqueous humor dynamics: a review. *Open Ophthalmol J* **2010,** *4*, 52-9.
12. Nickla, D. L.; Wallman, J., The multifunctional choroid. *Prog Retin Eye Res* **2010,** *29* (2), 144-68.
13. Hejtmancik, J. F.; Shiels, A., Overview of the Lens. *Prog Mol Biol Transl Sci* **2015,** *134*, 119-27.
14. Tram, N. K.; Swindle-Reilly, K. E., Rheological Properties and Age-Related Changes of the Human Vitreous Humor. *Front Bioeng Biotechnol* **2018,** *6*, 199.
15. Kolb, H., Simple Anatomy of the Retina. In *Webvision: The Organization of the Retina and Visual System*, Kolb, H.; Fernandez, E.; Nelson, R., Eds. Salt Lake City (UT), 1995.

16. Spadea, L.; Maraone, G.; Verboschi, F.; Vingolo, E. M.; Tognetto, D., Effect of corneal light scatter on vision: a review of the literature. *Int J Ophthalmol* **2016,** *9* (3), 459-64.
17. Masland, R. H., The neuronal organization of the retina. *Neuron* **2012,** *76* (2), 266-80.
18. Mahabadi, N.; Al Khalili, Y., Neuroanatomy, Retina. In *StatPearls*, Treasure Island (FL), 2021.
19. Morgan, J.; Wong, R., Development of Cell Types and Synaptic Connections in the Retina. In *Webvision: The Organization of the Retina and Visual System*, Kolb, H.; Fernandez, E.; Nelson, R., Eds. Salt Lake City (UT), 1995.
20. Chirco, K. R.; Sohn, E. H.; Stone, E. M.; Tucker, B. A.; Mullins, R. F., Structural and molecular changes in the aging choroid: implications for age-related macular degeneration. *Eye (Lond)* **2017,** *31* (1), 10-25.
21. Sung, C. H.; Chuang, J. Z., The cell biology of vision. *J Cell Biol* **2010,** *190* (6), 953-63.
22. Mehra, D.; Le, P. H., Physiology, Night Vision. In *StatPearls*, Treasure Island (FL), 2021.
23. Molday, R. S.; Moritz, O. L., Photoreceptors at a glance. *J Cell Sci* **2015,** *128* (22), 4039-45.
24. Lamb, T. D., Why rods and cones? *Eye (Lond)* **2016,** *30* (2), 179-85.
25. Mustafi, D.; Engel, A. H.; Palczewski, K., Structure of cone photoreceptors. *Prog Retin Eye Res* **2009,** *28* (4), 289-302.
26. Costa, M.; Bonetti, L.; Vignali, V.; Lantieri, C.; Simone, A., The role of peripheral vision in vertical road sign identification and discrimination. *Ergonomics* **2018,** *61* (12), 1619-1634.
27. Goldberg, A. F.; Moritz, O. L.; Williams, D. S., Molecular basis for photoreceptor outer segment architecture. *Prog Retin Eye Res* **2016,** *55*, 52-81.
28. Lamb, T. D.; Pugh, E. N., Jr., Phototransduction, dark adaptation, and rhodopsin regeneration the proctor lecture. *Invest Ophthalmol Vis Sci* **2006,** *47* (12), 5137-52.
29. Fu, Y.; Yau, K. W., Phototransduction in mouse rods and cones. *Pflugers Arch* **2007,** *454* (5), 805-19.
30. Baker, S. A.; Kerov, V., Photoreceptor inner and outer segments. *Curr Top Membr* **2013,** *72*, 231-65.
31. Morgans, C. W., Neurotransmitter release at ribbon synapses in the retina. *Immunol Cell Biol* **2000,** *78* (4), 442-6.
32. Veleri, S.; Lazar, C. H.; Chang, B.; Sieving, P. A.; Banin, E.; Swaroop, A., Biology and therapy of inherited retinal degenerative disease: insights from mouse models. *Dis Model Mech* **2015,** *8* (2), 109-29.
33. Simo, R.; Villarroel, M.; Corraliza, L.; Hernandez, C.; Garcia-Ramirez, M., The retinal pigment epithelium: something more than a constituent of the blood-retinal barrier--implications for the pathogenesis of diabetic retinopathy. *J Biomed Biotechnol* **2010,** *2010*, 190724.

34. Kay, P.; Yang, Y. C.; Paraoan, L., Directional protein secretion by the retinal pigment epithelium: roles in retinal health and the development of age-related macular degeneration. *J Cell Mol Med* **2013,** *17* (7), 833-43.
35. Sparrow, J. R.; Hicks, D.; Hamel, C. P., The retinal pigment epithelium in health and disease. *Curr Mol Med* **2010,** *10* (9), 802-23.
36. Bonilha, V. L.; Rayborn, M. E.; Bhattacharya, S. K.; Gu, X.; Crabb, J. S.; Crabb, J. W.; Hollyfield, J. G., The retinal pigment epithelium apical microvilli and retinal function. *Adv Exp Med Biol* **2006,** *572*, 519-24.
37. Bok, D., The retinal pigment epithelium: a versatile partner in vision. *J Cell Sci Suppl* **1993,** *17*, 189-95.
38. Kocaoglu, O. P.; Liu, Z.; Zhang, F.; Kurokawa, K.; Jonnal, R. S.; Miller, D. T., Photoreceptor disc shedding in the living human eye. *Biomed Opt Express* **2016,** *7* (11), 4554-4568.
39. Young, R. W., The renewal of photoreceptor cell outer segments. *J Cell Biol* **1967,** *33* (1), 61-72.
40. Kevany, B. M.; Palczewski, K., Phagocytosis of retinal rod and cone photoreceptors. *Physiology (Bethesda)* **2010,** *25* (1), 8-15.
41. Young, R. W., The renewal of rod and cone outer segments in the rhesus monkey. *J Cell Biol* **1971,** *49* (2), 303-18.
42. Young, R. W.; Bok, D., Participation of the retinal pigment epithelium in the rod outer segment renewal process. *J Cell Biol* **1969,** *42* (2), 392-403.
43. Ban, Y.; Rizzolo, L. J., Differential regulation of tight junction permeability during development of the retinal pigment epithelium. *Am J Physiol Cell Physiol* **2000,** *279* (3), C744-50.
44. Ao, J.; Wood, J. P.; Chidlow, G.; Gillies, M. C.; Casson, R. J., Retinal pigment epithelium in the pathogenesis of age-related macular degeneration and photobiomodulation as a potential therapy? *Clin Exp Ophthalmol* **2018,** *46* (6), 670-686.
45. Fu, Z.; Kern, T. S.; Hellstrom, A.; Smith, L. E. H., Fatty acid oxidation and photoreceptor metabolic needs. *J Lipid Res* **2021,** *62*, 100035.
46. Adijanto, J.; Du, J.; Moffat, C.; Seifert, E. L.; Hurle, J. B.; Philp, N. J., The retinal pigment epithelium utilizes fatty acids for ketogenesis. *J Biol Chem* **2014,** *289* (30), 20570-82.
47. Boulton, M.; Dayhaw-Barker, P., The role of the retinal pigment epithelium: topographical variation and ageing changes. *Eye (Lond)* **2001,** *15* (Pt 3), 384-9.
48. Choi, E. H.; Daruwalla, A.; Suh, S.; Leinonen, H.; Palczewski, K., Retinoids in the visual cycle: role of the retinal G protein-coupled receptor. *J Lipid Res* **2021,** *62*, 100040.
49. Tsin, A.; Betts-Obregon, B.; Grigsby, J., Visual cycle proteins: Structure, function, and roles in human retinal disease. *J Biol Chem* **2018,** *293* (34), 13016-13021.
50. Kiser, P. D.; Golczak, M.; Maeda, A.; Palczewski, K., Key enzymes of the retinoid (visual) cycle in vertebrate retina. *Biochim Biophys Acta* **2012,** *1821* (1), 137-51.

51. Strauss, O., The retinal pigment epithelium in visual function. *Physiol Rev* **2005,** *85* (3), 845-81.
52. Miceli, M. V.; Liles, M. R.; Newsome, D. A., Evaluation of oxidative processes in human pigment epithelial cells associated with retinal outer segment phagocytosis. *Exp Cell Res* **1994,** *214* (1), 242-9.
53. Beatty, S.; Boulton, M.; Henson, D.; Koh, H. H.; Murray, I. J., Macular pigment and age related macular degeneration. *Br J Ophthalmol* **1999,** *83* (7), 867-77.
54. Feeney, L., Lipofuscin and melanin of human retinal pigment epithelium. Fluorescence, enzyme cytochemical, and ultrastructural studies. *Invest Ophthalmol Vis Sci* **1978,** *17* (7), 583-600.
55. Nita, M.; Grzybowski, A., The Role of the Reactive Oxygen Species and Oxidative Stress in the Pathomechanism of the Age-Related Ocular Diseases and Other Pathologies of the Anterior and Posterior Eye Segments in Adults. *Oxid Med Cell Longev* **2016,** *2016*, 3164734.
56. Colak, E.; Ignjatovic, S.; Radosavljevic, A.; Zoric, L., The association of enzymatic and non-enzymatic antioxidant defense parameters with inflammatory markers in patients with exudative form of age-related macular degeneration. *J Clin Biochem Nutr* **2017,** *60* (2), 100-107.
57. Wang, Y.; Subramanian, P.; Shen, D.; Tuo, J.; Becerra, S. P.; Chan, C. C., Pigment epithelium-derived factor reduces apoptosis and pro-inflammatory cytokine gene expression in a murine model of focal retinal degeneration. *ASN Neuro* **2013,** *5* (5), e00126.
58. Saint-Geniez, M.; Maldonado, A. E.; D'Amore, P. A., VEGF expression and receptor activation in the choroid during development and in the adult. *Invest Ophthalmol Vis Sci* **2006,** *47* (7), 3135-42.
59. Kim, J.; Gee, H. Y.; Lee, M. G., Unconventional protein secretion - new insights into the pathogenesis and therapeutic targets of human diseases. *J Cell Sci* **2018,** *131* (12).
60. Keller, P.; Simons, K., Post-Golgi biosynthetic trafficking. *J Cell Sci* **1997,** *110 (Pt 24)*, 3001-9.
61. Mostov, K. E., Regulation of protein traffic in polarized epithelial cells. *Histol Histopathol* **1995,** *10* (2), 423-31.
62. Rodriguez-Boulan, E.; Zurzolo, C., Polarity signals in epithelial cells. *J Cell Sci Suppl* **1993,** *17*, 9-12.
63. Fields, M. A.; Del Priore, L. V.; Adelman, R. A.; Rizzolo, L. J., Interactions of the choroid, Bruch's membrane, retinal pigment epithelium, and neurosensory retina collaborate to form the outer blood-retinal-barrier. *Prog Retin Eye Res* **2020,** *76*, 100803.
64. Edwards, M.; Lutty, G. A., Bruch's Membrane and the Choroid in Age-Related Macular Degeneration. *Adv Exp Med Biol* **2021,** *1256*, 89-119.
65. Liu, L.; Liu, X., Roles of Drug Transporters in Blood-Retinal Barrier. *Adv Exp Med Biol* **2019,** *1141*, 467-504.

66. Bhutto, I.; Lutty, G., Understanding age-related macular degeneration (AMD): relationships between the photoreceptor/retinal pigment epithelium/Bruch's membrane/choriocapillaris complex. *Mol Aspects Med* **2012,** *33* (4), 295-317.
67. Grover, L. L., Making Eye Health a Population Imperative: A Vision for Tomorrow-A Report by the Committee on Public Health Approaches to Reduce Vision Impairment and Promote Eye Health. *Optom Vis Sci* **2017,** *94* (4), 444-445.
68. Swenor, B. K.; Ehrlich, J. R., Ageing and vision loss: looking to the future. *Lancet Glob Health* **2021,** *9* (4), e385-e386.
69. Lopez-Otin, C.; Blasco, M. A.; Partridge, L.; Serrano, M.; Kroemer, G., The hallmarks of aging. *Cell* **2013,** *153* (6), 1194-217.
70. Rebelo-Marques, A.; De Sousa Lages, A.; Andrade, R.; Ribeiro, C. F.; Mota-Pinto, A.; Carrilho, F.; Espregueira-Mendes, J., Aging Hallmarks: The Benefits of Physical Exercise. *Front Endocrinol (Lausanne)* **2018,** *9*, 258.
71. Gipson, I. K., Age-related changes and diseases of the ocular surface and cornea. *Invest Ophthalmol Vis Sci* **2013,** *54* (14), ORSF48-53.
72. Faragher, R. G.; Mulholland, B.; Tuft, S. J.; Sandeman, S.; Khaw, P. T., Aging and the cornea. *Br J Ophthalmol* **1997,** *81* (10), 814-7.
73. Salvi, S. M.; Akhtar, S.; Currie, Z., Ageing changes in the eye. *Postgrad Med J* **2006,** *82* (971), 581-7.
74. Panda-Jonas, S.; Jonas, J. B.; Jakobczyk-Zmija, M., Retinal photoreceptor density decreases with age. *Ophthalmology* **1995,** *102* (12), 1853-9.
75. Bonilha, V. L., Age and disease-related structural changes in the retinal pigment epithelium. *Clin Ophthalmol* **2008,** *2* (2), 413-24.
76. Hashemi, H.; Khabazkhoob, M.; Nabovati, P.; Ostadimoghaddam, H.; Shafaee, S.; Doostdar, A.; Yekta, A., The Prevalence of Age-Related Eye Disease in an Elderly Population. *Ophthalmic Epidemiol* **2017,** *24* (4), 222-228.
77. Umfress, A. C.; Brantley, M. A., Jr., Eye Care Disparities and Health-Related Consequences in Elderly Patients with Age-Related Eye Disease. *Semin Ophthalmol* **2016,** *31* (4), 432-8.
78. Ehrlich, R.; Harris, A.; Kheradiya, N. S.; Winston, D. M.; Ciulla, T. A.; Wirostko, B., Age-related macular degeneration and the aging eye. *Clin Interv Aging* **2008,** *3* (3), 473-82.
79. Klein, R.; Klein, B. E.; Jensen, S. C.; Meuer, S. M., The five-year incidence and progression of age-related maculopathy: the Beaver Dam Eye Study. *Ophthalmology* **1997,** *104* (1), 7-21.
80. Gehrs, K. M.; Anderson, D. H.; Johnson, L. V.; Hageman, G. S., Age-related macular degeneration--emerging pathogenetic and therapeutic concepts. *Ann Med* **2006,** *38* (7), 450-71.
81. Pennington, K. L.; DeAngelis, M. M., Epidemiology of age-related macular degeneration (AMD): associations with cardiovascular disease phenotypes and lipid factors. *Eye Vis (Lond)* **2016,** *3*, 34.

82. Wong, W. L.; Su, X.; Li, X.; Cheung, C. M.; Klein, R.; Cheng, C. Y.; Wong, T. Y., Global prevalence of age-related macular degeneration and disease burden projection for 2020 and 2040: a systematic review and meta-analysis. *Lancet Glob Health* **2014,** *2* (2), e106-16.
83. Fine, S. L.; Berger, J. W.; Maguire, M. G.; Ho, A. C., Age-related macular degeneration. *N Engl J Med* **2000,** *342* (7), 483-92.
84. Seddon, J. M.; Rosner, B.; Sperduto, R. D.; Yannuzzi, L.; Haller, J. A.; Blair, N. P.; Willett, W., Dietary fat and risk for advanced age-related macular degeneration. *Arch Ophthalmol* **2001,** *119* (8), 1191-9.
85. Velilla, S.; Garcia-Medina, J. J.; Garcia-Layana, A.; Dolz-Marco, R.; Pons-Vazquez, S.; Pinazo-Duran, M. D.; Gomez-Ulla, F.; Arevalo, J. F.; Diaz-Llopis, M.; Gallego-Pinazo, R., Smoking and age-related macular degeneration: review and update. *J Ophthalmol* **2013,** *2013*, 895147.
86. Coleman, A. L.; Seitzman, R. L.; Cummings, S. R.; Yu, F.; Cauley, J. A.; Ensrud, K. E.; Stone, K. L.; Hochberg, M. C.; Pedula, K. L.; Thomas, E. L.; Mangione, C. M.; Study Of Osteoporotic Fractures Research, G., The association of smoking and alcohol use with age-related macular degeneration in the oldest old: the Study of Osteoporotic Fractures. *Am J Ophthalmol* **2010,** *149* (1), 160-9.
87. Chan, D., Cigarette smoking and age-related macular degeneration. *Optom Vis Sci* **1998,** *75* (7), 476-84.
88. Colijn, J. M.; Buitendijk, G. H. S.; Prokofyeva, E.; Alves, D.; Cachulo, M. L.; Khawaja, A. P.; Cougnard-Gregoire, A.; Merle, B. M. J.; Korb, C.; Erke, M. G.; Bron, A.; Anastasopoulos, E.; Meester-Smoor, M. A.; Segato, T.; Piermarocchi, S.; de Jong, P.; Vingerling, J. R.; Topouzis, F.; Creuzot-Garcher, C.; Bertelsen, G.; Pfeiffer, N.; Fletcher, A. E.; Foster, P. J.; Silva, R.; Korobelnik, J. F.; Delcourt, C.; Klaver, C. C. W.; consortium, E.-R.; European Eye Epidemiology, c., Prevalence of Age-Related Macular Degeneration in Europe: The Past and the Future. *Ophthalmology* **2017,** *124* (12), 1753-1763.
89. Bourne, R. R.; Jonas, J. B.; Flaxman, S. R.; Keeffe, J.; Leasher, J.; Naidoo, K.; Parodi, M. B.; Pesudovs, K.; Price, H.; White, R. A.; Wong, T. Y.; Resnikoff, S.; Taylor, H. R.; Vision Loss Expert Group of the Global Burden of Disease, S., Prevalence and causes of vision loss in high-income countries and in Eastern and Central Europe: 1990-2010. *Br J Ophthalmol* **2014,** *98* (5), 629-38.
90. Landowski, M.; Kelly, U.; Klingeborn, M.; Groelle, M.; Ding, J. D.; Grigsby, D.; Bowes Rickman, C., Human complement factor H Y402H polymorphism causes an age-related macular degeneration phenotype and lipoprotein dysregulation in mice. *Proc Natl Acad Sci U S A* **2019,** *116* (9), 3703-3711.
91. Geerlings, M. J.; de Jong, E. K.; den Hollander, A. I., The complement system in age-related macular degeneration: A review of rare genetic variants and implications for personalized treatment. *Mol Immunol* **2017,** *84*, 65-76.
92. Tuo, J.; Bojanowski, C. M.; Chan, C. C., Genetic factors of age-related macular degeneration. *Prog Retin Eye Res* **2004,** *23* (2), 229-49.

93. Chen, Y.; Bedell, M.; Zhang, K., Age-related macular degeneration: genetic and environmental factors of disease. *Mol Interv* **2010,** *10* (5), 271-81.
94. Pool, F. M.; Kiel, C.; Serrano, L.; Luthert, P. J., Repository of proposed pathways and protein-protein interaction networks in age-related macular degeneration. *NPJ Aging Mech Dis* **2020,** *6*, 2.
95. Garcia-Layana, A.; Cabrera-Lopez, F.; Garcia-Arumi, J.; Arias-Barquet, L.; Ruiz-Moreno, J. M., Early and intermediate age-related macular degeneration: update and clinical review. *Clin Interv Aging* **2017,** *12*, 1579-1587.
96. Cornel, S.; Adriana, I. D.; Mihaela, T. C.; Speranta, S.; Algerino, S.; Mehdi, B.; Jalaladin, H. R., Anti-vascular endothelial growth factor indications in ocular disease. *Rom J Ophthalmol* **2015,** *59* (4), 235-242.
97. Ambati, J.; Fowler, B. J., Mechanisms of age-related macular degeneration. *Neuron* **2012,** *75* (1), 26-39.
98. Bressler, N. M., Early detection and treatment of neovascular age-related macular degeneration. *J Am Board Fam Pract* **2002,** *15* (2), 142-52.
99. Abdelsalam, A.; Del Priore, L.; Zarbin, M. A., Drusen in age-related macular degeneration: pathogenesis, natural course, and laser photocoagulation-induced regression. *Surv Ophthalmol* **1999,** *44* (1), 1-29.
100. Zhang, X.; Sivaprasad, S., Drusen and pachydrusen: the definition, pathogenesis, and clinical significance. *Eye (Lond)* **2021,** *35* (1), 121-133.
101. Spaide, R. F.; Curcio, C. A., Drusen characterization with multimodal imaging. *Retina* **2010,** *30* (9), 1441-54.
102. Age-Related Eye Disease Study Research, G., The Age-Related Eye Disease Study (AREDS): design implications. AREDS report no. 1. *Control Clin Trials* **1999,** *20* (6), 573-600.
103. Age-Related Eye Disease Study Research, G., A randomized, placebo-controlled, clinical trial of high-dose supplementation with vitamins C and E, beta carotene, and zinc for age-related macular degeneration and vision loss: AREDS report no. 8. *Arch Ophthalmol* **2001,** *119* (10), 1417-36.
104. Institute, N. N. E., AREDS/AREDS2 Clinical Trials. **2020**.
105. Group, A. R.; Chew, E. Y.; Clemons, T.; SanGiovanni, J. P.; Danis, R.; Domalpally, A.; McBee, W.; Sperduto, R.; Ferris, F. L., The Age-Related Eye Disease Study 2 (AREDS2): study design and baseline characteristics (AREDS2 report number 1). *Ophthalmology* **2012,** *119* (11), 2282-9.
106. Aronow, M. E.; Chew, E. Y., Age-related Eye Disease Study 2: perspectives, recommendations, and unanswered questions. *Curr Opin Ophthalmol* **2014,** *25* (3), 186-90.
107. Chew, E. Y.; Clemons, T. E.; Agron, E.; Launer, L. J.; Grodstein, F.; Bernstein, P. S.; Age-Related Eye Disease Study 2 Research, G., Effect of Omega-3 Fatty Acids, Lutein/Zeaxanthin, or Other Nutrient Supplementation on Cognitive Function: The AREDS2 Randomized Clinical Trial. *JAMA* **2015,** *314* (8), 791-801.

108. Carneiro, A.; Andrade, J. P., Nutritional and Lifestyle Interventions for Age-Related Macular Degeneration: A Review. *Oxid Med Cell Longev* **2017,** *2017*, 6469138.
109. Cabral de Guimaraes, T. A.; Daich Varela, M.; Georgiou, M.; Michaelides, M., Treatments for dry age-related macular degeneration: therapeutic avenues, clinical trials and future directions. *Br J Ophthalmol* **2021**.
110. Livingstone, I.; Uversky, V. N.; Furniss, D.; Wiberg, A., The Pathophysiological Significance of Fibulin-3. *Biomolecules* **2020,** *10* (9).
111. Stone, E. M.; Lotery, A. J.; Munier, F. L.; Heon, E.; Piguet, B.; Guymer, R. H.; Vandenburgh, K.; Cousin, P.; Nishimura, D.; Swiderski, R. E.; Silvestri, G.; Mackey, D. A.; Hageman, G. S.; Bird, A. C.; Sheffield, V. C.; Schorderet, D. F., A single EFEMP1 mutation associated with both Malattia Leventinese and Doyne honeycomb retinal dystrophy. *Nat Genet* **1999,** *22* (2), 199-202.
112. Duvvari, M. R.; van de Ven, J. P.; Geerlings, M. J.; Saksens, N. T.; Bakker, B.; Henkes, A.; Neveling, K.; del Rosario, M.; Westra, D.; van den Heuvel, L. P.; Schick, T.; Fauser, S.; Boon, C. J.; Hoyng, C. B.; de Jong, E. K.; den Hollander, A. I., Whole Exome Sequencing in Patients with the Cuticular Drusen Subtype of Age-Related Macular Degeneration. *PLoS One* **2016,** *11* (3), e0152047.
113. Marmorstein, L. Y.; Munier, F. L.; Arsenijevic, Y.; Schorderet, D. F.; McLaughlin, P. J.; Chung, D.; Traboulsi, E.; Marmorstein, A. D., Aberrant accumulation of EFEMP1 underlies drusen formation in Malattia Leventinese and age-related macular degeneration. *Proc Natl Acad Sci U S A* **2002,** *99* (20), 13067-72.
114. Meyer, K. J.; Davis, L. K.; Schindler, E. I.; Beck, J. S.; Rudd, D. S.; Grundstad, A. J.; Scheetz, T. E.; Braun, T. A.; Fingert, J. H.; Alward, W. L.; Kwon, Y. H.; Folk, J. C.; Russell, S. R.; Wassink, T. H.; Stone, E. M.; Sheffield, V. C., Genome-wide analysis of copy number variants in age-related macular degeneration. *Hum Genet* **2011,** *129* (1), 91-100.
115. Varshney, S.; Hunter, D. D.; Brunken, W. J., Extracellular Matrix Components Regulate Cellular Polarity and Tissue Structure in the Developing and Mature Retina. *J Ophthalmic Vis Res* **2015,** *10* (3), 329-39.
116. Al-Ubaidi, M. R.; Naash, M. I.; Conley, S. M., A perspective on the role of the extracellular matrix in progressive retinal degenerative disorders. *Invest Ophthalmol Vis Sci* **2013,** *54* (13), 8119-24.
117. Hubmacher, D.; Apte, S. S., The biology of the extracellular matrix: novel insights. *Curr Opin Rheumatol* **2013,** *25* (1), 65-70.
118. Argraves, W. S.; Dickerson, K.; Burgess, W. H.; Ruoslahti, E., Fibulin, a novel protein that interacts with the fibronectin receptor beta subunit cytoplasmic domain. *Cell* **1989,** *58* (4), 623-9.
119. Argraves, W. S.; Greene, L. M.; Cooley, M. A.; Gallagher, W. M., Fibulins: physiological and disease perspectives. *EMBO Rep* **2003,** *4* (12), 1127-31.
120. Timpl, R.; Sasaki, T.; Kostka, G.; Chu, M. L., Fibulins: a versatile family of extracellular matrix proteins. *Nat Rev Mol Cell Biol* **2003,** *4* (6), 479-89.

121. Yanagisawa, H.; Schluterman, M. K.; Brekken, R. A., Fibulin-5, an integrin-binding matricellular protein: its function in development and disease. *J Cell Commun Signal* **2009,** *3* (3-4), 337-47.
122. Cangemi, C.; Hansen, M. L.; Argraves, W. S.; Rasmussen, L. M., Fibulins and their role in cardiovascular biology and disease. *Adv Clin Chem* **2014,** *67*, 245-65.
123. Vogel, B. E.; Hedgecock, E. M., Hemicentin, a conserved extracellular member of the immunoglobulin superfamily, organizes epithelial and other cell attachments into oriented line-shaped junctions. *Development* **2001,** *128* (6), 883-94.
124. Giltay, R.; Timpl, R.; Kostka, G., Sequence, recombinant expression and tissue localization of two novel extracellular matrix proteins, fibulin-3 and fibulin-4. *Matrix Biol* **1999,** *18* (5), 469-80.
125. Djokic, J.; Fagotto-Kaufmann, C.; Bartels, R.; Nelea, V.; Reinhardt, D. P., Fibulin-3, -4, and -5 are highly susceptible to proteolysis, interact with cells and heparin, and form multimers. *J Biol Chem* **2013,** *288* (31), 22821-35.
126. Zhang, Y.; Marmorstein, L. Y., Focus on molecules: fibulin-3 (EFEMP1). *Exp Eye Res* **2010,** *90* (3), 374-5.
127. Nakamura, T.; Ruiz-Lozano, P.; Lindner, V.; Yabe, D.; Taniwaki, M.; Furukawa, Y.; Kobuke, K.; Tashiro, K.; Lu, Z.; Andon, N. L.; Schaub, R.; Matsumori, A.; Sasayama, S.; Chien, K. R.; Honjo, T., DANCE, a novel secreted RGD protein expressed in developing, atherosclerotic, and balloon-injured arteries. *J Biol Chem* **1999,** *274* (32), 22476-83.
128. Ehlermann, J.; Weber, S.; Pfisterer, P.; Schorle, H., Cloning, expression and characterization of the murine Efemp1, a gene mutated in Doyne-Honeycomb retinal dystrophy. *Gene Expr Patterns* **2003,** *3* (4), 441-7.
129. de Vega, S.; Iwamoto, T.; Nakamura, T.; Hozumi, K.; McKnight, D. A.; Fisher, L. W.; Fukumoto, S.; Yamada, Y., TM14 is a new member of the fibulin family (fibulin-7) that interacts with extracellular matrix molecules and is active for cell binding. *J Biol Chem* **2007,** *282* (42), 30878-88.
130. Yanagisawa, H.; Davis, E. C.; Starcher, B. C.; Ouchi, T.; Yanagisawa, M.; Richardson, J. A.; Olson, E. N., Fibulin-5 is an elastin-binding protein essential for elastic fibre development in vivo. *Nature* **2002,** *415* (6868), 168-71.
131. Loeys, B.; Van Maldergem, L.; Mortier, G.; Coucke, P.; Gerniers, S.; Naeyaert, J. M.; De Paepe, A., Homozygosity for a missense mutation in fibulin-5 (FBLN5) results in a severe form of cutis laxa. *Hum Mol Genet* **2002,** *11* (18), 2113-8.
132. McLaughlin, P. J.; Chen, Q.; Horiguchi, M.; Starcher, B. C.; Stanton, J. B.; Broekelmann, T. J.; Marmorstein, A. D.; McKay, B.; Mecham, R.; Nakamura, T.; Marmorstein, L. Y., Targeted disruption of fibulin-4 abolishes elastogenesis and causes perinatal lethality in mice. *Mol Cell Biol* **2006,** *26* (5), 1700-9.
133. Kumra, H.; Nelea, V.; Hakami, H.; Pagliuzza, A.; Djokic, J.; Xu, J.; Yanagisawa, H.; Reinhardt, D. P., Fibulin-4 exerts a dual role in LTBP-4L-mediated matrix assembly and function. *Proc Natl Acad Sci U S A* **2019,** *116* (41), 20428-20437.

134. Driver, S. G. W.; Jackson, M. R.; Richter, K.; Tomlinson, P.; Brockway, B.; Halliday, B. J.; Markie, D. M.; Robertson, S. P.; Wade, E. M., Biallelic variants in EFEMP1 in a man with a pronounced connective tissue phenotype. *Eur J Hum Genet* **2020,** *28* (4), 445-452.
135. Bizzari, S.; El-Bazzal, L.; Nair, P.; Younan, A.; Stora, S.; Mehawej, C.; El-Hayek, S.; Delague, V.; Megarbane, A., Recessive marfanoid syndrome with herniation associated with a homozygous mutation in Fibulin-3. *Eur J Med Genet* **2020,** *63* (5), 103869.
136. Lecka-Czernik, B.; Lumpkin, C. K., Jr.; Goldstein, S., An overexpressed gene transcript in senescent and quiescent human fibroblasts encoding a novel protein in the epidermal growth factor-like repeat family stimulates DNA synthesis. *Mol Cell Biol* **1995,** *15* (1), 120-8.
137. McLaughlin, P. J.; Bakall, B.; Choi, J.; Liu, Z.; Sasaki, T.; Davis, E. C.; Marmorstein, A. D.; Marmorstein, L. Y., Lack of fibulin-3 causes early aging and herniation, but not macular degeneration in mice. *Hum Mol Genet* **2007,** *16* (24), 3059-70.
138. Bizzari, S.; El-Bazzal, L.; Nair, P.; Younan, A.; Stora, S.; Mehawej, C.; El-Hayek, S.; Delague, V.; Megarbane, A., Recessive marfanoid syndrome with herniation associated with a homozygous mutation in Fibulin-3. *Eur J Med Genet* **2020**, 103869.
139. Papke, C. L.; Yanagisawa, H., Fibulin-4 and fibulin-5 in elastogenesis and beyond: Insights from mouse and human studies. *Matrix Biol* **2014,** *37*, 142-9.
140. Souied, E. H.; Leveziel, N.; Querques, G.; Darmon, J.; Coscas, G.; Soubrane, G., Indocyanine green angiography features of Malattia leventinese. *Br J Ophthalmol* **2006,** *90* (3), 296-300.
141. Heon, E.; Piguet, B.; Munier, F.; Sneed, S. R.; Morgan, C. M.; Forni, S.; Pescia, G.; Schorderet, D.; Taylor, C. M.; Streb, L. M.; Wiles, C. D.; Nishimura, D. Y.; Sheffield, V. C.; Stone, E. M., Linkage of autosomal dominant radial drusen (malattia leventinese) to chromosome 2p16-21. *Arch Ophthalmol* **1996,** *114* (2), 193-8.
142. Takeuchi, T.; Hayashi, T.; Bedell, M.; Zhang, K.; Yamada, H.; Tsuneoka, H., A novel haplotype with the R345W mutation in the EFEMP1 gene associated with autosomal dominant drusen in a Japanese family. *Invest Ophthalmol Vis Sci* **2010,** *51* (3), 1643-50.
143. Zhang, K.; Sun, X.; Chen, Y.; Zhong, Q.; Lin, L.; Gao, Y.; Hong, F., Doyne honeycomb retinal dystrophy/malattia leventinese induced by EFEMP1 mutation in a Chinese family. *BMC Ophthalmol* **2018,** *18* (1), 318.
144. Gelvez, N.; Hurtado-Villa, P.; Florez, S.; Brieke, A. C.; Rodriguez, F.; Bertolotto, A. M.; Tamayo, M. L., [Definicion diagnostica en una familia con malattia leventinese en Colombia]. *Biomedica* **2021,** *41* (3), 388-395.
145. Vaclavik, V.; Tran, H. V.; Schorderet Md Ph, D. D., Malattia Leventinese: EFEMP1 R345W Variant Is a Hot Spot Mutation, Not a Founder Mutation. *Ophthalmol Retina* **2020,** *4* (10), 1023.

146. Haimovici, R.; Wroblewski, J.; Piguet, B.; Fitzke, F. W.; Holder, G. E.; Arden, G. B.; Bird, A. C., Symptomatic abnormalities of dark adaptation in patients with EFEMP1 retinal dystrophy (Malattia Leventinese/Doyne honeycomb retinal dystrophy). *Eye (Lond)* **2002,** *16* (1), 7-15.
147. Michaelides, M.; Jenkins, S. A.; Brantley, M. A., Jr.; Andrews, R. M.; Waseem, N.; Luong, V.; Gregory-Evans, K.; Bhattacharya, S. S.; Fitzke, F. W.; Webster, A. R., Maculopathy due to the R345W substitution in fibulin-3: distinct clinical features, disease variability, and extent of retinal dysfunction. *Invest Ophthalmol Vis Sci* **2006,** *47* (7), 3085-97.
148. Hulleman, J. D.; Kaushal, S.; Balch, W. E.; Kelly, J. W., Compromised mutant EFEMP1 secretion associated with macular dystrophy remedied by proteostasis network alteration. *Mol Biol Cell* **2011,** *22* (24), 4765-75.
149. Fernandez-Godino, R.; Garland, D. L.; Pierce, E. A., A local complement response by RPE causes early-stage macular degeneration. *Hum Mol Genet* **2015,** *24* (19), 5555-69.
150. Garland, D. L.; Pierce, E. A.; Fernandez-Godino, R., Complement C5 is not critical for the formation of sub-RPE deposits in Efemp1 mutant mice. *Sci Rep* **2021,** *11* (1), 10416.
151. Fraser, P. E., Prions and prion-like proteins. *J Biol Chem* **2014,** *289* (29), 19839-40.
152. Fu, L.; Garland, D.; Yang, Z.; Shukla, D.; Rajendran, A.; Pearson, E.; Stone, E. M.; Zhang, K.; Pierce, E. A., The R345W mutation in EFEMP1 is pathogenic and causes AMD-like deposits in mice. *Hum Mol Genet* **2007,** *16* (20), 2411-22.
153. Marmorstein, L. Y.; McLaughlin, P. J.; Peachey, N. S.; Sasaki, T.; Marmorstein, A. D., Formation and progression of sub-retinal pigment epithelium deposits in Efemp1 mutation knock-in mice: a model for the early pathogenic course of macular degeneration. *Hum Mol Genet* **2007,** *16* (20), 2423-32.
154. Cheng, L.; Chen, C.; Guo, W.; Liu, K.; Zhao, Q.; Lu, P.; Yu, F.; Xu, X., EFEMP1 Overexpression Contributes to Neovascularization in Age-Related Macular Degeneration. *Front Pharmacol* **2020,** *11*, 547436.
155. Chakraborty, P.; Dash, S. P.; Sarangi, P. P., The role of adhesion protein Fibulin7 in development and diseases. *Mol Med* **2020,** *26* (1), 47.
156. Sabanayagam, C.; Cheng, C. Y., Global causes of vision loss in 2015: are we on track to achieve the Vision 2020 target? *Lancet Glob Health* **2017,** *5* (12), e1164-e1165.
157. Varma, R.; Vajaranant, T. S.; Burkemper, B.; Wu, S.; Torres, M.; Hsu, C.; Choudhury, F.; McKean-Cowdin, R., Visual Impairment and Blindness in Adults in the United States: Demographic and Geographic Variations From 2015 to 2050. *JAMA Ophthalmol* **2016,** *134* (7), 802-9.
158. Lin, J. B.; Tsubota, K.; Apte, R. S., A glimpse at the aging eye. *NPJ Aging Mech Dis* **2016,** *2*, 16003.

159. Chader, G. J.; Taylor, A., Preface: The aging eye: normal changes, age-related diseases, and sight-saving approaches. *Invest Ophthalmol Vis Sci* **2013,** *54* (14), ORSF1-4.
160. Swaroop, A.; Chew, E. Y.; Rickman, C. B.; Abecasis, G. R., Unraveling a multifactorial late-onset disease: from genetic susceptibility to disease mechanisms for age-related macular degeneration. *Annu Rev Genomics Hum Genet* **2009,** *10*, 19-43.
161. Johnson, P. T.; Lewis, G. P.; Talaga, K. C.; Brown, M. N.; Kappel, P. J.; Fisher, S. K.; Anderson, D. H.; Johnson, L. V., Drusen-associated degeneration in the retina. *Invest Ophthalmol Vis Sci* **2003,** *44* (10), 4481-8.
162. Bahadorani, S.; Singer, M., Recent advances in the management and understanding of macular degeneration. *F1000Res* **2017,** *6*, 519.
163. Girmens, J. F.; Sahel, J. A.; Marazova, K., Dry age-related macular degeneration: A currently unmet clinical need. *Intractable Rare Dis Res* **2012,** *1* (3), 103-14.
164. Clemons, T. E.; Milton, R. C.; Klein, R.; Seddon, J. M.; Ferris, F. L., 3rd; Age-Related Eye Disease Study Research, G., Risk factors for the incidence of Advanced Age-Related Macular Degeneration in the Age-Related Eye Disease Study (AREDS) AREDS report no. 19. *Ophthalmology* **2005,** *112* (4), 533-9.
165. Thornton, J.; Edwards, R.; Mitchell, P.; Harrison, R. A.; Buchan, I.; Kelly, S. P., Smoking and age-related macular degeneration: a review of association. *Eye (Lond)* **2005,** *19* (9), 935-44.
166. Klein, R.; Peto, T.; Bird, A.; Vannewkirk, M. R., The epidemiology of age-related macular degeneration. *Am J Ophthalmol* **2004,** *137* (3), 486-95.
167. Hulleman, J. D., Malattia Leventinese/Doyne Honeycomb Retinal Dystrophy: Similarities to Age-Related Macular Degeneration and Potential Therapies. *Adv Exp Med Biol* **2016,** *854*, 153-8.
168. Daniel, S.; Renwick, M.; Chau, V. Q.; Datta, S.; Maddineni, P.; Zode, G.; Wade, E. M.; Robertson, S. P.; Petroll, W. M.; Hulleman, J. D., Fibulin-3 knockout mice demonstrate corneal dysfunction but maintain normal retinal integrity. *J Mol Med (Berl)* **2020,** *98* (11), 1639-1656.
169. Roybal, C. N.; Marmorstein, L. Y.; Vander Jagt, D. L.; Abcouwer, S. F., Aberrant accumulation of fibulin-3 in the endoplasmic reticulum leads to activation of the unfolded protein response and VEGF expression. *Invest Ophthalmol Vis Sci* **2005,** *46* (11), 3973-9.
170. Hulleman, J. D.; Brown, S. J.; Rosen, H.; Kelly, J. W., A high-throughput cell-based Gaussia luciferase reporter assay for identifying modulators of fibulin-3 secretion. *J Biomol Screen* **2013,** *18* (6), 647-58.
171. Hulleman, J. D.; Balch, W. E.; Kelly, J. W., Translational attenuation differentially alters the fate of disease-associated fibulin proteins. *FASEB J* **2012,** *26* (11), 4548-60.
172. Mackay, D. S.; Bennett, T. M.; Shiels, A., Exome Sequencing Identifies a Missense Variant in EFEMP1 Co-Segregating in a Family with Autosomal Dominant Primary Open-Angle Glaucoma. *PLoS One* **2015,** *10* (7), e0132529.

173. Landrum, M. J.; Lee, J. M.; Riley, G. R.; Jang, W.; Rubinstein, W. S.; Church, D. M.; Maglott, D. R., ClinVar: public archive of relationships among sequence variation and human phenotype. *Nucleic Acids Res* **2014,** *42* (Database issue), D980-5.
174. Hulleman, J. D.; Kelly, J. W., Genetic ablation of N-linked glycosylation reveals two key folding pathways for R345W fibulin-3, a secreted protein associated with retinal degeneration. *FASEB J* **2015,** *29* (2), 565-75.
175. Daniel, S.; Renwick, M.; Chau, V. Q.; Datta, S.; Maddineni, P.; Zode, G.; Wade, E. M.; Robertson, S. P.; Petroll, W. M.; Hulleman, J. D., Fibulin-3 knockout mice demonstrate corneal dysfunction but maintain normal retinal integrity. *J Mol Med (Berl)* **2020**.
176. Ho, B. K.; Coutsias, E. A.; Seok, C.; Dill, K. A., The flexibility in the proline ring couples to the protein backbone. *Protein Sci* **2005,** *14* (4), 1011-8.
177. Williamson, M. P., The structure and function of proline-rich regions in proteins. *Biochem J* **1994,** *297 (Pt 2)*, 249-60.
178. Nguyen, A.; Hulleman, J. D., Differential tolerance of 'pseudo-pathogenic' tryptophan residues in calcium-binding EGF domains of short fibulin proteins. *Exp Eye Res* **2015,** *130*, 66-72.
179. Zadoo, S.; Nguyen, A.; Zode, G.; Hulleman, J. D., A Novel Luciferase Assay For Sensitively Monitoring Myocilin Variants in Cell Culture. *Invest Ophthalmol Vis Sci* **2016,** *57* (4), 1939-50.
180. Burns, J. N.; Orwig, S. D.; Harris, J. L.; Watkins, J. D.; Vollrath, D.; Lieberman, R. L., Rescue of glaucoma-causing mutant myocilin thermal stability by chemical chaperones. *ACS Chem Biol* **2010,** *5* (5), 477-87.
181. Jacobson, N.; Andrews, M.; Shepard, A. R.; Nishimura, D.; Searby, C.; Fingert, J. H.; Hageman, G.; Mullins, R.; Davidson, B. L.; Kwon, Y. H.; Alward, W. L.; Stone, E. M.; Clark, A. F.; Sheffield, V. C., Non-secretion of mutant proteins of the glaucoma gene myocilin in cultured trabecular meshwork cells and in aqueous humor. *Hum Mol Genet* **2001,** *10* (2), 117-25.
182. Liu, Y.; Vollrath, D., Reversal of mutant myocilin non-secretion and cell killing: implications for glaucoma. *Hum Mol Genet* **2004,** *13* (11), 1193-204.
183. Klenotic, P. A.; Munier, F. L.; Marmorstein, L. Y.; Anand-Apte, B., Tissue inhibitor of metalloproteinases-3 (TIMP-3) is a binding partner of epithelial growth factor-containing fibulin-like extracellular matrix protein 1 (EFEMP1). Implications for macular degenerations. *J Biol Chem* **2004,** *279* (29), 30469-73.
184. Weber, B. H.; Vogt, G.; Pruett, R. C.; Stohr, H.; Felbor, U., Mutations in the tissue inhibitor of metalloproteinases-3 (TIMP3) in patients with Sorsby's fundus dystrophy. *Nat Genet* **1994,** *8* (4), 352-6.
185. Hulleman, J. D.; Genereux, J. C.; Nguyen, A., Mapping wild-type and R345W fibulin-3 intracellular interactomes. *Exp Eye Res* **2016,** *153*, 165-169.
186. Wyatt, M. K.; Tsai, J. Y.; Mishra, S.; Campos, M.; Jaworski, C.; Fariss, R. N.; Bernstein, S. L.; Wistow, G., Interaction of complement factor h and fibulin3 in age-related macular degeneration. *PLoS One* **2013,** *8* (6), e68088.

187. Tasaki, M.; Ueda, M.; Hoshii, Y.; Mizukami, M.; Matsumoto, S.; Nakamura, M.; Yamashita, T.; Ueda, A.; Misumi, Y.; Masuda, T.; Inoue, Y.; Torikai, T.; Nomura, T.; Tsuda, Y.; Kanenawa, K.; Isoguchi, A.; Okada, M.; Matsui, H.; Obayashi, K.; Ando, Y., A novel age-related venous amyloidosis derived from EGF-containing fibulin-like extracellular matrix protein 1. *J Pathol* **2019,** *247* (4), 444-455.
188. Nguyen, A.; Hulleman, J. D., Evidence of Alternative Cystatin C Signal Sequence Cleavage Which Is Influenced by the A25T Polymorphism. *PLoS One* **2016,** *11* (2), e0147684.
189. Curcio, C. A., Soft Drusen in Age-Related Macular Degeneration: Biology and Targeting Via the Oil Spill Strategies. *Invest Ophthalmol Vis Sci* **2018,** *59* (4), AMD160-AMD181.
190. Spraul, C. W.; Lang, G. E.; Grossniklaus, H. E.; Lang, G. K., Histologic and morphometric analysis of the choroid, Bruch's membrane, and retinal pigment epithelium in postmortem eyes with age-related macular degeneration and histologic examination of surgically excised choroidal neovascular membranes. *Surv Ophthalmol* **1999,** *44 Suppl 1*, S10-32.
191. Sarks, S.; Cherepanoff, S.; Killingsworth, M.; Sarks, J., Relationship of Basal laminar deposit and membranous debris to the clinical presentation of early age-related macular degeneration. *Invest Ophthalmol Vis Sci* **2007,** *48* (3), 968-77.
192. Sura, A. A.; Chen, L.; Messinger, J. D.; Swain, T. A.; McGwin, G., Jr.; Freund, K. B.; Curcio, C. A., Measuring the Contributions of Basal Laminar Deposit and Bruch's Membrane in Age-Related Macular Degeneration. *Invest Ophthalmol Vis Sci* **2020,** *61* (13), 19.
193. Sohn, E. H.; Wang, K.; Thompson, S.; Riker, M. J.; Hoffmann, J. M.; Stone, E. M.; Mullins, R. F., Comparison of drusen and modifying genes in autosomal dominant radial drusen and age-related macular degeneration. *Retina* **2015,** *35* (1), 48-57.
194. Marshall, G. E.; Konstas, A. G.; Reid, G. G.; Edwards, J. G.; Lee, W. R., Type IV collagen and laminin in Bruch's membrane and basal linear deposit in the human macula. *Br J Ophthalmol* **1992,** *76* (10), 607-14.
195. Garland, D. L.; Fernandez-Godino, R.; Kaur, I.; Speicher, K. D.; Harnly, J. M.; Lambris, J. D.; Speicher, D. W.; Pierce, E. A., Mouse genetics and proteomic analyses demonstrate a critical role for complement in a model of DHRD/ML, an inherited macular degeneration. *Hum Mol Genet* **2014,** *23* (1), 52-68.
196. Stanton, J. B.; Marmorstein, A. D.; Zhang, Y.; Marmorstein, L. Y., Deletion of Efemp1 Is Protective Against the Development of Sub-RPE Deposits in Mouse Eyes. *Invest Ophthalmol Vis Sci* **2017,** *58* (3), 1455-1461.
197. Dinculescu, A.; Min, S. H.; Dyka, F. M.; Deng, W. T.; Stupay, R. M.; Chiodo, V.; Smith, W. C.; Hauswirth, W. W., Pathological Effects of Mutant C1QTNF5 (S163R) Expression in Murine Retinal Pigment Epithelium. *Invest Ophthalmol Vis Sci* **2015,** *56* (11), 6971-80.

198. Naso, M. F.; Tomkowicz, B.; Perry, W. L., 3rd; Strohl, W. R., Adeno-Associated Virus (AAV) as a Vector for Gene Therapy. *BioDrugs* **2017,** *31* (4), 317-334.
199. Schon, C.; Biel, M.; Michalakis, S., Retinal gene delivery by adeno-associated virus (AAV) vectors: Strategies and applications. *Eur J Pharm Biopharm* **2015,** *95* (Pt B), 343-52.
200. Xiao, W.; Chirmule, N.; Berta, S. C.; McCullough, B.; Gao, G.; Wilson, J. M., Gene therapy vectors based on adeno-associated virus type 1. *J Virol* **1999,** *73* (5), 3994-4003.
201. Backovic, A.; Cervelli, T.; Salvetti, A.; Zentilin, L.; Giacca, M.; Galli, A., Capsid protein expression and adeno-associated virus like particles assembly in Saccharomyces cerevisiae. *Microb Cell Fact* **2012,** *11*, 124.
202. Wang, D.; Tai, P. W. L.; Gao, G., Adeno-associated virus vector as a platform for gene therapy delivery. *Nat Rev Drug Discov* **2019,** *18* (5), 358-378.
203. Ziccardi, L.; Cordeddu, V.; Gaddini, L.; Matteucci, A.; Parravano, M.; Malchiodi-Albedi, F.; Varano, M., Gene Therapy in Retinal Dystrophies. *Int J Mol Sci* **2019,** *20* (22).
204. Wang, X.; Yu, C.; Tzekov, R. T.; Zhu, Y.; Li, W., The effect of human gene therapy for RPE65-associated Leber's congenital amaurosis on visual function: a systematic review and meta-analysis. *Orphanet J Rare Dis* **2020,** *15* (1), 49.
205. Jacobson, S. G.; Cideciyan, A. V.; Ratnakaram, R.; Heon, E.; Schwartz, S. B.; Roman, A. J.; Peden, M. C.; Aleman, T. S.; Boye, S. L.; Sumaroka, A.; Conlon, T. J.; Calcedo, R.; Pang, J. J.; Erger, K. E.; Olivares, M. B.; Mullins, C. L.; Swider, M.; Kaushal, S.; Feuer, W. J.; Iannaccone, A.; Fishman, G. A.; Stone, E. M.; Byrne, B. J.; Hauswirth, W. W., Gene therapy for leber congenital amaurosis caused by RPE65 mutations: safety and efficacy in 15 children and adults followed up to 3 years. *Arch Ophthalmol* **2012,** *130* (1), 9-24.
206. Maguire, A. M.; Simonelli, F.; Pierce, E. A.; Pugh, E. N., Jr.; Mingozzi, F.; Bennicelli, J.; Banfi, S.; Marshall, K. A.; Testa, F.; Surace, E. M.; Rossi, S.; Lyubarsky, A.; Arruda, V. R.; Konkle, B.; Stone, E.; Sun, J.; Jacobs, J.; Dell'Osso, L.; Hertle, R.; Ma, J. X.; Redmond, T. M.; Zhu, X.; Hauck, B.; Zelenaia, O.; Shindler, K. S.; Maguire, M. G.; Wright, J. F.; Volpe, N. J.; McDonnell, J. W.; Auricchio, A.; High, K. A.; Bennett, J., Safety and efficacy of gene transfer for Leber's congenital amaurosis. *N Engl J Med* **2008,** *358* (21), 2240-8.
207. Pang, J. J.; Lei, L.; Dai, X.; Shi, W.; Liu, X.; Dinculescu, A.; McDowell, J. H., AAV-mediated gene therapy in mouse models of recessive retinal degeneration. *Curr Mol Med* **2012,** *12* (3), 316-30.
208. Reid, C. A.; Ertel, K. J.; Lipinski, D. M., Improvement of Photoreceptor Targeting via Intravitreal Delivery in Mouse and Human Retina Using Combinatory rAAV2 Capsid Mutant Vectors. *Invest Ophthalmol Vis Sci* **2017,** *58* (14), 6429-6439.
209. Qi, Y.; Dai, X.; Zhang, H.; He, Y.; Zhang, Y.; Han, J.; Zhu, P.; Zhang, Y.; Zheng, Q.; Li, X.; Zhao, C.; Pang, J., Trans-Corneal Subretinal Injection in Mice and

Its Effect on the Function and Morphology of the Retina. *PLoS One* **2015,** *10* (8), e0136523.
210. Parikh, S.; Le, A.; Davenport, J.; Gorin, M. B.; Nusinowitz, S.; Matynia, A., An Alternative and Validated Injection Method for Accessing the Subretinal Space via a Transcleral Posterior Approach. *J Vis Exp* **2016,** (118).
211. Woodard, D. R.; Nakahara, E.; Hulleman, J. D., Clinically-identified C-terminal mutations in fibulin-3 are prone to misfolding and destabilization. *Sci Rep* **2021,** *11* (1), 2998.
212. Rajasekaran, S. A.; Hu, J.; Gopal, J.; Gallemore, R.; Ryazantsev, S.; Bok, D.; Rajasekaran, A. K., Na,K-ATPase inhibition alters tight junction structure and permeability in human retinal pigment epithelial cells. *Am J Physiol Cell Physiol* **2003,** *284* (6), C1497-507.
213. Georgiadis, A.; Tschernutter, M.; Bainbridge, J. W.; Balaggan, K. S.; Mowat, F.; West, E. L.; Munro, P. M.; Thrasher, A. J.; Matter, K.; Balda, M. S.; Ali, R. R., The tight junction associated signalling proteins ZO-1 and ZONAB regulate retinal pigment epithelium homeostasis in mice. *PLoS One* **2010,** *5* (12), e15730.
214. Lewis, G. P.; Fisher, S. K., Up-regulation of glial fibrillary acidic protein in response to retinal injury: its potential role in glial remodeling and a comparison to vimentin expression. *Int Rev Cytol* **2003,** *230*, 263-90.
215. Finch, C. E., Neurons, glia, and plasticity in normal brain aging. *Adv Gerontol* **2002,** *10*, 35-9.
216. Hausmann, O. N., Post-traumatic inflammation following spinal cord injury. *Spinal Cord* **2003,** *41* (7), 369-78.
217. Tuccari, G.; Trombetta, C.; Giardinelli, M. M.; Arena, F.; Barresi, G., Distribution of glial fibrillary acidic protein in normal and gliotic human retina. *Basic Appl Histochem* **1986,** *30* (4), 425-32.
218. Kimura, T.; Ferran, B.; Tsukahara, Y.; Shang, Q.; Desai, S.; Fedoce, A.; Pimentel, D. R.; Luptak, I.; Adachi, T.; Ido, Y.; Matsui, R.; Bachschmid, M. M., Production of adeno-associated virus vectors for in vitro and in vivo applications. *Sci Rep* **2019,** *9* (1), 13601.
219. Mehta, A. K.; Majumdar, S. S.; Alam, P.; Gulati, N.; Brahmachari, V., Epigenetic regulation of cytomegalovirus major immediate-early promoter activity in transgenic mice. *Gene* **2009,** *428* (1-2), 20-4.
220. Buck, T. M.; Wijnholds, J., Recombinant Adeno-Associated Viral Vectors (rAAV)-Vector Elements in Ocular Gene Therapy Clinical Trials and Transgene Expression and Bioactivity Assays. *Int J Mol Sci* **2020,** *21* (12).
221. Zolotukhin, S.; Byrne, B. J.; Mason, E.; Zolotukhin, I.; Potter, M.; Chesnut, K.; Summerford, C.; Samulski, R. J.; Muzyczka, N., Recombinant adeno-associated virus purification using novel methods improves infectious titer and yield. *Gene Ther* **1999,** *6* (6), 973-85.
222. Galibert, L.; Savy, A.; Dickx, Y.; Bonnin, D.; Bertin, B.; Mushimiyimana, I.; van Oers, M. M.; Merten, O. W., Origins of truncated supplementary capsid proteins in

rAAV8 vectors produced with the baculovirus system. *PLoS One* **2018,** *13* (11), e0207414.
223. Abisambra, J. F.; Jinwal, U. K.; Blair, L. J.; O'Leary, J. C., 3rd; Li, Q.; Brady, S.; Wang, L.; Guidi, C. E.; Zhang, B.; Nordhues, B. A.; Cockman, M.; Suntharalingham, A.; Li, P.; Jin, Y.; Atkins, C. A.; Dickey, C. A., Tau accumulation activates the unfolded protein response by impairing endoplasmic reticulum-associated degradation. *J Neurosci* **2013,** *33* (22), 9498-507.
224. Murray, H. C.; Dieriks, B. V.; Swanson, M. E. V.; Anekal, P. V.; Turner, C.; Faull, R. L. M.; Belluscio, L.; Koretsky, A.; Curtis, M. A., The unfolded protein response is activated in the olfactory system in Alzheimer's disease. *Acta Neuropathol Commun* **2020,** *8* (1), 109.
225. Colla, E., Linking the Endoplasmic Reticulum to Parkinson's Disease and Alpha-Synucleinopathy. *Front Neurosci* **2019,** *13*, 560.
226. Athanasiou, D.; Aguila, M.; Bellingham, J.; Kanuga, N.; Adamson, P.; Cheetham, M. E., The role of the ER stress-response protein PERK in rhodopsin retinitis pigmentosa. *Hum Mol Genet* **2017,** *26* (24), 4896-4905.
227. Lee, E. J.; Chan, P.; Chea, L.; Kim, K.; Kaufman, R. J.; Lin, J. H., ATF6 is required for efficient rhodopsin clearance and retinal homeostasis in the P23H rho retinitis pigmentosa mouse model. *Sci Rep* **2021,** *11* (1), 16356.
228. Kincaid, M. M.; Cooper, A. A., Misfolded proteins traffic from the endoplasmic reticulum (ER) due to ER export signals. *Mol Biol Cell* **2007,** *18* (2), 455-63.
229. Ruberg, F. L.; Berk, J. L., Transthyretin (TTR) cardiac amyloidosis. *Circulation* **2012,** *126* (10), 1286-300.
230. Rao, R. V.; Bredesen, D. E., Misfolded proteins, endoplasmic reticulum stress and neurodegeneration. *Curr Opin Cell Biol* **2004,** *16* (6), 653-62.
231. Kozlowski, M. R., The ARPE-19 cell line: mortality status and utility in macular degeneration research. *Curr Eye Res* **2015,** *40* (5), 501-9.
232. Samuel, W.; Jaworski, C.; Postnikova, O. A.; Kutty, R. K.; Duncan, T.; Tan, L. X.; Poliakov, E.; Lakkaraju, A.; Redmond, T. M., Appropriately differentiated ARPE-19 cells regain phenotype and gene expression profiles similar to those of native RPE cells. *Mol Vis* **2017,** *23*, 60-89.
233. Adijanto, J.; Philp, N. J., Cultured primary human fetal retinal pigment epithelium (hfRPE) as a model for evaluating RPE metabolism. *Exp Eye Res* **2014,** *126*, 77-84.
234. Ablonczy, Z.; Dahrouj, M.; Tang, P. H.; Liu, Y.; Sambamurti, K.; Marmorstein, A. D.; Crosson, C. E., Human retinal pigment epithelium cells as functional models for the RPE in vivo. *Invest Ophthalmol Vis Sci* **2011,** *52* (12), 8614-20.
235. Toops, K. A.; Tan, L. X.; Lakkaraju, A., A detailed three-step protocol for live imaging of intracellular traffic in polarized primary porcine RPE monolayers. *Exp Eye Res* **2014,** *124*, 74-85.
236. Bouabe, H.; Fassler, R.; Heesemann, J., Improvement of reporter activity by IRES-mediated polycistronic reporter system. *Nucleic Acids Res* **2008,** *36* (5), e28.

237. Khabou, H.; Cordeau, C.; Pacot, L.; Fisson, S.; Dalkara, D., Dosage Thresholds and Influence of Transgene Cassette in Adeno-Associated Virus-Related Toxicity. *Hum Gene Ther* **2018,** *29* (11), 1235-1241.
238. Ildefonso, C. J.; Jaime, H.; Biswal, M. R.; Boye, S. E.; Li, Q.; Hauswirth, W. W.; Lewin, A. S., Gene therapy with the caspase activation and recruitment domain reduces the ocular inflammatory response. *Mol Ther* **2015,** *23* (5), 875-884.
239. Beltran, W. A.; Boye, S. L.; Boye, S. E.; Chiodo, V. A.; Lewin, A. S.; Hauswirth, W. W.; Aguirre, G. D., rAAV2/5 gene-targeting to rods:dose-dependent efficiency and complications associated with different promoters. *Gene Ther* **2010,** *17* (9), 1162-74.
240. Watanabe, S.; Sanuki, R.; Ueno, S.; Koyasu, T.; Hasegawa, T.; Furukawa, T., Tropisms of AAV for subretinal delivery to the neonatal mouse retina and its application for in vivo rescue of developmental photoreceptor disorders. *PLoS One* **2013,** *8* (1), e54146.
241. Petit, L.; Ma, S.; Cheng, S. Y.; Gao, G.; Punzo, C., Rod Outer Segment Development Influences AAV-Mediated Photoreceptor Transduction After Subretinal Injection. *Hum Gene Ther* **2017,** *28* (6), 464-481.
242. Allocca, M.; Mussolino, C.; Garcia-Hoyos, M.; Sanges, D.; Iodice, C.; Petrillo, M.; Vandenberghe, L. H.; Wilson, J. M.; Marigo, V.; Surace, E. M.; Auricchio, A., Novel adeno-associated virus serotypes efficiently transduce murine photoreceptors. *J Virol* **2007,** *81* (20), 11372-80.
243. Xue, K.; MacLaren, R. E., Antisense oligonucleotide therapeutics in clinical trials for the treatment of inherited retinal diseases. *Expert Opin Investig Drugs* **2020,** *29* (10), 1163-1170.
244. Collin, R. W.; Garanto, A., Applications of antisense oligonucleotides for the treatment of inherited retinal diseases. *Curr Opin Ophthalmol* **2017,** *28* (3), 260-266.
245. Gerard, X.; Garanto, A.; Rozet, J. M.; Collin, R. W., Antisense Oligonucleotide Therapy for Inherited Retinal Dystrophies. *Adv Exp Med Biol* **2016,** *854*, 517-24.
246. Di Fusco, D.; Dinallo, V.; Marafini, I.; Figliuzzi, M. M.; Romano, B.; Monteleone, G., Antisense Oligonucleotide: Basic Concepts and Therapeutic Application in Inflammatory Bowel Disease. *Front Pharmacol* **2019,** *10*, 305.
247. Murray, S. F.; Jazayeri, A.; Matthes, M. T.; Yasumura, D.; Yang, H.; Peralta, R.; Watt, A.; Freier, S.; Hung, G.; Adamson, P. S.; Guo, S.; Monia, B. P.; LaVail, M. M.; McCaleb, M. L., Allele-Specific Inhibition of Rhodopsin With an Antisense Oligonucleotide Slows Photoreceptor Cell Degeneration. *Invest Ophthalmol Vis Sci* **2015,** *56* (11), 6362-75.
248. Niu, C.; Prakash, T. P.; Kim, A.; Quach, J. L.; Huryn, L. A.; Yang, Y.; Lopez, E.; Jazayeri, A.; Hung, G.; Sopher, B. L.; Brooks, B. P.; Swayze, E. E.; Bennett, C. F.; La Spada, A. R., Antisense oligonucleotides targeting mutant Ataxin-7 restore visual function in a mouse model of spinocerebellar ataxia type 7. *Sci Transl Med* **2018,** *10* (465).

249. Dulla, K.; Slijkerman, R.; van Diepen, H. C.; Albert, S.; Dona, M.; Beumer, W.; Turunen, J. J.; Chan, H. L.; Schulkens, I. A.; Vorthoren, L.; den Besten, C.; Buil, L.; Schmidt, I.; Miao, J.; Venselaar, H.; Zang, J.; Neuhauss, S. C. F.; Peters, T.; Broekman, S.; Pennings, R.; Kremer, H.; Platenburg, G.; Adamson, P.; de Vrieze, E.; van Wijk, E., Antisense oligonucleotide-based treatment of retinitis pigmentosa caused by USH2A exon 13 mutations. *Mol Ther* **2021,** *29* (8), 2441-2455.
250. Dhuri, K.; Bechtold, C.; Quijano, E.; Pham, H.; Gupta, A.; Vikram, A.; Bahal, R., Antisense Oligonucleotides: An Emerging Area in Drug Discovery and Development. *J Clin Med* **2020,** *9* (6).
251. Crooke, S. T.; Vickers, T. A.; Liang, X. H., Phosphorothioate modified oligonucleotide-protein interactions. *Nucleic Acids Res* **2020,** *48* (10), 5235-5253.
252. Sahel, J. A.; Marazova, K.; Audo, I., Clinical characteristics and current therapies for inherited retinal degenerations. *Cold Spring Harb Perspect Med* **2014,** *5* (2), a017111.
253. Hamel, C. P., Cone rod dystrophies. *Orphanet J Rare Dis* **2007,** *2*, 7.
254. Hamel, C., Retinitis pigmentosa. *Orphanet J Rare Dis* **2006,** *1*, 40.
255. Ferrari, S.; Di Iorio, E.; Barbaro, V.; Ponzin, D.; Sorrentino, F. S.; Parmeggiani, F., Retinitis pigmentosa: genes and disease mechanisms. *Curr Genomics* **2011,** *12* (4), 238-49.
256. Ullah, I.; Kabir, F.; Iqbal, M.; Gottsch, C. B.; Naeem, M. A.; Assir, M. Z.; Khan, S. N.; Akram, J.; Riazuddin, S.; Ayyagari, R.; Hejtmancik, J. F.; Riazuddin, S. A., Pathogenic mutations in TULP1 responsible for retinitis pigmentosa identified in consanguineous familial cases. *Mol Vis* **2016,** *22*, 797-815.
257. Adzhubei, I. A.; Schmidt, S.; Peshkin, L.; Ramensky, V. E.; Gerasimova, A.; Bork, P.; Kondrashov, A. S.; Sunyaev, S. R., A method and server for predicting damaging missense mutations. *Nat Methods* **2010,** *7* (4), 248-9.
258. Paloma, E.; Hjelmqvist, L.; Bayes, M.; Garcia-Sandoval, B.; Ayuso, C.; Balcells, S.; Gonzalez-Duarte, R., Novel mutations in the TULP1 gene causing autosomal recessive retinitis pigmentosa. *Invest Ophthalmol Vis Sci* **2000,** *41* (3), 656-9.
259. Iqbal, M.; Naeem, M. A.; Riazuddin, S. A.; Ali, S.; Farooq, T.; Qazi, Z. A.; Khan, S. N.; Husnain, T.; Riazuddin, S.; Sieving, P. A.; Hejtmancik, J. F.; Riazuddin, S., Association of pathogenic mutations in TULP1 with retinitis pigmentosa in consanguineous Pakistani families. *Arch Ophthalmol* **2011,** *129* (10), 1351-7.
260. Milam, A. H.; Hendrickson, A. E.; Xiao, M.; Smith, J. E.; Possin, D. E.; John, S. K.; Nishina, P. M., Localization of tubby-like protein 1 in developing and adult human retinas. *Invest Ophthalmol Vis Sci* **2000,** *41* (8), 2352-6.
261. Hagstrom, S. A.; Adamian, M.; Scimeca, M.; Pawlyk, B. S.; Yue, G.; Li, T., A role for the Tubby-like protein 1 in rhodopsin transport. *Invest Ophthalmol Vis Sci* **2001,** *42* (9), 1955-62.
262. Xi, Q.; Pauer, G. J.; Marmorstein, A. D.; Crabb, J. W.; Hagstrom, S. A., Tubby-like protein 1 (TULP1) interacts with F-actin in photoreceptor cells. *Invest Ophthalmol Vis Sci* **2005,** *46* (12), 4754-61.

263. Hagstrom, S. A.; Duyao, M.; North, M. A.; Li, T., Retinal degeneration in tulp1-/- mice: vesicular accumulation in the interphotoreceptor matrix. *Invest Ophthalmol Vis Sci* **1999,** *40* (12), 2795-802.
264. Lobo, G. P.; Au, A.; Kiser, P. D.; Hagstrom, S. A., Involvement of Endoplasmic Reticulum Stress in TULP1 Induced Retinal Degeneration. *PLoS One* **2016,** *11* (3), e0151806.
265. Hulleman, J. D.; Nguyen, A.; Ramprasad, V. L.; Murugan, S.; Gupta, R.; Mahindrakar, A.; Angara, R.; Sankurathri, C.; Mootha, V. V., A novel H395R mutation in MKKS/BBS6 causes retinitis pigmentosa and polydactyly without other findings of Bardet-Biedl or McKusick-Kaufman syndrome. *Mol Vis* **2016,** *22*, 73-81.
266. Martin-Merida, I.; Avila-Fernandez, A.; Del Pozo-Valero, M.; Blanco-Kelly, F.; Zurita, O.; Perez-Carro, R.; Aguilera-Garcia, D.; Riveiro-Alvarez, R.; Arteche, A.; Trujillo-Tiebas, M. J.; Tahsin-Swafiri, S.; Rodriguez-Pinilla, E.; Lorda-Sanchez, I.; Garcia-Sandoval, B.; Corton, M.; Ayuso, C., Genomic Landscape of Sporadic Retinitis Pigmentosa: Findings from 877 Spanish Cases. *Ophthalmology* **2019,** *126* (8), 1181-1188.
267. Gruppuso, P. A.; Gorden, P.; Kahn, C. R.; Cornblath, M.; Zeller, W. P.; Schwartz, R., Familial hyperproinsulinemia due to a proposed defect in conversion of proinsulin to insulin. *N Engl J Med* **1984,** *311* (10), 629-34.
268. GenomeAsia, K. C., The GenomeAsia 100K Project enables genetic discoveries across Asia. *Nature* **2019,** *576* (7785), 106-111.
269. Davydov, E. V.; Goode, D. L.; Sirota, M.; Cooper, G. M.; Sidow, A.; Batzoglou, S., Identifying a high fraction of the human genome to be under selective constraint using GERP++. *PLoS Comput Biol* **2010,** *6* (12), e1001025.
270. Kircher, M.; Witten, D. M.; Jain, P.; O'Roak, B. J.; Cooper, G. M.; Shendure, J., A general framework for estimating the relative pathogenicity of human genetic variants. *Nat Genet* **2014,** *46* (3), 310-5.
271. Choi, Y.; Chan, A. P., PROVEAN web server: a tool to predict the functional effect of amino acid substitutions and indels. *Bioinformatics* **2015,** *31* (16), 2745-7.
272. He, W.; Ikeda, S.; Bronson, R. T.; Yan, G.; Nishina, P. M.; North, M. A.; Naggert, J. K., GFP-tagged expression and immunohistochemical studies to determine the subcellular localization of the tubby gene family members. *Brain Res Mol Brain Res* **2000,** *81* (1-2), 109-17.
273. Arpino, J. A.; Rizkallah, P. J.; Jones, D. D., Crystal structure of enhanced green fluorescent protein to 1.35 A resolution reveals alternative conformations for Glu222. *PLoS One* **2012,** *7* (10), e47132.
274. den Hollander, A. I.; Lopez, I.; Yzer, S.; Zonneveld, M. N.; Janssen, I. M.; Strom, T. M.; Hehir-Kwa, J. Y.; Veltman, J. A.; Arends, M. L.; Meitinger, T.; Musarella, M. A.; van den Born, L. I.; Fishman, G. A.; Maumenee, I. H.; Rohrschneider, K.; Cremers, F. P.; Koenekoop, R. K., Identification of novel mutations in patients with Leber congenital amaurosis and juvenile RP by genome-wide

homozygosity mapping with SNP microarrays. *Invest Ophthalmol Vis Sci* **2007,** *48* (12), 5690-8.

275. Kannabiran, C.; Singh, H.; Sahini, N.; Jalali, S.; Mohan, G., Mutations in TULP1, NR2E3, and MFRP genes in Indian families with autosomal recessive retinitis pigmentosa. *Mol Vis* **2012,** *18*, 1165-74.
276. Abbasi, A. H.; Garzozi, H. J.; Ben-Yosef, T., A novel splice-site mutation of TULP1 underlies severe early-onset retinitis pigmentosa in a consanguineous Israeli Muslim Arab family. *Mol Vis* **2008,** *14*, 675-82.
277. Hagstrom, S. A.; North, M. A.; Nishina, P. L.; Berson, E. L.; Dryja, T. P., Recessive mutations in the gene encoding the tubby-like protein TULP1 in patients with retinitis pigmentosa. *Nat Genet* **1998,** *18* (2), 174-6.
278. RetNet, the Retinal Information Network. **August 27, 2019**.
279. den Hollander, A. I.; van Lith-Verhoeven, J. J.; Arends, M. L.; Strom, T. M.; Cremers, F. P.; Hoyng, C. B., Novel compound heterozygous TULP1 mutations in a family with severe early-onset retinitis pigmentosa. *Arch Ophthalmol* **2007,** *125* (7), 932-5.
280. Lewis, C. A.; Batlle, I. R.; Batlle, K. G.; Banerjee, P.; Cideciyan, A. V.; Huang, J.; Aleman, T. S.; Huang, Y.; Ott, J.; Gilliam, T. C.; Knowles, J. A.; Jacobson, S. G., Tubby-like protein 1 homozygous splice-site mutation causes early-onset severe retinal degeneration. *Invest Ophthalmol Vis Sci* **1999,** *40* (9), 2106-14.
281. Hebrard, M.; Manes, G.; Bocquet, B.; Meunier, I.; Coustes-Chazalette, D.; Herald, E.; Senechal, A.; Bolland-Auge, A.; Zelenika, D.; Hamel, C. P., Combining gene mapping and phenotype assessment for fast mutation finding in non-consanguineous autosomal recessive retinitis pigmentosa families. *Eur J Hum Genet* **2011,** *19* (12), 1256-63.
282. McKenna, A.; Hanna, M.; Banks, E.; Sivachenko, A.; Cibulskis, K.; Kernytsky, A.; Garimella, K.; Altshuler, D.; Gabriel, S.; Daly, M.; DePristo, M. A., The Genome Analysis Toolkit: a MapReduce framework for analyzing next-generation DNA sequencing data. *Genome Res* **2010,** *20* (9), 1297-303.
283. Cingolani, P.; Platts, A.; Wang le, L.; Coon, M.; Nguyen, T.; Wang, L.; Land, S. J.; Lu, X.; Ruden, D. M., A program for annotating and predicting the effects of single nucleotide polymorphisms, SnpEff: SNPs in the genome of Drosophila melanogaster strain w1118; iso-2; iso-3. *Fly (Austin)* **2012,** *6* (2), 80-92.